Carbon Stars in the Hamburg/ESO Survey: Abundances[1]

Judith G. Cohen[2], Andrew McWilliam[2], Stephen Shectman[2], Ian Thompson[2], Norbert Christlieb[4], Jorge Melendez[2], Solange Ramirez[5], Amber Swensson[2] & Franz-Josef Zickgraf[4]

ABSTRACT

We have carried out a detailed abundance analysis using high dispersion spectra from HIRES at Keck for a sample of 16 carbon stars found among candidate extremely metal-poor (EMP) stars from the Hamburg/ESO Survey. We find that the Fe-metallicities for the cooler C-stars ($T_{\rm eff}$ ∼5100 K) have been underestimated by a factor of ∼10 by the standard HES survey tools. The results presented here provided crucial supporting data used by Cohen *et al.* (2006a) to derive the frequency of C-stars among EMP stars.

C-enhancement in these EMP C-stars appears to be independent of Fe-metallicity and approximately constant at ∼1/5 the solar ϵ(C). The C-enhancement shows some evidence of decreasing with decreasing $T_{\rm eff}$ (increasing luminosity), presumably due to mixing and dredge-up of C-depleted material. The mostly low ^{12}C/^{13}C ratios (∼4) and the high N abundances in many of these stars suggest that material which has been through proton burning via the CN cycle comprises most of the stellar envelope.

C-enhancement in this sample is associated with strong enrichment of heavy nuclei beyond the Fe-peak for 12 of the 16 stars. The remaining C-stars from the HES, which tend to be the most Fe-metal poor, show no evidence for enhancement of the heavy elements. Very high enhancements of lead are detected in some of

[1]Based in part on observations obtained at the W.M. Keck Observatory, which is operated jointly by the California Institute of Technology, the University of California, and the National Aeronautics and Space Administration.

[2]Palomar Observatory, Mail Stop 105-24, California Institute of Technology, Pasadena, Ca., 91125, jlc@astro.caltech.edu, aswenson@caltech.edu

[3]Carnegie Observatories of Washington, 813 Santa Barbara Street, Pasadena, Ca. 91101, andy, ian, shec@ociw.edu

[4]Hamburger Sternwarte, Universität Hamburg, Gojenbergsweg 112, D-21029 Hamburg, Germany, nchristlieb, fzickgraf@hs.uni-hamburg.de

[5]Spitzer Science Center, Mail Stop 100-22, California Institute of Technology, Pasadena, Ca., 91125, solange@ipac.caltech.edu

the C-stars with highly enhanced Ba. The strong lead lines, the high Ba/Eu ratios, and the high ratios of abundances of the diagnostic elements in the first and second *s*-process peak demonstrate that the *s*-process is responsible for the enhancement of the heavy elements for the majority of the C-stars in our sample.

The low $^{12}C/^{13}C$ ratios and large C and N enhancements of the EMP C-stars are more extreme than those of intrinsic AGB C-stars of near solar Fe-metallicity, but closer to the composition of CH stars. Our subsample of EMP C-stars without *s*-process enhancement is reminiscent of the R-type C-stars in the solar neighborhood; thus we expect that they are formed by similar mechanisms.

We suggest that both the *s*-process rich and Ba-normal C-stars result from phenomena associated with mass transfer in binary systems. This leads directly to the progression from C-stars to CH stars and then to Ba stars as the Fe-metallicity increases.

Subject headings: halo stars, Carbon enhancement, stars: abundances

1. Introduction

We are engaged in a large scale project to find extremely metal-poor (henceforth EMP) stars, characterized by [Fe/H] ≤ -3.0 dex[1], by exploiting the Hamburg/ESO Survey (HES) database. The HES is an objective prism survey from which it is possible to efficiently select a variety of interesting stellar objects, among them EMP stars (Christlieb 2003). The discovery of a number of very metal-poor, carbon-rich, objects, with diverse additional peculiarities, particularly *s*-process or/and *r*-process enrichment, and the discovery of the most iron-poor star known, HE0107−5240 (Christlieb *et al.* 2004), at [Fe/H]=−5.3, which is also very C-rich, recently surpassed by HE1327–2326, with similar characteristics at [Fe/H] ~ -5.6 dex (Frebel *et al.* 2005), as well as the known C-rich binary M dwarf G77–61 established by Plez & Cohen (2005) to have [Fe/H] ~ -4 dex, all contribute to a renewed interest in EMP carbon-rich halo stars.

Broadly speaking, when ϵ(O) exceeds ϵ(C) in cool stars, the oxide molecules (CO, TiO, etc) dominate in the outer layers of the stellar atmosphere. (This is the normal condition for solar abundance ratios.) However, if ϵ(C) is larger than ϵ(O), after the formation of CO, extra C remains rather than extra O, and carbon compounds such as C_2, CH and CN

[1]The standard nomenclature is adopted; the abundance of element X is given by $\epsilon(X) = N(X)/N(H)$ on a scale where $N(H) = 10^{12}$ H atoms. Then [X/H] = $\log_{10}$[N(X)/N(H)] − $\log_{10}$[N(X)/N(H)]$_\odot$, and similarly for [X/Fe].

will dominate. The strong bands of C_2 are then prominent in the optical spectrum of such stars, if they are cool enough, hence the origin of the name Carbon stars (C-stars). Our operational definition of a C-star is one whose spectrum shows the blue-degraded band of C_2 at 5160 Å, which is the most prominent band of this molecule within the wavelength range of the spectra discussed here. If no C_2 bands are detected, but [C/Fe] > 1 dex, we denote a star to be C-enhanced. The strength of the C_2 bands will be a function of $T_{\rm eff}$, ϵ(C), and to a lesser extent, log(g), [Fe/H] and ϵ(O).

The purpose of the present paper is to carry out detailed chemical abundance analyses of a sample of 16 EMP C-stars selected from the HES. This provides a broad database to establish the Fe-metallicity for EMP C-stars. The results presented here provided crucial supporting data used by Cohen *et al.* (2006a) to derive the frequency of C-stars among EMP stars. We use the abundance ratios derived here for EMP C-stars to discuss the origin of the C-star phenomenon among EMP stars, which we attribute *in toto* to phenomena associated with binary systems.

After a description of the stellar sample in §2, readers who are not interested in the details of the abundance analyses should proceed to §4, then §4.1, then skip to §5.

We favor scenarios of C-star formation among the EMP halo stars resulting from the evolution of binary systems, including mass transfer. The evidence supporting this is described in §5. Section §5.5 compares the derived abundances of the EMP C-stars to those of various types of near solar [Fe/H] disk C-stars. The implications of our hypothesis for C-star formation among the EMP stars as applied to stars of higher and lower Fe-metallicity are described in §6. A brief summary concludes the paper.

2. The Stellar Sample

The normal procedures outlined by Christlieb (2003) to isolate extremely metal-poor (EMP) stars from the candidate lists produced by the HES were followed. In brief, candidate EMP stars were selected from the HES. This was followed by vetting via moderate resolution spectroscopy at 5-m class telescopes to eliminate the numerous higher abundance interlopers. The follow up spectra for the stars discussed here were obtained either with the Double Spectrograph (Oke & Gunn 1982) at the Hale Telescope at Palomar Mountain or with the Boller and Chivens spectrograph on the Baade and Clay Telescopes at the Las Campanas Observatory during the period from 2001 to the present.

These follow up spectra are used to determine an estimate of the metallicity of the star, which is much more accurate than can be derived from the low resolution objective prism

spectra of the HES itself. This is accomplished via a combination of strength of absorption in Hδ (determining $T_{\rm eff}$) and in the Ca II line at 3933 Å (the KP index), which determines [Fe/H], once $T_{\rm eff}$, and hence log(g), are specified. The calibration of Hδ plus KP index to [Fe/H] is ultimately based on the results from high resolution abundance studies of standard stars; but such calibrations implicitly assume that the relation between these line indices and [Fe/H] is the same for both program and standard stars. We denote the resulting metallicity value as [Fe/H](HES). The specific algorithm adopted by the HES is described in Beers *et al.* (1999) and is identical to that used until recently by the HK Survey of Beers, Preston & Shectman (1985) and Beers, Preston & Shectman (1992). Stars were chosen for observation at high resolution with HIRES (Vogt *et al.* 1994) at the Keck I Telescope primarily on the basis of low predicted metallicity; all stars with [Fe/H](HES) ≤ -2.9 dex were put on the HIRES observing list, as well as selected other stars of interest.

This paper is dedicated to an exploration of these stars which turned out from their moderate resolution spectra to be C-stars. A more complete discussion of the selection of our C-star sample from the HES and the frequency of C-stars within this sample will be given in Cohen *et al.* (2006c). We present here detailed abundance analyses for 15 C-stars from the HES observed at the Keck I telescope. One of these is a newly discovered short period double lined spectroscopic binary. We denote this group plus the dwarf C-star HE0007–1832 discussed in Cohen *et al.* (2004) as the primary sample. The augmented sample also includes two C-enhanced dwarfs selected from the HES and analyzed in the same way by our group in our previously published papers, HE0024–2523, discussed in Cohen *et al.* (2002), Carretta *et al.* (2002), and in great detail in Lucatello *et al.* (2003), and HE2148–1247, discussed in Cohen *et al.* (2003), both of which show highly enhanced lead in their spectra, plus a third C-enhanced star whose analysis will be presented in Cohen *et al.* (2006b).

Throughout this paper we ignore the two known ultra-metal poor stars HE0107–5240 (Christlieb *et al.* 2004) and HE1327–2326 (Frebel *et al.* 2005). More than 7,000 EMP candidates were searched to turn up these two stars, and there are no stars in the Galaxy known to us with $-5.2 \leq$ [Fe/H] ≤ -4.3 dex. Although both of the known ultra-metal-poor stars are C-stars with extremely large C-enhancements, we are not certain that they represent a continuation towards lower Fe-metallicities of the stars discussed here, and hence we have chosen to not consider them here.

2.1. Stellar Parameters

In order to determine stellar parameters for these stars, particularly the cooler ones, ideally we would compute a special set of model atmosphere which would have the abundances,

particularly those of CNO, set to values appropriate for each star. This would ensure that a proper accounting of the molecular absorption would be made. We have not done this. Instead we have followed our normal procedures described in Cohen *et al.* (2002) of matching observed broad band photometry V–I, V–J, and V–K to predicted grids of synthetic colors by Houdashelt, Bell & Sweigart (2000). Cohen *et al.* (2002) demonstrate that there is good agreement between the Kurucz and MARCS temperature scale. They find that the $V-K$ relations of Alonso, Arribas & Martinez-Roger (1996, 1999) extrapolated to EMP stars gives $T_{\rm eff}$ values $\sim$100 K cooler than those adopted here for giants, while the deduced $T_{\rm eff}$ from $V-K$ for stars near the main sequence turnoff are in good agreement.

We then rely on an appropriate 12 Gyr isochrone from the grid of Yi *et al.* (2002) to obtain the surface gravity for each star. The resulting stellar parameters, which have been derived with no reference to the spectra themselves, are given in Table 2. By using the larger wavelength differences of V–I, and of V–J and V–K to determine our $T_{\rm eff}$ values, avoiding B–V and J–K, we achieve consistency to within $\pm$150 K between the $T_{\rm eff}$ determinations from each of these three colors for all stars. We have noticed that the B–V colors of the HES C-stars appear too red. This behavior is expected, since the flux in the B band is reduced much more by molecular bands in C-stars than is the flux in the V band. B–V colors thus tend to give $T_{\rm eff}$ that are too low, presumably due to the effect of molecular absorption in one or both of the filter bandpasses altering a color which because of its small wavelength coverage is, even under the best of circumstances, relatively insensitive to $T_{\rm eff}$. This problem with B–V colors was pointed out by, among others, Preston & Sneden (2001). J–K is not very sensitive to $T_{\rm eff}$, changing in color by only 0.02 mag for $\Delta T_{\rm eff}$ of 100 K. Given that many of the HES stars are sufficiently faint that the errors in their 2MASS photometry exceed 0.05 mag at K, we avoid the use of J–K colors here.

The IR photometry we use is taken from 2MASS (Skrutskie *et al.* 1997; Cutri *et al.* 2003). We have obtained new photometry at V and I for many of the stars in our sample. We use ANDICAM images taken for this purpose over the past year via a service observing queue on the 1.3m telescope at CTIO operated by the SMARTS consortium. ANDICAM is a dual channel camera constructed by the Ohio State University instrument group[2]. Our ANDICAM program requires photometric conditions, and additional standard star fields, charged to our ANDICAM allocation through NOAO, are always taken for us.

Our new Andicam photometry for our sample of C-stars from the HES, as well as other relevant observational data for these stars, is presented in Table 1. Table 2 gives the resulting stellar parameters for these stars.

[2]See http://www.astronomy.ohio-state.edu/ANDICAM and http://www.astro.yale.edu/smarts.

The uncertainty in log(g) arising from our 150 K uncertainty in $T_{\rm eff}$ depends on the slope of the relationship between $T_{\rm eff}$ and log(g) along the adopted isochrone. For stars close to the main sequence turnoff and for subgiants, this is small, and the uncertainty in log(g) is 0.1 dex. However, for stars along the RGB, it reaches 0.4 dex.

3. HIRES Observations and Abundance Analysis

Observations with HIRES at the Keck I Telescope were obtained during several runs from Sep 2001 to June 2005. The weather conditions varied from night to night. A spectral resolution of 45,000 was achieved using a 0.86 arcsec wide slit projecting to 3 pixels in the HIRES focal plane CCD detector. For those stars presented here with $V > 15$ mag, a spectral resolution of 34,000 was used, with the exception of HE1410−0004, which was observed at the higher spectral resolution. The spectra cover the region from 3840 to 5330 Å with no gaps between orders for $\lambda < 5000$ Å, and only small gaps thereafter. Each exposure was broken up into 1200 sec segments to expedite removal of cosmic rays. The goal was to achieve a SNR of 100 per spectral resolution element in the continuum at 4500 Å; a few spectra have lower SNR. This SNR calculation utilizes only Poisson statistics, ignoring issues of cosmic ray removal, night sky subtraction, flattening, etc. The observations were carried out with the slit length aligned to the parallactic angle.

The recently installed upgraded HIRES detector designed and built by the Lick Observatory engineering staff, led by S. Vogt, was used for three C-stars observed in 2005: HE1410−0004, HE1443+0113, and HE1434−1442. HIRES-R was used for the first star, and HIRES-B for the other two. We thus obtain, among other desirable things, more complete spectral coverage, reaching in a single exposure from 4020 to 7800 Å with HIRES-R and from 3200 to 5900 Å with HIRES-B for the instrument configurations we use. Note that only for one star in the present sample does the included spectral range reach beyond 6000 Å. Details of the HIRES exposures, including the exposure times and the SNR per spectral resolution element in the continuum, are given in Table 1.

This set of HIRES data was reduced using a combination of Figaro scripts and the software package MAKEE[3]. Insofar as possible, both the spectral reduction and abundance analyses presented here are identical to the procedures described in our earlier paper on EMP dwarfs from the HES (Cohen *et al.* 2004).

[3]MAKEE was developed by T.A. Barlow specifically for reduction of Keck HIRES data. It is freely available on the world wide web at the Keck Observatory home page, http://www2.keck.hawaii.edu:3636/.

3.1. Equivalent Widths and Abundance Analysis

The search for absorption features present in our HIRES data and the measurement of their equivalent width (W_λ) was done automatically with a FORTRAN code, EWDET, developed for a globular cluster project. Details of this code and its features are given in Ramírez *et al.* (2001). The strong molecular bands made it impossible to use the full spectral range; selected regions were eliminated prior to searching for absorption features. This also applied to the radial velocity determination procedure we use, described in Cohen *et al.* (2004). Extensive hand checking of the W_λ for blending by molecular features was necessary in many cases, such as when the line profiles were frequently distorted by blends, due to strong molecular blanketing, or low S/N conditions. The spectrum of HE1410+0213 is so severely affected by its very strong molecular bands that only the region beyond 5160 Å (plus a few strong lines near 4920 Å) could be used. For HE1443+0113 there is only one exposure available which had to be terminated at 550 sec due to deteriorating weather conditions. It has a very low SNR, and only the strongest features could be measured, i.e. CH, the Na doublet, the Mg triplet, a few Fe I lines, and two Ba II lines. The W_λ for this spectrum are more uncertain than those of the others presented here.

The atomic data and list of unblended lines used (ignoring those in the regions cut out due to the strong molecular bands), are identical to those of Cohen *et al.* (2004). We adopt $\log\epsilon$(Fe) = 7.45 dex for iron following the revisions in the solar photospheric abundances suggested by Asplund *et al.* (2000), Prochaska *et al.* (2000) and Holweger (2001). Abundances were determined from equivalent widths, except for C, N (where we synthesized the region of the CN bandhead near 3885 Å), and Pb. For C, we synthesized the region of the CH band near 4320 Å, which is considerably weaker than the main bandhead of the G band near 4305 Å, and hence still usable even in these C-stars. For the coolest C-stars with the strongest bands, even this region off the main bandhead is close to saturation. The solar abundances we adopt are those of Anders & Grevesse (1989), slightly updated as described in Cohen *et al.* (2004). A synthesis using our line list of CH and CN features combined with the Kurucz (1993) solar model matches the solar FTS spectrum of Wallace, Hinkle & Livingston (1998) with our initially adopted C and N solar abundances, $\log\epsilon$(C) = 8.59 dex and $\log\epsilon$(N) = 7.93 dex. These are close to those of Grevesse & Sauval (1998), but larger than those of Asplund *et al.* (2004, 2005), which are are 0.2 dex smaller for C and 0.13 dex smaller for N. Once the C and N abundances were determined for a star, we synthesized the region of the 4057 Å Pb I line to derive the Pb abundance.

The equivalent widths and atomic parameters used in the analysis of the primary sample of 16 C-stars selected as EMP candidates from the HES are tabulated in Table 3, 4 and 5. W_λ for the additional redder lines seen only in the three C-stars observed with the upgraded

HIRES detector are given in Table 6. Occasionally, for crucial elements where no line was securely detected in a star, we tabulate upper limits to W_λ.

As in our previous work, we use the HFS components from Prochaska *et al.* (2000) for the lines we utilize here of Sc II, Mn I, and Co I. For Ba II, we adopt the HFS from McWilliam (1998). We use the laboratory spectroscopy of Lawler, Bonvallet & Sneden (2001a) and Lawler *et al.* (2001b) to calculate the HFS patterns for La II and for Eu II. We adopt the isotopic and HFS shifts for the 4057 Å line of Pb I given by Van Eck *et al.* (2003); see her paper for references for the laboratory and theoretical atomic physics. McWilliam *et al.* (1995b) gives the HFS pattern for the NaD lines. Although the difference between log(ϵ(Na)) derived from the full HFS pattern and by just using two lines to represent the double is small, <0.08 dex, we use the full HFS pattern for these lines. A synthesis incorporating the list of hyperfine and isotopic components given by Hobbs, Thorburn & Rebull (1999) was used for the Li I resonance line for which an upper limit for its W_λ was measured in one star. Spectral syntheses are carried out for each of the features with HFS to match the observed W_λ and thus derive the abundance of the relevant species. For Pb, because of the strong blending by CH features, the spectral synthesis used to determine the Pb abundance included lines of ^{12}CH, ^{13}CH, Pb and other metals.

Recall that the amount of C_2, CH, and CN formed is dependent upon the amount of free carbon present (i.e. the amount not locked-up in CO), and that in general we do not have measurements of the O abundance in these EMP C-stars. Thus our derived C abundances are dependent on the choice made for the O abundance through molecular formation and equilibrium.

The abundance analysis is carried out using a current version of the LTE spectral synthesis program MOOG (Sneden 1973). We employ the grid of stellar atmospheres from Kurucz (1993) without convective overshoot, when available. We compute the abundances of the species observed in each star using the measured W_λ values and the four stellar atmosphere models from this grid with the closest $T_{\rm eff}$ and log(g) to each star's parameters. The abundances were interpolated using results from the closest stellar model atmospheres to the appropriate $T_{\rm eff}$ and log(g) for each star given in Table 2.

Our HIRES spectra show that HE0012−1441 is a double lined spectroscopic binary. Since it is rather faint, spectra were taken on each of three consecutive nights with the intention of summing them to reach a high SNR. Comparison of the summed spectra for each of the three nights revealed the presence of double lines as well as obvious differences in the velocity separation of the two components over the timespan of 48 hours, as is shown in Fig. 1. The v_r of the primary decreased by 6 km s^{-1} over that timespan. The separation of the two components was largest on the last night, when it reached 28 km s^{-1}. Thus, this

binary must have a relatively short period, and is probably similar to HE0024–2523 (Cohen et al. 2002; Carretta et al. 2002; Lucatello et al. 2003). Only the sum of the three 1200 sec HIRES exposures from the third night was used to determine W_λ; this night had the largest velocity separation, hence was the easiest from which to measure the W_λ of the primary component. This, of course, reduces the SNR of the spectrum below that expected on the basis of the total integration time and below the desired value. We have assumed that the secondary, which contributes perhaps 1/5 of the total W_λ for selected lines, does not seriously affect the colors used to determine $T_{\rm eff}$, which may not be a valid assumption. Furthermore, the lines from the secondary appear to be wider than those of the primary, suggesting a faint cool dwarf as the secondary star. (The secondary is too luminous to be a white dwarf with age $\sim$10 Gyr.) For this star only, the W_λ were not used; the W_λ listed in Table 3 for this star are for guidance only. Instead the abundance was determined by matching the observed line profile for each spectral feature with the predicted one, varying ϵ(X). This ensured proper treatment of the partially blended lines due to the second component in the binary system. A luminosity ratio for the two components of 4 throughout the relevant wavelength range of the HIRES spectra was assumed to determine the W_λ for this star.

The microturbulent velocity (v_t) of a star can be determined spectroscopically by requiring the abundance to be independent of the strength of the lines. However, there are fewer usable Fe I lines in the complex spectra of these C-stars than in stars with normal C and N and the same stellar parameters due to the rejection of large regions of the spectrum where the molecular features are strongest. Furthermore the uncertainties in measurement of the remaining lines are larger, again due to possible molecular contamination and difficulties with continuum determination that do not occur in EMP stars with normal C and N. Based on our as yet unpublished analyses of a large sample of EMP giants from the HES, we set the v_t to 1.6 to 1.8 km s^{-1}, depending on $T_{\rm eff}$. We checked in each case that a plot of derived Fe I abundance as a function of W_λ looked reasonable, but did not try to iterate on v_t to achieve a perfectly constant Fe I abundance.

The abundances presented here could be improved. Spectral syntheses could be used for additional elements. A better determination of $T_{\rm eff}$ and of v_t could be attempted. However, Table 7 demonstrates that the results achieved here are reasonably good. This table gives the slope of a linear fit to the derived Fe I abundance from each observed line as a function of EP, W_λ/λ, and line wavelength. Assuming a perfect analysis, these slopes should all be zero[4].

[4]We ignore contributions from any issues that vary as a function of $T_{\rm eff}$ that may not be included in our analysis, such as non-LTE effects, which might contribute to the measured slopes and their rms disperion. Large contributions to the σ of the measured slopes from terms such can be excluded.

The full range in EP for the observed Fe I lines is only 3 eV. The mean slope for the derived Fe I abundance with EP for the 11 C-stars with entries in Table 7 is +0.02 dex/eV with $\sigma = 0.05$ dex/eV. We need to demonstrate that this mean and σ are consistent with our known uncertainties. The value of 0.05 dex/eV found for σ corresponds to a change in $T_{\rm eff}$ of 250 K, somewhat larger than our adopted uncertainty in $T_{\rm eff}$ discussed in §2.1 of 150 K. However, the random component of the uncertainty in the Fe abundance derived from a single Fe I line in a single star due primarily to errors in the gf value assigned to the line is at least 0.2 dex. This leads to a σ for the measured slopes Fe I abundance versus EP beyond that expected purely from the adopted $T_{\rm eff}$ uncertainty. To support this assertion we note that the correlation coefficients for the relationship within each star are low ($|r| < 0.25$ in all cases).

The slopes for the Fe I abundance versus reduced equivalent width for the same set of 11 stars have a mean of -0.04 dex with $\sigma = 0.12$ dex. The spread in this slope is completely consistent with our adopted uncertainty in v_t of 0.2 km s^{-1}. The set of correlation coefficients are low ($|r| < 0.35$ in all cases) here also.

The results for the abundances of typically 20 species in each star (only 9 in HE1410+0213, and only five for HE1443+0113) are given in Tables 8 to Table 10. We tabulate both log$\epsilon(X)$ and [X/Fe]; our adopted solar abundances can be inferred directly from these tables. The ^{12}C/^{13}C ratios determined from the CH and the C_2 bands are given in Table 12.

Table 13 gives the changes in the deduced abundances for small changes in $T_{\rm eff}$, log(g), v_t and W_λ in the [Fe/H] of the model atmosphere used for an EMP giant with $T_{\rm eff}$ ∼5200 K. The last column gives expected random uncertainties for [X/Fe] appropriate for for a single star, combining in quadrature the uncertainties in [X/Fe] resulting from the errors in stellar parameters established in §2.1, i.e. an uncertainty of ±150 K in $T_{\rm eff}$, of ±0.4 dex in log(g), of ±0.5 dex in the metallicity assumed in the model atmosphere used for the analysis, of ±0.2 km s^{-1} for v_t, and a contribution representing the errors in the measured equivalent widths. This last term is set at 20% (approximately equivalent to 0.08 dex abundance uncertainty, but depends upon line strength) for a single detected line (which may be an underestimate for the complex spectra of the C-stars), and is scaled based on the number of detected lines. The contribution of the various terms, particularly that of log(g),, which will be smaller for hotter stars, may vary somewhat with $T_{\rm eff}$. Systematic uncertainties, such as might arise from errors in the scale of the transition probabilities for an element, are not included in the entries in Table 13. Random errors in the gf value for a particular line are not relevant to this calculation provided that the same line list is used throughout.

3.2. The $^{12}C/^{13}C$ Ratios

We have measured the isotopic ratio $^{12}C/^{13}C$ for the C-stars from our sample with the highest SNR spectra using the line list for the 4300 Å region of the G band of CH as described in Cohen *et al.* (2003). Spectral syntheses of the features of ^{13}CH at 4211.3, 4213.1, 4219.2, and 4221.8 Å were used. We have verified for three stars whose HDS spectra were supplied by W. Aoki that our line list combined with our standard analysis procedures gives $^{12}C/^{13}C$ ratios derived from CH features differing from those derived by Aoki *et al.* (2001) or Aoki *et al.* (2002a) by 15% or less.

Spectrum synthesis for the C_2 bands was carried out based on the C_2 line list of Querci, Querci & Kunde (1971) and Querci, Querci & Tsuji (1974), as updated and supported on the web site of U. Jørgensen[5]. The dissociation potential for C_2 was taken as 6.30 eV (Urdahl, Bao & Jackson 1991). The isotopic line shift depends on the ratio of the reduced mass of a diatomic molecule AB, $m_A m_B/(m_A + m_B)$, for its two isotopic variants. This ratio is 1.04 for C_2 and only 1.007 for CH when considering ^{12}C versus ^{13}C. Thus, as has been know for a long time, isotopic effects are considerably easier to detect in certain C_2 bands than in those of CH. For the G band of CH, one must study detailed profiles of individual lines within the band which are often blends of multiple components of ^{12}CH or ^{13}CH. The situation for C_2 is very different. The strongest C_2 band within our spectral range is the (0,0) Swan band at 5160 Å, which has a very small isotopic shift. However, the (1,0) bandhead for $^{12}C^{13}C$ at 4744 Å is separated from that of $^{12}C^{12}C$ at 4737 Å by ∼7 Å, which is easily resolved even on moderate resolution spectra. The $^{13}C^{13}C$ bandhead is ∼8 Å further to the red at 4752 Å; it can be glimpsed in the C-stars in our sample with the smallest $^{12}C/^{13}C$ ratios. Plates 26 and 29 of Keenan & McNeil (1976) show examples of spectra of C-stars stars with high and low $^{12}C/^{13}C$ ratios in this spectral region. Figure 2 illustrates the ease of separating the the bandheads $^{12}C^{12}C$ and $^{12}C^{13}C$ with the present much higher resolution data. Any uncertainty in the band electronic oscillator strength does not affect the determination of $^{12}C/^{13}C$ ratio.

Because $^{12}C^{13}C$ is a heteronuclear molecule, and ^{13}C has a non-zero nuclear spin, it has a different number of states than does $^{12}C^{12}C$, affecting the partition function as well as the number of transitions in a band. Since the spectrum synthesis program, MOOG, which we use does not distinguish between isotopic molecular species it is necessary to reduce the gf value of each $^{12}C^{13}C$ line by a factor of 2, to account for the partition function difference with $^{12}C^{12}C$; $^{13}C^{13}C$ lines would require a factor of 4 reduction (e.g. see Amoit 1983). [6] We

[5]http://stella.nbi.dk/pub/scan

[6]Notes on the web site of U. Jørgensen (http://stella.nbi.dk/pub/scan) suggest that this arguement may

note that the band oscillator strengths for the isotopic species may not be exactly equal, due to wavefunction differences.

We performed a sanity check on our isotopic C_2 band line lists by synthesizing the $^{12}C^{13}C$ and $^{12}C^{12}C$ (1,0) bandheads. In this test we adopted a carbon abundance low enough that the bandheads were unsaturated. If we set $^{12}C/^{13}C = 1$, and synthesize the spectrum in the region of the bandhead of the (1,0) Swan C_2 band, the $^{12}C^{13}C$ and $^{12}C^{12}C$ bandheads should then be roughly equal in strength, because although the $^{13}C_2$ isotopic bandhead has twice as many lines, its partition function is a factor two larger. The ratio of absorption at the appropriate resulting bandheads in the synthesized spectrum is within 15% of unity, as expected.

3.3. Ionization Equilibrium and non-LTE

Since we have not used the high resolution spectra themselves to determine $T_{\rm eff}$ or $\log(g)$, the ionization equilibrium is a stringent test of our analysis and procedures, including the determination of $T_{\rm eff}$ and of $\log(g)$, as well as the assumption of LTE. For the 16 candidate EMP C-stars from the HES we analyze here, the Fe ionization equilibrium is shown in Fig. 3; we obtain a mean for $\log\epsilon$(Fe:Fe II) − $\log\epsilon$(Fe:Fe I) of −0.07 dex, with a 1σ rms scatter about the mean of 0.16 dex. This is an extremely good ionization equilibrium for stars with such complex spectra, and it demonstrates the validity of our determination of stellar parameters from photometry and isochrones. The ionization equilibrium for Ti is almost as good, with a mean of +0.08 dex, $\sigma = 0.28$ dex. The dispersion falls to 0.22 dex (and the mean becomes −0.03 dex) if one outlier with extremely weak Ti I lines is eliminated.

The Fe abundances derived from the neutral and ionized lines shift out of equilibrium by ∼0.25 dex for a 250 K change in $T_{\rm eff}$ in this temperature regime (see Table 13). Our adopted uncertainty in $T_{\rm eff}$ is ±150 K and the resulting uncertainty in $\log(g)$ is discussed in §2.1. Table 13 demonstrates these two factors alone can give rise to the dispersion observed among the sample stars in the Fe ionization equilibrium.

Following Cohen *et al.* (2004), we implement a non-LTE correction to $\log\epsilon$(Al) of +0.60 dex for the lines of the Al I doublet near 3950 Å (Baumüller & Gehren 1997). Only the 3961 Å line can be used for most of these C-stars; the other line of this doublet is blended with molecular features. The 3905 Å line of Si I, the only suitable line of this element in the

be too simplistic, and that a factor of 4 should be used instead to correct the gf values for the $^{12}C^{13}C$ lines. If true, our derived ^{13}C abundances will need to be reduced by a factor of two.

wavelength range covered in most of our spectra, is also heavily blended with CH lines; we do not use it. Si abundances have been determined only for the small number of C-stars with the redder wavelength coverage achieved with the new HIRES detector, where unblended Si I lines near 5800 Å become available. We use a non-LTE correction for Na abundances from the 5889,5895 Å doublet of −0.20 dex following Baumüller, Butler & Gehren (1998) and Takeda *et al.* (2003). Only one star (HE1410−0004) has a spectrum which reaches any of the O I features, yielding an upper limit to the 6300 Å forbidden line and a marginal detection of the strongest line in the triplet at 7772 Å. Kisselman (2001) pointed out the need for non-LTE corrections for the IR triplet line, and we use those calculated by Takeda (2003). We adopt a non-LTE correction for O for this star of −0.2 dex.

3.4. Comparison with Previous High Dispersion Analyses

Two of the 16 C-stars studied here are rediscoveries of stars found in the HK Survey (Beers, Preston & Shectman 1985, 1992), and have been previously observed at high dispersion. HE0058–0244 (CS 22183–015) was analyzed by Johnson & Bolte (2002). They relied on stellar parameters determined from the spectra themselves; their adopted $T_{\rm eff}$ (5200±100 K) is 400 K lower than our value, and their $\log(g)$ is correspondingly 1 dex higher to preserve ionization equilibrium. The difference in their derived [Fe/H], which is 0.35 dex lower than our value, is due entirely to the differences in the adopted stellar parameters. We attempt to compare [X/Fe], modifying their values to our adopted $T_{\rm eff}$,$\log(g)$ using the sensitivity table (Table 13). With these corrections, which in some cases are large, we find pretty good agreement (within 0.25 dex), except for [Y/Fe] and [La/Fe], where our abundances are 0.4 dex lower than theirs.

Norris, Ryan & Beers (1997), Bonifacio *et al.* (1998), Preston & Sneden (2001) and recently Aoki *et al.* (2002b) observed HE2356–0410 (CS 22957–027). The first two groups used B–V to establish $T_{\rm eff}$; they both use a value 350 K cooler than that we adopted here. Preston & Sneden (2001) uses a hybrid method with B–V corrected for molecular absorption to determine $T_{\rm eff}$, while Aoki *et al.* (2002b) used B–V and V–K for this purpose, ending up with a value for $T_{\rm eff}$ only 100 K lower than ours. These differences in adopted stellar parameters directly produce the differences in derived metallicity: the first two analyses yield [Fe/H] values 0.3 dex lower than adopted here, while that of the last is only 0.05 dex lower. Although there is overall good agreement for the C abundances, the derived [N/Fe] ranges over 0.9 dex among the five analyses.

We compare our derived abundance ratios with those of Aoki *et al.* (2002b), as the stellar parameters adopted in these two analyses are similar. Their $^{12}C/^{13}C$ ratio is 8±2, in

reasonable agreement with our value of 4.0±1.3 (see Table 12). Our [C/Fe] is 0.2 dex lower than theirs, while our derived [N/Fe] is a similar amount larger, as it must be to compensate in order to fit the CN band strength. The abundance ratios for all the species in common agree fairly well, with [Al/Fe], [Ca/Fe], [Sr/Fe] and [Ba/Fe] showing the largest differences, -0.42[7], $+0.58$, -0.42 and $+0.45$ dex respectively for the values of [X/Fe] derived here minus those of Aoki *et al.* (2002b). Large differences also occur in abundance ratios for many species in comparing our results with the other earlier analyses.

To isolate the cause of the large differences between the various analyses of these C-stars, we have compared our measured W_λ with those published, when available. For HE0058–0244, the measured W_λ for the 12 weak lines in common (mean W_λ of 27.7 mÅ) tabulated by Johnson & Bolte (2002) for n-capture elements agree with ours with a mean difference of 1.1 mÅ and a σ of 3.2 mÅ. The only strong line in common is the 4554 Å line of Ba II with measured a W_λ of 177.5 and 166.2 mÅ in the two studies. For HE2356–0410 we have 18 lines in common with those tabulated by Norris, Ryan & Beers (1997). The W_λ again agree well, with a mean difference of 0.3 mÅ and a σ of 12.2 mÅ. (The set of lines in common in this case are in general stronger lines, with a mean W_λ of 62 mÅ.) The agreement with the W_λ for this star tabulated by Bonifacio *et al.* (1998) is also very good, with σ of 6.1 mÅ.

Thus the differences in deduced abundances between the analysis presented here and those previously published for these two C-stars are not due to differences in measured W_λ. They must arise from the choices made for the stellar parameters and in the details of the abundance analyses. In spite of these discrepancies, the overall characteristics of the abundance distribution in these two C-stars are inferred as identical by each of the analyses. All five groups, for example, agree that HE2356–0410 has an extremely large enhancement of C, and has a very low [Ba/Fe]. The deviations from "normal" EMP stars are in general and for this particular star very large, larger than the errors made by any of the independent analyses.

We previously published an analysis of the dwarf C-star HE0143–0441 in Cohen *et al.* (2004). The analysis presented here supersedes that one; the adopted $T_{\rm eff}$ is 130 K cooler due to acquisition of better optical photometry in the interim and the W_λ have also been rechecked for molecular blends since our earlier effort. The resulting [Fe/H] is 0.14 dex smaller than that of our previous work. The abundance ratios [X/Fe] derived from our two analyses are in good agreement, except for N. It appears there was a typo in the entry for logϵ(N) in Table 5 of Cohen *et al.* (2004) which is corrected in Table 8 here.

[7]The difference in adopted non-LTE correction for the lines of the 3950 Å doublet of Al I has been removed.

S. Lucatello's PhD thesis (Lucatello *et al.* 2006) will present a detailed abundance analysis for five of the C-stars analyzed here. That analysis should be definitive, with extensive use of spectral syntheses and maximum care in all aspects. The Si abundance should be recoverable with such syntheses, and a careful synthesis of the region of the 3961 Å line of Al I would improve the Al abundances presented here.

4. Comments on Individual Elements

4.1. Iron

We confirm that our [Fe/H] determinations are largely free of molecular contamination by looking at the derived Fe-abundance in regions where molecular bands are absent as compared to those where they are (weakly) present. Regions where the molecular bands are strong in the spectrum of a sample star were ignored. Every star in our sample was checked to make sure that the Fe I abundance deduced from lines redward of 5160 Å to the end of our spectral coverage, a region within which there are no molecular features, was the same as that for lines to the blue. For only two stars did a possible systematic difference appear, and it was only 0.1 dex, with the redder lines giving slightly lower Fe abundances. This supports the validity of our Fe-abundances.

The [Fe/H] values derived here are in some cases considerably higher than those predicted by the algorithm used on the moderate resolution HES follow-up spectra. Fig. 4 shows Δ[Fe/H], the difference between [Fe/H] as determined from a detailed abundance analysis of high dispersion spectra versus that from the application of the Beers *et al.* (1999) algorithm to the moderate resolution spectra. Initially, both for the HES and for the HK Survey, the B−V color was used to indicate $T_{\rm eff}$. Such a procedure is very convenient for the HES, for example, as rough colors can be measured directly from the objective prism spectra. This procedure, however, is a disaster for C-stars, as the B bandpass is much more affected by molecular absorption from CH and CN, than is the V bandpass. Spuriously red B−V colors lead to spuriously low deduced $T_{\rm eff}$, which in turn lead to spuriously low deduced Fe-abundances. In practice this affects all C-stars cooler than 6000 K, and almost certainly some even hotter than that. The literature is full of references to C-star abundance analyses where the resulting high resolution [Fe/H] grossly (by $\sim$1 dex) exceeds [Fe/H](HK), see, for example, Norris, Ryan & Beers (1997) or Hill *et al.* (2000), for which the relevant [Fe/H](HK) are given in Barbuy *et al.* (1997). The origin of this problem was realized several years ago by several groups, see, for example, Preston & Sneden (2001). Both the HES and the HK Survey then switched to using the strength of absorption at Hδ as a $T_{\rm eff}$ indicator.

However, there is still a problem for the cooler C-stars, as is shown in Fig. 4. The five C-stars HE0212−0557, HE1031−0020, HE1434−1442, HE1443+0113 and HE1509−0806 show Δ[Fe/H] $\sim$1 dex. Something is still wrong, but now only the cooler giants, $T_{\rm eff} \sim 5100$ K, and not all of them, are affected. As was shown by Cohen *et al.* (2006a), the problem is the molecular absorption in the specific bandpasses used, particularly in the red continuum bandpass for the Hδ index. For the most extreme C-stars in our sample, the HP2 index measuring the Hδ absorption defined and used by the HK Survey becomes negative (i.e. implies that Hδ is in emission), which is not the case when one examines high dispersion spectra. This again leads to spuriously low $T_{\rm eff}$ estimates and hence to spuriously low deduced Fe-abundances from the moderate resolution follow up HES or HK Survey spectra. Both CN and CH contribute to the absorption there, with that of CN dominating at solar metallicity in the relevant $T_{\rm eff}$ range. At the low Fe-metallicities considered here, the relative contribution of CN and of CH will depend primarily on $T_{\rm eff}$, with C/N ratio and Fe-abundance also playing a role. The five C-stars with large Δ[Fe/H] (those discrepant in Fig. 4) are the five stars with the strongest absorption over the specific spectral region of interest (4144 to 4164 Å).

In the regime of KP and HP2 corresponding to EMP giants, a change in HP2 of 0.5 Å can produce a change in predicted [Fe/H](HES) of 0.5 dex. The filter bandpass of HP2 is 12 Å wide (Beers *et al.* 1999). Thus, a 0.5 Å error in the measured HP2 index corresponds to a 4% error in the continuum level. Looking at the spectra of the coolest C-stars in the 4000-4200 A region shown in Fig. 2 of Cohen *et al.* (2006a) in the relevant region for the feature and sideband bandpasses of HP2, it is difficult to see how an underestimate of the continuum level of this size will not occur.

Thus, the algorithm adopted by the HES, and until recently the HK Survey (Rossi et al. 2005), to deduce a Fe-metallicity from the low dispersion spectra, systematically underestimates [Fe/H](HES) by a factor of $\sim$10, for certain cool C-stars ($T_{\rm eff} \lesssim 5100$ K). The important implications of this are: the overestimate of the frequency of C-stars among EMP stars, and the overestimate of the yield of EMP stars in the HES and, by implication, the HK Survey. These issues are discussed briefly in Cohen *et al.* (2006a) and will be discussed at length in Cohen *et al.* (2006c).

We demonstrate that the systematic [Fe/H] underestimate for EMP C-stars does not arise from the random uncertainty in the measurement of the HP2 indices. Comparison of HP2 indices measured from moderate dispersion spectra for 57 stars, most of which are C-normal, with observations on different runs at the P200 or observed at both the P200 and Magellan telescopes show a mean difference in measured HP2 indices of 0.18 Å, with a rms dispersion about the mean of 0.65 Å; details will be presented in Cohen *et al.* (2006c). Also note that the moderate resolution spectra of the 5 C-stars which show large Δ[Fe/H](HES)

are from four different runs with the Double Spectrograph on the Hale Telescope.

The slight overlap of high and low Δ[Fe/H](HES) values at the boundary in $T_{\rm eff}$ where this effect becomes important ($\sim$5200 K) can be explained as resulting from observational uncertainties; recall that our adopted uncertainty in $T_{\rm eff}$ for these C-stars is 150 K. Furthermore, this effect depends on the C abundance, the C/N ratio, and to a smaller extent [Fe/H], although the primary dependence is on $T_{\rm eff}$. Clearly, while using Hδ is better than using B–V as a $T_{\rm eff}$ indicator, it has its limitations, particularly for cool C-rich giants, as shown here. Using a V–K color is better. J–K is not useful for the faint stars found in the HES; the errors of the 2MASS database are too large compared to the sensitivity of J–K to $T_{\rm eff}$ which is, as discussed in §2.1, small. This statement may not hold for the HK Survey, where the stars are in the mean significantly brighter than the HES, and hence the 2MASS errors are much smaller.

4.2. C and N

Since a band of CN is used to derive the N abundance, the N abundance is linked to the choice of C. Systematic errors not included in Table 13 in the C and N abundances are possible in the case of unusually large oxygen abundance, because the CN and CH densities depend upon the amount of free carbon left given CO formation.

HE1150–0428 has extremely strong CN bands; the bandheads at 3885, 3875 and 3865 Å are all present and the first two of these reach maximum absorption of $\sim$85% of the continuum. The continuum was very hard to define in this region of the spectrum of this star. Combining that with saturation issues, the N abundance this star is not well determined; appropriate errors might be $\log[\epsilon(\rm N)] = 7.15$ (+0.5,−0.3) dex.

The determination of ^{12}C/^{13}C from the C_2 and CH bands is described in §3.2. Fig. 5 displays the measured absorption of the stellar continuum at ^{12}C^{12}C and ^{12}C^{13}C bandheads for the C-stars in our sample; see also Figure 2. The deduced isotopic ratios for C derived from these two bands are shown as a function of $T_{\rm eff}$ in Fig. 6. ^{12}C/^{13}C is easy to determine from the 4740 Å C_2 band, and the many values given in Table 12 demonstrate that the ^{12}C/^{13}C ratio is low, with a typical value of 4. The isotopic ratios for our sample of C-stars as determined from C_2 bands, ignoring the lower limits, are consistent to within 1.5σ with a constant value of ^{12}C/^{13}C of $\sim$3.5. Similar values have been found among luminous moderately metal poor field giant stars with normal C-abundances and with luminosities near the tip of the RGB by Carretta, Gratton, Sneden & Bragaglia (2000). The hottest stars in the sample yield only lower limits to ^{12}C/^{13}C using either of the molecular features.

More measurements of $^{12}C/^{13}C$ ratios at the extremes of the range of $T_{\rm eff}$ would be required to search for any trend with $T_{\rm eff}$.

4.3. Barium

In many cases, the Ba II lines are very strong, and the resulting derived Ba abundances must be regarded as quite uncertain. Their HFS corrections are sometimes large and vary considerably with W_λ. The HFS corrections calculated by McWilliam (1998) which we adopt are for a r-process isotopic distribution. We have rescaled them for the s-process Ba isotopic distribution; this in general reduces the deduced Ba abundance by $\sim$0.1 dex.

4.4. Lead

There is only one usable Pb I line in the spectral region we cover. This line, at 4057.8 Å, is badly blended by CH features in these C-stars. Our spectral synthesis for this feature uses the isotopic and HFS pattern for Pb described in § 3.1, as well as features of ^{12}CH, ^{13}CH and various atomic species. A reasonable uncertainty for our Pb measurements based on spectral synthesis is $\pm$0.3 dex. Non-detections, in cases where there is no problem indicated by notes in Table 8 to 11, correspond to upper limits of $\log[\epsilon({\rm Pb})] = +1.5$ dex.

4.5. Use of Strong Lines

It is desirable in carrying out a detailed abundance analysis to use only absorption lines with W_λ less than $\sim$170 mÅ to keep the errors as small as possible. Stronger lines will be formed in the outermost layers of the stellar atmosphere, where the $T(\tau)$ relationship is more uncertain, and where LTE is less likely to prevail. Hence the W_λ predicted from a model atmosphere for such strong lines are more uncertain, as is the derived abundance of the species from which the line originates. However, the wavelength coverage of our spectra, almost all of which were taken prior to the HIRES detector upgrade, is restricted, and CH, CN and C_2 molecular bands in the spectra of these stars further cut down the useful wavelength range. Some elements have very few detectable lines of any state of ionization within the allowed region. In a few cases only strong lines are available, while in others one or two weak lines are sometimes present together with the strong ones, at least for a few of the C-stars in our sample.

Examination of Tables 3 to 6 reveals the elements of concern. The Na I D lines are too

strong for reliable abundance analysis in the spectrum of our coolest C-star, HE1443+0113, and are the only lines detected of that species in the only available HIRES spectrum of that star, which has low SNR. Two lines of the Mg triplet at 5170 Å are always detected (the third is blended and not used) and are sometimes stronger than 170 mÅ, but often one or more of the weaker subordinate Mg I lines are seen as well. The Sr II line at 4077 Å is the only one measured in many of the sample stars, as the 4215 Å line is often swamped by CN. In the most *s*-process rich cool C-stars, this line exceeds the W_λ cutoff suggested above; unfortunately there are no other detectable Sr lines in the available wavelength region. The Ba II lines at 4554 and 4934 Å are extremely strong, far beyond the limit in W_λ suggested above, in several of the cooler Ba-rich C-stars. But in many of these, the weaker 4130 Å line is seen as well, and in the one star with a HIRES-R spectrum, the weaker 5854, 6141 and 6496 Å Ba II lines are picked up as well. Caution is necessary for these particular elements, but we believe that the magnitude of the potential errors is sufficiently small that the fundamental conclusions of our work are not affected.

5. Abundance Ratios

5.1. C/H Ratios

We have two indicators in the present work for the carbon abundances, the strength of the bands of CH and of C_2. The upper panel of Fig. 7 shows ϵ(C) inferred from the G band of CH as a function of [Fe/H](HIRES) for the full sample of 16 C-stars and the three EMP C-enhanced stars with [C/Fe] > 1.0 dex from our work. Eleven additional very metal-poor C-stars, mostly from the HK Survey, with recent analyses from the literature, are indicated as small open circles in this figure as well as in Fig. 8 and in Fig. 10. The details for the additional stars are given in Table 14. This produces a total sample of 27 Fe-poor C-stars and three EMP C-enhanced dwarfs.

The dashed horizontal line in the upper panel of Fig. 7 indicates a constant C/H ratio of 20% of the solar value independent of [Fe/H]. This constant ϵ(C), which we denote as ϵ_0(C), is a reasonable fit to all the available data, given the uncertainties. The inferred ϵ(C) reach a maximum value of $\sim$1/3 Solar, consistent with ϵ_0(C). Fig. 7 shows that EMP C-stars, even though they are of very low [Fe/H], can, by whatever processes are relevant, achieve C-enrichment up to near the Solar abundance, but not beyond it. This is also true of the two known ultra-metal-poor stars (Christlieb *et al.* 2004; Frebel *et al.* 2005). Marsteller *et al.* (2004) also have reached similar conclusions using the HK Survey sample.

The most metal-poor star shown in this figure is G77–61, with [Fe/H] about -4.0 dex.

This star is a M dwarf in a binary system. Since the star is so cool compared to the C-stars studied here, it has a much more complex spectrum with very strong molecular features. As part of a recent study by Plez & Cohen (2005) a search was made for a detectable feature of O in the optical spectrum of this star. However, given the very strong molecular bands in this M dwarf, none could be found even in high precision Keck/HIRES spectra covering the full optical spectral regime from 0.4 to 1.0μ. Thus in the abundance analysis for G77–61 carried out by Plez & Cohen (2005), it was assumed that O was enhanced by +0.3 dex (i.e. [O/Fe] = +0.3 dex). The resulting enhancement of C was found to be [C/Fe] +2.6 dex. A recently obtained Keck high resolution near IR spectrum yielded a detection of CO, and hence enabled determination of the O abundance. Plez, Cohen & Melendez (2006) found an unexpectedly high O-enhancement, [O/Fe] about +2.2 dex, much higher than the previously assumed value. With the original value for ϵ(C), this star would not be an extreme C-star, which its spectrum clearly demonstrates that it is. The new higher O abundance thus in turn led to a revised [C/Fe] value of +3.2 dex. The values plotted in the figures for this star (which is included in the additional sample from the literature) are these updated values.

In this context it is important to note that we also in general lack a determination of the O abundance for the C-stars in our sample (although clearly near IR spectra of the CO bands would yield such), and have assumed [O/Fe] to be the maximum of +0.5 dex or ([C/Fe] – 0.8 dex) in calculating the molecular equilibria for all the C-stars analyzed here. Only one star in our sample has a measured O abundance; HE1410−0004 has [C/Fe] +2.0 dex, [O/Fe] + 1.2 dex, and C/O = 5. This O abundance is in accord with the assumption we have chosen to make regarding [O/Fe] when no O abundance in available. If the O abundance in this star is in fact even lower, which it might be given the marginal detection of the strongest line of the 7770 Å IR triplet, the molecular equilibrium for CH and for C_2 would not change significantly. We expect the largest change in the deduced C abundance (i.e. the largest shift in the molecular equilibrium of CH and C_2) for C-stars as the O abundance is increased from that of C-normal stars to occur when ϵ(O) is only slightly less than ϵ(C). (Recall that ϵ(O) must be less than ϵ(C) since these are C-stars.) For changes in ϵ(O) from the nominal value for HE1410−0004 given in Table 10 not exceeding a factor of 4, the change in ϵ(C) deduced from the CH band in this star is modest, less than ±0.15 dex.

The interpretation of the CH band strengths as a measure of the C abundance in the sample C-stars is straightforward, ignoring the issue of the linkage to the assumed O abundance discussed above. With regard to C_2, we look again at the upper panel of Fig. 5 (a plot of the absorption at several bandheads of C_2 versus $T_{\rm eff}$). Although C_2 band strengths were not used to determine the C abundance, spectral synthesis in the region of the 5160 Å bandhead with the fixed CNO abundances log[ϵ(C,N,O)] 7.56, 6.55, and 7.13 dex (a C/O ratio of 2.7) (for the value of f_{00}, the band oscillator strength, adopted by Querci and col-

laborators) were used to predict the depth of absorption at the 5160 Å band head. The $T_{\rm eff}$, $\log(g)$ pairs were chosen to follow the isochrone for an age of 12 Gyr with [Fe/H] −2.5 dex. The result is shown as the solid curve in the upper panel the figure, and clearly indicates that increasing absorption at the C_2 bandhead as $T_{\rm eff}$ decreases is due to the shift in the molecular equilibrium with $T_{\rm eff}$. Additional curves in this figure are shown for a C/O ratio of 1.0 and of 1/2.7, keeping ϵ(O) fixed, as would occur in a star to which C-rich material is added. The rapid decline in the strength of absorption at the C_2 bandhead is obvious and is due largely to the dependence of $\epsilon(C_2)$ on $\epsilon(CI)^2$. Our ability to match the observed strength of the C_2 bandhead in our sample of C-stars shown in Fig. 5 by varying only $T_{\rm eff}$ is consistent with the key result from analysis of the G band of CH that an approximately constant ϵ(C) is a satisfactory fit to the existing data on highly C-enhanced stars.

There are no stars in the upper right area of Fig. 5. This is, in terms of C_2 band detectability, an allowed area. Thus sufficiently strong bands of C_2, equivalent to sufficiently large C-enhancements, do not exist in real stars with $T_{\rm eff}$ ∼6200 K with their higher continuum flux. The required very large C-enhancements in such hot stars must substantially exceed the constant ϵ_0(C) deduced from the CH analysis. The maximum C_2 band strength, presumably that corresponding to ϵ_0(C), is very weak among the hotter stars in our sample (the main sequence turnoff region stars), and so stars with lower C-enhancements will simply have no detectable C_2. One might wonder why no stars appear in the lower left corner of this plot, where weaker C_2 features could easily be detected. This appears to be a consequence of the fact that a C-star must have $\epsilon(C) > \epsilon(O)$, otherwise oxides will dominate the molecular equilibrium. At the solar composition, $\epsilon(C)/\epsilon(O)$ is about 1/2. Normal-C EMP unevolved and hence unmixed stars (i.e. low luminosity giants or dwarfs) have [O/Fe] about +0.7 dex, while they have [C/Fe] about +0.4 dex (see, e.g. for the giants Spite *et al.* 2005). A C-enhancement of a factor of four for a normal-C unmixed EMP star will lead to $\epsilon(C) = \epsilon(O)$, and that required to produce a C-star must be slightly higher. The C_2 becomes stronger as the C-enhancement increases above the minimum required to produce a C-star. We suggest that the duration of this phase of C-enhancement is short compared to the age of the EMP C-star, and that this phase did not in general occur recently as compared to the timescale for mixing, making this region of Fig. 5 unpopulated.

Among more highly evolved EMP and VMP C-stars, we would expect to see some evidence for depletion of C at the stellar surface as a result of mixing and dredge up, which will depend on the mass included in the mixing region. We use $T_{\rm eff}$ as a surrogate for evolutionary stage, as the star cools as it moves up the RGB; the M dwarf and EMP star G77–61 is plotted as though its $T_{\rm eff}$ were 6000 K to place it at the proper position corresponding to its evolutionary state in this figure. Fig. 8 displays $\log[\epsilon(C)]$ as a function of $T_{\rm eff}$; the 11 additional Fe-poor C-stars from the literature are included. There is a suggestion in

this figure of decreasing ϵ(C) as $T_{\rm eff}$ decreases, i.e. as the star moves up the giant branch, reminiscent of mixing and dredge up phenomena studied among EMP giants by Spite *et al.* (2005) and among globular cluster giants by Cohen, Briley & Stetson (2005). The slope of a linear fit to the data in this figure is statistically different from 0.0 at more than the 3σ level. The existence of such a correlation, should further work demonstrate conclusively that it is real, would again suggest that the C-enhancement could not have occurred recently; sufficient time for C-depletion and mixing in the giant EMP C-stars is required.

It is interesting to note that the highest value of ^{12}C/^{13}C we measured was obtained using the G band of CH for the hottest and least luminous (and presumably least evolved) of the C-stars with a high signal-to-noise ratio HIRES spectrum. Ryan *et al.* (2006) compiled ^{12}C/^{13}C ratios for Fe-poor C-rich stars from the literature. Their compilation also supports the suggestion that there is a general trend of declining ^{12}C/^{13}C with increasing luminosity. This trend, which needs further confirmation, together with the generally low ^{12}C/^{13}C ratios, is reproduced by the models of Boothroyd & Sackmann (1999) as a consequence of deep mixing and "cool bottom processing" after the first and second dredge up in low mass red giants. They establish that the latter increases dramatically as [Fe/H] decreases. Additional determinations of ^{12}C/^{13}C for EMP C-stars from the C_2 bandhead at 4740 Å will be straightforward, and are now underway.

5.2. Abundance Ratios for Other Elements

Table 15 gives statistics for selected abundance ratios for the sample of 16 C-stars from the HES analyzed here. Upper limits are ignored. Only the sample of 16 C-stars analyzed here is used to compute the statistical measures given in Table 15. The mean abundance ratios for various elements are compared with those obtained by Cohen *et al.* (2004) for a large sample of EMP dwarfs, and in some cases to those from the First Stars project at the VLT for EMP giants (Cayrel *et al.* 2004; Spite *et al.* 2005).

The median [C/Fe] is +1.9 dex, with a small dispersion (0.3 dex) about the mean. The lower limit of ϵ(C) is defined by the requirement that the star be a C-star to be included in the present sample, but the upper bound is not constrained; it is determined by the stellar characteristics themselves. N is also highly enhanced, with a median [N/Fe] of +1.7 dex, only slightly below the median C-enhancement. The scatter is perhaps slightly larger than that seen for ϵ(C) in Fig. 8. The lower panel of Fig. 7 shows [C/N] as a function of [Fe/H]. The mean is somewhat higher than the Solar value, but there is no obvious trend of C/N with [Fe/H]. Among the giants, there is a suggestion that ϵ(N) increases and [C/N] decreases as $T_{\rm eff}$ decreases and luminosity along the giant branch increases, but the scatter is large and

this may not be statistically significant.

We include in our analysis two of the Mg triplet lines, which lie in a region free of molecular features. Hence the Mg abundance should be reliable[8]. The median abundance ratio [Mg/Fe] of our C-star sample agrees well with that of the EMP dwarfs from Cohen *et al.* (2004), but the range of derived [Mg/Fe] is quite large (a factor of 10). The highest value, [Mg/Fe] = +1.04 dex (for HE0336+0113), is comparable to that of the small number of other extremely Mg enhanced C-rich stars known, i.e. CS 29498–043 discussed by Aoki *et al.* (2002b) and BS 14934–002 (Aoki *et al.* 2005). The lowest value of [Mg/Fe] among the C-stars in our sample (+0.04 dex, for HE0212–0557) is comparable to the lowest seen among VMP and EMP stars (see, e.g. the compilation in Fig.5 of Aoki *et al.* 2005). [Mg/Fe] almost certainly shows a real range from star-to-star among EMP stars.

The abundance of Ti should be well determined as there are many strong Ti II lines in the spectra of these C-stars, some of which lie in regions completely free of molecular contamination. Cr benefits from the strong line at 5206 Å, again a region unaffected by molecular features. It is thus gratifying that the [Ti/Fe] and [Cr/Fe] abundance ratios among the C-stars from the HES show relatively small dispersion, with mean values in good agreement with the results for EMP dwarfs from Cohen *et al.* (2004). The remaining elements up to the Fe-peak suffer from a paucity of unblended lines with strengths sufficiently large for a reliable abundance analysis.

We find that 12 of our C-stars show an enhancement of Ba (see Fig. 9) and other *s*-process neutron capture heavy elements approximately equal to that of C. The other four show [Ba/C] ≤ -1.6 dex, i.e. a strong C enhancement, with normal heavy elements, as contrasted to enhancement of both C and the *s*-process elements in the majority of the C-stars. In the full sample of 27 C-stars and three C-enhanced dwarfs, 6 stars do not show a strong Ba enhancement, while $\sim$85% of the full sample do show a strong Ba-enhancement. Fig. 10 shows the [Ba/C] ratio for our sample of HES EMP stars. There is a strong suggestion that the stars with low [Ba/C] ratios are the most Fe-metal-poor of the sample. The bifurcation into *s*-normal and highly C-enhanced stars is not an artifact of relying on the Fe-abundances, which are decoupled from the C-abundances.

We can examine whether the process that produces highly enhanced C in these C-stars also leads to abnormalities in the abundances of other elements beyond those established above, i.e. CNO and the heavy elements beyond the Fe-peak. We define $\Delta(X)$ as the difference between the median [X/Fe] in our C-star sample with HIRES abundance analyses

[8]There is a minor caveat regarding the issue of internal consistency of the gf values between the various Mg lines discussed in Cohen *et al.* (2004), but this is a small effect, $\sim$0.2 dex at most.

and that found for C-normal EMP dwarfs and giants. From the values given in Table 15, for elements from Na to Fe we find only two with $\mid \Delta(X) \mid \; > \; 0.25$ dex. These are Al (Δ(Al) = +0.36 dex) and Mn (Δ(Mn) = +0.38 dex). There is only one reliable line for Al I (at 3961 Å) and only two for Mn I (two of the three lines of the 4030 Å triplet, ignoring a few very weak lines of Mn which are only rarely detected in the HIRES spectra of these C-stars) and each of these is located in regions of strong CH absorption. It is likely that there is still some contamination of the atomic features by molecular ones that we were not successful in removing. With this caveat, we thus conclude that the C-star phenomenon in EMP stars is confined to the elements CNO and to the elements heavier than the Fe-peak. The abundance ratios [X/Fe] of elements from Na to Fe for which we can detect suitable lines are normal.

5.3. Evidence that *s*-process Neutron Capture Dominates Among the EMP C-stars

We discuss here the evidence that enhancement of the neutron capture elements seen in EMP C-stars arises from the *s*-process, with no substantial/detectable contribution from the *r*-process. When we look at the elements beyond the Fe-peak, we notice that the median and the mean [Eu/Ba] (both about −0.8 dex) closely correspond to that characteristic of the main component of the solar *s*-process given by Arlandini *et al.* (1999). The detection of large amounts of lead is another clue that the *s*-process is responsible. The median value of [Pb/Ba] (+0.79 dex, with σ about the mean of 0.34 dex) is close to that of other *s*-process dominated stars: Sivarani *et al.* (2004) has compiled all the data for Pb in such stars available to date (their Table 5 and Figure 11).

Additional abundance ratios give clues to the detailed behavior of the *s*-process. For example, we find a smaller range in [Y/Fe] and in [Sr/Fe] than in [Ba/Fe], which shows a range of a factor of 1000; this is consistent with metal-poor *s*-processing in AGB stars. Busso, Gallino & Wasserburg (1999), for example, predict the *s*-process enhancement will be relatively larger for the second peak elements than for the lighter *s*-process nuclei in stars with lower Fe-metallicity. A recent extensive theoretical discussion of the nucleosynthesis of Sr, Y and Zr was given by Travaglio *et al.* (2004).

Ignoring the upper limits, σ[Y/Sr] and σ[La/Ba] are small (0.32 and 0.26 dex respectively), confirming previous work suggesting that within each of the peaks, the *s*-process element ratios for the Ba-rich EMP C-stars are approximately constant for elements within that particular peak, while the variation from star-to-star of the ratio of the strength of the various peaks is much larger. Aoki *et al.* (2005) also present relevant data for a sample of

18 very metal-poor stars supporting this.

5.4. The Ba-poor C-stars

Fig. 10 shows [Ba/C] as a function of Fe-metallicity for this sample of C and C-enhanced stars. Just as was seen in Fig. 9, 12 of the C-stars from the HES that we have analyzed show an enhancement of Ba (and of the other *s*-process neutron capture heavy elements) approximately equal to that of C. The other four show [Ba/C] ≤ -1.2 dex, i.e. a strong C enhancement, with more normal heavy elements. Including 10 additional C-stars compiled from the literature, 25 of the 30 stars in the full sample of EMP/VMP C-rich stars (83%) show highly enhanced Ba, while 1/6 have [Ba/C] ≤ -1.2 dex. It is clear from the evidence described above that the *s*-process is responsible for the enhancement of the heavy neutron-capture elements in these C-stars, when they are highly enhanced. We note the Ba-poor C-stars that are cooler than $T_{\rm eff}$ = 5700 K have the same low ^{12}C/^{13}C ratios as do the Ba-rich C-stars.

We first consider whether the Ba in the Ba-poor stars is from the *s* or the *r*-process. One might argue for the former, claiming that Ba is in fact enhanced even in the Ba-poor stars. The influence of the very low Fe-metallicity on the heavy neutron capture rates might give rise to a very low *s*-process production, with the *r*-process making no or an even lower contribution. However, Fig. 9 shows that [Ba/Fe] in the Ba-poor stars is consistent with that observed among the C-normal stars from the HES that we have analyzed to date. We know that the Ba in C-normal EMP stars must be largely produced in the *r*-process based on their [Ba/Eu] and [La/Eu] ratios (e.g. McWilliam et al. 1995b, McWilliam 1997, 1998a, Simmerer 2004). Thus we infer that the Ba in the Ba-poor EMP C-stars has its origin in the *r*-process as well.

At first sight, the existence of two more or less distinct classes of EMP C-stars suggests that two distinct processes are required to produce the C-stars which are Ba-enhanced and those that are not Ba-rich. Nucleosynthesis within an intermediate mass AGB star can reproduce the first set of characteristics. If the mass of the EMP C-stars is assumed to be the turnoff mass of the halo with an age of $\sim$12 Gyr, near 0.8 $M_{\odot}$, they are not massive enough to produce s-process elements at any time (e.g. see the review by Busso et al. 2004). Also, their $T_{\rm eff}$ are too warm and the luminosities are too low for our C-stars to be AGB stars. Thus intrinsic nucleosynthesis production and transport to the stellar surface of large amounts of C is not possible for such unevolved stars.

We suppose instead that the EMP C-stars are the former secondaries of binary systems

across which mass transfer has occurred. This is the mechanism originally suggested for the CH stars by McClure (1985), which also have enhanced C and Ba and low Fe-metallicities (e.g. Wallerstein & Greenstein 1964; Vanture 1992), although with ϵ(Fe) still a factor of 50 to 100 times higher than the EMP C-stars discussed here, so the apparent enhancements are not as large in the CH stars. McClure (1984) (see also McClure & Woodsworth 1990) established that essentially all CH stars are members of binary systems. The higher metallicity Ba stars appear to be another example of the same phenomenon (McClure & Woodsworth 1990); Bohm-Vitense *et al.* (2000) have established from UV HST spectra the presence of white dwarf companions for several of these stars.

What about the 1/6 of the C-rich stars without heavy element enhancements? We suggest that there is no need to resort to intrinsic production or any other additional mechanism; in our view, essentially *all* of these stars could be produced by mass transfer and other phenomena in binary systems. There are several possibilities for explaining these stars within the context of our hypothesis that all EMP C-stars are or were binaries. We can ascribe the differing enhancement of the *s*-process elements from C-star to C-star within our sample to some dependence in the nucleosynthetic yields involving, for example, the initial [Fe/H] or mass of the original primary star. At the lowest metallicities, Busso, Gallino & Wasserburg (1999) (see especially their Fig. 12) predict that when n(Fe seed) becomes very small, there are so many neutrons available for each seed nucleus that the *s*-process runs to completion, with lead the main product, and very little Ba enhancement. Lead is the third *s*-process peak, and ϵ(Pb) is considerably higher in the Sun than that of its neighbors in the periodic table. Any heavier elements produced, which are all unstable except for Bi at atomic number 83, decay to lead. Although the prediction of Busso, Gallino & Wasserburg (1999) for the Fe-metallicity at which the peak Ba *s*-process production occurs in AGB stars may be slightly too high, their Fig. 12 shows a drop of more than a factor of 100 for the predicted [Ba/Fe] enhancement as [Fe/H] drops 1 dex lower than that at which maximum Ba production occurs.

We attempt to estimate the expected Pb abundance for a EMP C-star assuming the *s*-process runs to completion to see if it is detectable. The highest [Ba/Fe] seen among the C-stars in our sample (see Table 15) has ϵ(Ba) approximately at the solar value for a C-star with [Fe/H] -2.3 dex. We make the reasonable assumption that *s*-process production is proportional to the number of Fe seed nuclei, and assume that all the *s*- process elements in the Sun, from Ba to Pb, end up as lead. But all the intervening elements have very low *s*-process abundances, see, e.g., the *s*-process solar abundances for the heavy elements tabulated by Burris *et al.* (2000). Thus for a [Fe/H] -3.5 dex star, we predict ϵ(Pb) to be $+1.5$ dex. This Pb abundance, which is roughly 2.5 times the solar Pb abundance, is a very high Pb abundance for such a low Fe-metallicity star. However, it is, as discussed in §4.4,

extremely difficult to detect in a highly C-enhanced (recall that ϵ_0(C) $\sim$1/5 solar) star with strong molecular bands given that the strongest Pb I line at optical wavelengths is weak and located in a thicket of CH features. Thus verification of this idea through an abundance determination extending to the third *s*-process peak will be very difficult in practice. We do, however, expect in this case that the Ba-poor EMP C-stars to be predominantly those of the lowest Fe-metallicity, which does appear to be the case in our sample (see Figures 9 and 10), in the somewhat smaller sample of Ryan *et al.* (2006), as well as in that of W. Aoki (private communication).

Another possible explanation for the absence of *s*-process enhancements in some of our EMP C-stars is that the neutron flux is strongly reduced in the AGB star, either due to low temperatures in the intershell region, or because the ^{13}C pocket fails to be injected into the intershell region of the AGB star, thus restricting the the ^{13}C(α,n)^{16}O reaction. This *n*-producing reaction competes with the reaction ^{13}C(p, γ)^{14}N. At lower T, the latter may dominate, which would reduce the production of neutrons available to create *s*-process elements. The circumstances which might lead to lower T are not clear, perhaps lower Fe-metallicity is in some way the dominant factor. In the absence of the neutron flux the *s*-process can not operate with vigor, thus producing the Ba-poor stars.

We view the trend for the Ba-poor C-stars to be among the most Fe-poor as a fundamental clue to the mechanism(s) involved in producing the Ba-poor C-stars. Any differences in the luminosity distribution of the two groups of C-stars might provide other useful clues for identifying the mechanisms involved. Fig. 11 shows a $T_{\rm eff}$, log(g) diagram for our sample of C-rich stars. Also shown there is the entire sample of EMP candidates from the HES for which we have carried out detailed abundance analyses to date. Our sample is selected from the HES and stars are chosen for HIRES observations and subsequent abundance analyses solely on the basis of apparent low [Fe/H][9]. Thus the distribution of stars, both C-rich and C-normal, along the locus they follow in the HR-diagram must represent some folding of the volume surveyed by the HES given the luminosity at each evolutionary stage, the IMF for EMP stars, and perhaps selection biases within the HES. The additional C-stars from the literature are not shown in this figure as they come from various sources and the selection criteria imposed for high resolution studies is not clear.

Fig. 11 suggests that the C-stars of both types are concentrated towards high luminosities, and are relatively rare among the turnoff region stars. We ascribe this to a selection

[9]It must be admitted that all the HIRES spectra of C-stars in hand as of Aug. 2005 have been analyzed, but not all the spectra of C-normal stars in hand have been analyzed yet. This bias only affects the relative ratio of C-rich to C-normal stars in Fig. 11, but not their distribution along the locus.

effect, as the G band of CH becomes weaker and harder to detect for such hot stars, even if the C-enhancement is very large. The C_2 bands become even weaker under such circumstances. Such hot stars can only be picked out as highly C-enhanced from a high resolution study. Fig. 5 demonstrates the weakness of the C_2 band in the hot turnoff stars. Low SNR moderate resolution spectra are inadequate to securely detect such weak bands. This is the case for the Ba-poor but C-rich star HE0007–1832 from our sample (this and the other Ba-poor C-rich stars are marked in the figure, as are the known binaries) which is a dwarf C-star whose analysis was published in Cohen *et al.* (2004). The somewhat hotter main sequence turnoff at a fixed age for lower metallicity stars ($T_{\rm eff}$ at the turnoff becomes hotter by 150 K when the Fe-metallicity decreases from −2.2 to −3.2 dex) makes the CH and C_2 bands in the lowest metallicity stars near the main sequence turnoff even weaker and harder to detect.

Ryan *et al.* (2006), in a very recent paper discussing the origin of the two classes of C-enhanced metal-poor stars described above, postulate two distinct mechanisms, with mass transfer in an AGB phase of a binary system giving rise to the Ba-rich and C-rich stars, while the Ba-poor, C-rich stars are assigned a completely different origin. However, the discussion given above indicates that there are several plausible scenarios for producing the Ba-poor EMP C-stars within the framework of the binary hypothesis adopted here. We do not find any reason at present to exclude them from also being formed via phenomena involving binary systems.

The path to resolve the origin of the Ba-poor EMP C-stars, which is in our view the only remaining area of considerable uncertainty in our scenario, is difficult. It requires assembling a larger sample of such stars, searching with exquisite high resolution spectra for the presence of Pb, and extensive radial velocity monitoring of these stars.

5.5. Comparison with Disk C-Stars

A comparison of the properties of the EMP C-stars with those having Fe-metallicity near solar is of interest. Wallerstein & Knapp (1998) present a review of the luminosities and abundances of the latter. Intrinsic C-stars stars which produce C internally, then dredge it up to the stellar surface, are AGB stars with luminosities much higher than those of the EMP C-stars in our sample. Lambert *et al.* (1986) have analyzed such luminous cool disk C-stars; their $T_{\rm eff}$ is considerably lower than the stars studied here. Their sample has [Fe/H] ~ -0.3 dex, and shows only modest C-enhancements (less than a factor of 2, far smaller than the factor of ∼100 seen in our sample), with no enhancement of N, and with $^{12}C/^{13}C$ typically large, 30 to 70. The $^{12}C/^{13}C$ in these intrinsic C-stars suggests the addition of

pure ^{12}C from He burning, with quite different abundance ratios among the CNO elements and also quite different ^{12}C/^{13}C ratios than those seen among much more Fe-poor C-stars studied here. The difference between the C/N ratios may arise if the former primary of the binary EMP C-stars in our sample had, in the mean, a different stellar mass when it was on the AGB than is typical of disk solar Fe-metallicity AGB stars, so as to produce different abundance ratios. Higher mass AGB stars produce higher C/N ratios. The predictions from the models of Boothroyd & Sackmann (1999) are also relevant here, in that a dependence of the nuclear reaction rates and hence the internal production ratios on [Fe/H] might also contribute to these differences.

It is now possible to investigate the abundances of C and N for luminous AGB C-stars in the LMC and the SMC. Preliminary results by Marigo *et al.* (2003), Matsuura *et al.* (2005) and Van Loon *et al.* (2005) suggest that the differences in abundance ratios between these more Fe-poor luminous AGB stars and Galactic disk intrinsic C-stars are small. There is, however, a well known decrease in mean luminosity and increase in the C-star to late M giant ratio as [Fe/H] decreases from the Galaxy to the LMC and then to the SMC, first discussed by Blanco, McCarthy & Blanco (1980). This presumably arises as a smaller amount of C (of intrinsic origin; these are luminous AGB stars) needs to be added to a very metal-poor star with a fixed [O/Fe] ratio to reach ϵ(C) = ϵ(O) and so produce a C-star as [Fe/H] decreases.

The early R-stars (a type of C-star) are much closer in some of their properties to the Ba-poor EMP C-stars found in the HES that are studied here. Dominy (1984) and Dominy (1985) studied their chemical compositions and evolutionary state. (See also the review of Wallerstein & Knapp 1998.) The R-stars are of lower luminosity than the intrinsic AGB C-stars, with $M_{bol} \sim -0.3$ mag, $L/L_{\odot} \sim 100$, and, with $T_{\rm eff} \sim 4600$ K, are warmer than AGB C-stars. Their space density is too high for them to be stars in the He shell burning phase of evolution (Scalo & Miller 1979). They have [Fe/H] $\sim$ solar, with moderate C enhancements ($\sim +0.7$ dex), and somewhat smaller N enhancements, but have ϵ(O) at the solar value. They, like the EMP C-stars, have low ^{12}C/^{13}C ratios. The R-stars do not in general show enhancements of the *s*-process elements. McClure (1997) has demonstrated, via extensive radial velocity monitoring, that they do not appear to be binaries; he suggested that they are coalesced binaries.

Among the various families of high Fe-metallicity C-stars, there appears to be a correlation that the stars with highest ^{12}C/^{13}C are those which have strong *s*-process enhancements, while those with the lowest ^{12}C/^{13}C have little or no enhancement of the elements past the Fe-peak. This correlation may be due to the variation with T in the rate of the reaction ^{13}C$(\alpha, n)^{16}$O, which provides the neutrons required for the *s*-process to occur, as compared to that of the reaction ^{13}C$(p, \gamma)^{14}$N, which suppresses the production of neutrons from ^{13}C

burning, or perhaps to some property of the ^{13}C pocket.

6. Implications of the Mass Transfer Scenario for EMP C-stars

We explore here the consequences of our assumption that mass transfer in binary systems produces all C-stars at all [Fe/H] whose luminosities are so low that they cannot be intrinsic C-stars. The stars being discussed here are very metal poor, so that by adding a small amount of processed material through binary mass transfer, a large change in surface abundances of the secondary star can be produced, which will lead to much more obvious changes in the star's spectral characteristics than would occur at solar metallicity. Furthermore the efficiency of the complex process of binary mass transfer depends on the mass of the primary star, which affects the mass loss rate, being higher for higher AGB luminosities, i.e. higher mass of primary, within certain limits. $\mathrm{d}M/\mathrm{dt}$ may also depend on the metallicity if the mass loss is driven by radiation pressure on dust grains. For a given $\mathrm{d}M/\mathrm{dt}$ of the AGB star, the accretion rate onto the secondary is a function of the binary separation and other orbital properties. The net result may be a highly variable efficiency for fixed initial [Fe/H] and the initial masses of the two components of the binary system.

A key result presented above is the approximately constant C/H ratio, $\epsilon(\mathrm{C}) = \epsilon_0(\mathrm{C})$, in the photospheres of the C-stars in our sample, which we derive from our analysis of their CH and C_2 bands. This is presumably a consequence of the primary nature of C production in AGB stars. We assume this constant level extends to higher Fe-metallicity, although a slight upward trend as [Fe/H] increases cannot be ruled out at this point (see Fig. 7). We consider adding this constant $\epsilon_0(\mathrm{C})$ to stars of both higher and lower Fe-metallicity than those studied here. As [Fe/H] rises, the impact of adding additional C (accompanied by additional H as well) is diluted. If we assume that C-normal EMP stars have [C/Fe] +0.3 dex and [O/Fe] +0.7 dex and that the stellar photosphere of the star we currently observe consists of equal amounts of its initial material and of material accreted from its AGB companion, then at [Fe/H] ~ -1.4 dex, the star, with its additional C, will just achieve $\epsilon(\mathrm{C}) = \epsilon(\mathrm{O})$ with the additional C-rich material. This falls to -2.0 dex if the final photosphere contains 20% accreted material. More Fe-rich C-normal stars cannot become C-stars through the mass transfer process with our assumptions unless the accreted material comprises more than 50% of the stellar photosphere.

In this scenario we thus expect for higher Fe-metallicities to see stars which are C-rich, but without C_2 bands. These presumably correspond to the CH stars. They occur in the right Fe-metallicity range, and essentially all of them were shown by McClure (1984) (see also McClure & Woodsworth 1990) to be binaries. The frequency of C-stars in the HES as

a function of [Fe/H] to be given in Cohen *et al.* (2006c) provides further support for this hypothesis. At still higher Fe-metallicities, the C-enhancement becomes too small to be noticeable. However, *s*-process production is to first order a secondary process proportional to the number of Fe seed nuclei (i.e. to [Fe/H]). Thus *s*-enhancement (i.e. the high levels of [*s*/Fe]) will still be present at high Fe-metallicity, although the details of the nucleosynthesis may shift the relative production of the *s*-process nuclei towards the first peak at Sr (see, e.g. Busso *et al.* 1999). Such stars presumably correspond to the Ba stars, which are of higher Fe-metallicity than the CH stars. According to McClure & Woodsworth (1990) (see also Luck & Bond 1991), the Ba stars are another example of the same phenomenon of mass-transfer in binary systems.

The situation at lower Fe-metallicities was explored in §5.4. We expect, as described earlier, the *s*-process to run through to lead, which will be extremely difficult to detect, with very low production of the more easily detected *s*-process elements such as Sr, Ba, La, etc.

The low $^{12}C/^{13}C$ ratios seen in these EMP C-stars, both Ba-enhanced and Ba-poor, provides another important clue. They, combined with the high C/N ratios, suggest that a two phase process is required. First, mass transfer across the binary system from a low Fe-metallicity AGB star with intrinsic production of C (and hence a high $^{12}C/^{13}C$ ratio) occurs. This is then followed by a phase of mixing combined with "cold bottom burning" as described by Boothroyd & Sackmann (1999) to produce the observed C/N and $^{12}C/^{13}C$ ratios. (See Carretta, Gratton, Sneden & Bragaglia 2000, for a description of the consequences of this mixing process in more metal-rich C-normal field stars.) Since the degree of C-depletion appears to depend on the luminosity of the C-star we observe today, that part of the processing cannot have occurred in the donor star of the binary.

6.1. Binarity

We have suggested that all EMP C-stars (i.e. those with $-4 \lesssim$ [Fe/H] $\lesssim -2$ dex) are the original secondary stars of binary systems in which mass transfer occurred. We have further suggested that this mass transfer from an AGB primary can produce the abundance anomalies we see among the EMP C-stars, specifically the high enhancement of *s*-process elements among ∼85% of these C-stars. Those VMP/EMP C-stars with low or no *s*-process enhancement are cases where some factor, most likely the low Fe-metallicity of the primary, while still producing, mixing to its surface, and transferring to the secondary star ample amounts of carbon, did not achieve such for the easily detectable heavy neutron-capture element Ba.

We consider here whether the statistics of binary detection among very metal-poor C-stars can support our hypothesis that all of these C-stars were once binaries. We expect most/all of them to still be binaries with (invisible) white dwarf companions. The HES C-stars of our sample are themselves not suitable for this purpose. They were only recently discovered to be interesting stars, and most have only been observed for a single epoch. They are in general faint for high dispersion spectroscopic analysis. There were no radial velocity monitoring programs for such stars until very recently. Even so, we have already found three confirmed binaries in our samples of candidate EMP stars from the HES.

So we look instead at the sample of additional C-stars from the literature. These stars are in general brighter than the HES C-stars in our sample, and they have been known as interesting objects for timescales of several years to a decade, giving more opportunity for radial velocity monitoring. Table 14 indicates which of these are known binaries and gives their periods and v_r amplitudes. Four of these 11 C-stars are confirmed binaries, consistent with the very preliminary results of the v_r monitoring program of Tsangarides, Ryan & Beers (2004) for *s*-process enhanced C-stars.

Although the sample is small, considering the lack of suitable long-term radial velocity monitoring programs, the length of the typical period, the small velocity amplitudes, the faintness of the stars, and the relatively short time they have been known to be interesting, we find our detection rate for binaries among very metal-poor and EMP C-stars to be consistent with all such stars being binaries; Monte Carlo simulations by Lucatello *et al.* (2004) support this. There is as yet insufficient v_r monitoring data for the small fraction of C-enhanced stars without *s*-process enhancement to assess their binarity.

7. Summary

We have studied a sample of 16 C-stars from the EMP candidate lists of the HES using high dispersion spectra from HIRES at Keck and new optical photometry. We have carried out a detailed abundance analysis using a $T_{\rm eff}$ scale based on V–I, V–J and V–K colors, while avoiding the effects of the molecular bands as much as possible. Earlier $T_{\rm eff}$ scale problems affecting the Fe-metallicity deduced for EMP stars as hot as 6000 K by the HES (and, until recently, the HK Survey) were solved by changing from B−V to Hδ as a $T_{\rm eff}$ indicator. Our results provide a broad database to establish the Fe-metallicity for EMP C-stars. We find that the Fe-metallicities for the cooler C-stars ($T_{\rm eff}$ ∼5100 K) are still being underestimated by a factor of ∼10 by the current standard HES (and until very recently HK) survey tools. This is due to strong molecular absorption primarily in the red continuum bandpass of the HP2 index which measures the strength of Hδ and acts as an indicator of $T_{\rm eff}$. The results

presented here provided crucial supporting data used by Cohen *et al.* (2006a) to derive the frequency of C-stars among EMP stars.

Carbon abundances in these very metal-poor stars appear to be constant, independent of Fe-metallicity, at about 1/5 the solar value. The C-abundances show marginal evidence of decreasing with decreasing $T_{\rm eff}$ or increasing luminosity, presumably due to mixing and dredge-up of C-depleted material. Such C-depletion is seen among "normal" halo field giants over a wide range of metallicity for sufficiently evolved stars with luminosities brighter than that of the RGB bump, which is high on the red giant branch. N is also highly enhanced in the EMP C-stars. Among the elements studied here, abundance anomalies in these stars appear to be confined to CNO and to those heavier than the Fe-peak.

C-enhancement in this sample is associated with strong enhancement of *s*-process heavy nuclei for 12 of the 16 stars, with [C/Ba] about −0.1 dex with small scatter. The remaining four C-stars from the HES show no evidence for enhancement of the heavy elements, with Ba providing the strongest constraint, [Ba/Fe] $\leq +0.20$ dex for each of the four stars. When 11 additional C-stars, mostly from the HK Survey, with recently published detailed abundance analyses are added, the same separation is seen, with ∼85% of the stars having [C/Ba] almost Solar.

Very high enhancements of lead are detected in some of the C-stars with highly enhanced Ba. The ratio Ba/Eu, the high Pb abundances, and the high ratios of diagnostic elements in the second to the first *s*-process peak for C-stars in our sample demonstrate that the *s*-process is responsible for the enhancement of the heavy elements for most of the C-stars in our sample. The mostly low $^{12}C/^{13}C$ ratios inferred from both the G band of CH and the 4740 Å band of C_2, where the isotope ratio is particularly easy to measure, as well as the high N-enhancements suggest that the bulk of the stellar envelope of these stars has been processed through the CN cycle of proton burning. Our data for the Ba-rich C-stars supports the suggestion that the abundance ratios for elements within a given *s*-process peak are to first order constant, while the ratio of the strength of the various peaks shows larger star-to-star variations.

The similarities and differences of the properties of the EMP C-stars to those of various types of near solar [Fe/H] disk C-stars are discussed. In particular, the early R stars show low $^{12}C/^{13}C$ ratios and no excess of the heavy elements, reminiscent of the Ba-poor EMP C-stars found (at a low rate) in our sample.

The abundance ratios we derive are used to discuss the origin of the C-rich stars among EMP stars. We suggest that both the *s*-process rich and Ba-normal C-stars result from phenomena associated with binary stars. The Ba-rich EMP C-stars presumably formed as

secondaries in a mass transfer binary system with an AGB primary. This was followed by proton burning at moderate T to reduce $^{12}C/^{13}C$ and increase the C/N ratio. The implications of this hypothesis for stars of both higher and lower Fe-metallicity than those in the present sample are discussed. Several possible origins for the small minority of Ba-poor EMP C-stars are suggested. In the most metal-poor stars, Busso, Gallino & Wasserburg (1999) predict that the *s*-process runs to completion through the Ba-peak to the heaviest stable element, lead, leaving little or no apparent Ba-excess. Heavier elements (all unstable except Bi) mostly decay to lead as well. The predicted ϵ(Pb) in a [Fe/H] -3.5 dex star, while very high for a star with such a low Fe-metallicity, will be very difficult to detect. Another possibility for explaining the Ba-poor EMP C-stars is a possible lack of neutrons due to ^{13}C burning via $^{13}C(p,\gamma)^{14}N$ instead of via $^{13}C(\alpha,n)^{16}O$. The former dominates at lower T, while the latter provides the neutrons required for the *s*-process to occur. If either of these suggestions is correct, the Ba-poor C-stars should have lower Fe-metallicities in the mean than the Ba-rich C-stars, which does appear to be the case in our sample. The frequency of known binaries among the samples appears consistent with our hypothesis for the origin of EMP C-stars given the lack of long term radial velocity monitoring programs, the long periods, the low velocity amplitudes, and other characteristics of the stars.

We thus see no reason at present to exclude the scenario adopted here, that *all* the EMP C-stars are formed via phenomena involving binary systems. For old stars of low Fe-metallicity, several mechanisms described above may lead to C-stars with little or no *s*-process enhancement, such as is occasionally seen in our sample. For old stars in binary mass transfer systems of higher [Fe/H] than those considered here, a progression with increasing [Fe/H] from C-stars to CH stars and finally to Ba stars is predicted for a constant donor ϵ_0(C), which successfully reproduces several key observed characteristics of the behavior of C-rich stars in the Galaxy.

The entire Keck/HIRES user community owes a huge debt to Jerry Nelson, Gerry Smith, Steve Vogt, and many other people who have worked to make the Keck Telescope and HIRES a reality and to operate and maintain the Keck Observatory. We are grateful to the W. M. Keck Foundation for the vision to fund the construction of the W. M. Keck Observatory. We are grateful to W. Aoki for providing his HDS/Subaru spectra of selected C-stars to verify our ^{13}CH line list. We thank G. Wasserburg for helpful discussions and moral support. This publication makes use of data products from the Two Micron All Sky Survey, which is a joint project of the University of Massachusetts and the Infrared Processing and Analysis Center/California Institute of Technology, funded by the National Aeronautics and Space Administration and the National Science Foundation. JGC is grateful for partial support from NSF grant AST-0205951. She is grateful for funds from the Ernest Fullam Award of the

Dudley Observatory for help in initiating this work. N.C. and F.J.Z. acknowledge support from Deutsche Forschungsgemeinschaft through grant Re 353/44. N.C. is also supported by a Henri Chretien International Research Grant administered by the American Astronomical Society.

REFERENCES

Alonso, A., Arrivas, S. & Martinez-Roger, C., 1996, A&A, 313, 873

Alonso, A., Arrivas, S. & Martinez-Roger, C., 1996, A&AS, 140, 261

Amiot C., 1983, ApJS, 52, 329

Anders, E. & Grevesse, N., 1989, Geochim. Cosmochim. Acta, 53, 197

Aoki, W. *et al.*, 2001, ApJ, 561, 346

Aoki, W. Norris, J. E., Ryan, S. G., Beers, T. C. & Ando, H., 2002a, ApJ, 567, 1166

Aoki, W. Norris, J. E., Ryan, S. G., Beers, T. C. & Ando, H., 2002b, ApJ, 576, L141

Aoki, W., Ryan, S. G., Norris, J. E., Beers, T. C., Ando, H. & Tsangarides, S., 2002, ApJ, 580, 1149

Aoki, W., *et al.*, 2005, ApJ, 632, 611

Arlandini, C., Käppeler, F., Wisshak, K., Gallino, R., Lugaro, M., Busso, M. & Straniero, O., 1999, ApJ, 525, 886

Asplund, M., Nordlund, A., Trampedach, R., Prieto, C. A. & Stein, R. F., 2000, A&A, 359, 729

Asplund, M., Grevesse, N., Sauval, A. J., Allende Prieto, C. & Kiselman, D., 2004, A&A, 417, 751

Asplund, M., Grevesse, N., Sauval, A. J., Allende Prieto, C. & Bloome, R., 2005, A&A, 431, 693

Barbuy, B. *et al.*, 1997, A&A, 317, L63

Baumüller, D. G. & Gehren, T., 1997, A&A, 325, 108

Baumüller, D. G., Butler, K. & Gehren, T., 1998, A&A, 338, 637

Beers, T.C., Preston, G.W. & Shectman, S., 1985, AJ, 90, 2089

Beers, T.C., Preston, G.W. & Shectman, S., 1992, AJ, 103, 1987

Beers, T. C., Rossi, S., Norris, J. E., Ryan, S. & Shefler, T., 1999, AJ, 117, 981

Beers, T. C. & Christlieb, N., 2005, ARA&A, 43, 531

Bessell, M. S., Christlieb, N. & Gustafsson, B., 2004, ApJ, 612, L61

Blanco, V. M., McCarthy, M. F. & Blanco, B. M., 1980, ApJ, 242, 938

Bohm-Vitense, E., Carpenter, K., Robinson, R., Ake, T. & Brown, J., 2000, ApJ, 533, 969

Bonifacio, Molaro, Beers, T.C., Vladilo, 1998, A&A, 332, 672

Boothroyd, A. I. & Sackmann, I. J., 1999, ApJ, 510, 232

Burris, D. L., Pilachowski, C. A., Armandroff, T. E., Sneden, C., Cowan, J. J. & Roe, H., 2000, ApJ, 544, 302

Busso, M., Gallino, R. & Wasserburg, G.J., 1999, ARA&A, 37, 239

Busso, M., Straniero, O., Gallino, R. & Abis, C., 2004, in "Origin and Evolution of the Elements", eds. A.McWilliam & M.Rauch, Pasadena, (CUP), page 67

Carretta, E., Gratton, R. G., Sneden, C. & Bragaglia, A., 2000, A&A, 354, 169

Carretta, E., Gratton, R. G., Cohen, J. G., Beers, T. C., Christlieb, N., 2002, AJ, 124, 481

Cayrel, R. *et al.* 2004, A&A, 416, 1117

Christlieb, N., Green, P. J., Wisotzki, L. & Reimers, D., 2001, A&A, 375, 366

Christlieb, N., 2003, Rev. Mod. Astron. 16, 191

Christlieb, N., Gustafsson, B., Korn, A. J., Barklem, P. S., Beers, T. C., Bessell, M. S., Karlsson, T. & Mizuno-Wiedner, M., 2004, ApJ, 603, 708

Cohen, J. G., Christlieb, N., Beers, T. C., Gratton, R. G., Carretta, E., 2002, AJ, 124, 470

Cohen, J. G., Christlieb, N., Qian, Y. Z. & Wasserburg, J. G., 2003, ApJ, 588, 1082

Cohen, J. G., Christlieb, N., McWilliam, A., Shectman, S., Thompson, I., Wasserburg, G. J., Ivans, I., Dehn, Karlsson & Melendez, J., 2004, ApJ, 612, 1107

Cohen, J. G., Briley, M. M. & Stetson, P. B., 2005, AJ, 130, 1177

Cohen, J. G., *et al.*, 2006a, ApJ, 633, L109

Cohen, J. G., *et al.*, 2006b, in preparation

Cohen, J. G., *et al.*, 2006c, in preparation

Cutri, R. M. *et al.*, 2003, "Explanatory Supplement to the 2MASS All-Sky Data Release, http://www.ipac.caltech.edu/2mass/releases/allsky/doc/explsup.html

Dearborn, D.S.P., Liebert, J., Aaronson, M., Dahn, C. C., Harrington, R., Mould, J. & Greenstein, J. L., 1986, ApJ, 300, 314

Dominy, J. F., 1984, ApJS, 55, 27

Dominy, J. F., 1984, PASP, 97, 104

Frebel, A., *et al.*, 2005, Nature

Grevesse, N. & Sauval, A. J., 1998, Space Science Reviews, 85, 161

Hill, V. *et al.*, 2000, A&A, 353, 557

Hobbs, L. M., Thorburn, J. A. & Rebull, L. M., 1999, ApJ, 523, 797

Holweger, H., 2001, in *Solar and Galactic Composition*, ed R.F.Wimmer-Schweingruber, AIP Conf. Proceedings, (see Astro-ph/0107426)

Houdashelt, M. L., Bell, R. A. & Sweigart, A. V., 2000, AJ, 119, 1448

Johnson, J. J. & Bolte, M., 2002, ApJ, 579, L87

Johnson, J. J. & Bolte, M., 2004, ApJ, 605, 462

Keenan, P. C. & McNeil, R. C., 1976, *An Atlas of Spectra of the Cooler Stars: Types G, K, M, S and C*, The Ohio State University Press

Kisselman, D., 2001, New Astronomy Review, 45, 559

Kurucz, R. L., 1993, ATLAS9 Stellar Atmosphere Programs and 2 km/s Grid, (Kurucz CD-ROM No. 13)

Lambert, D. L., Gustaffson, B., Eriksson, H. & Hinkle, K. H., 1986, ApJS, 62, 373

Lawler, J. E., Bonvallet, G. & Sneden, C., 2001, ApJ, 556, 452

Lawler, J. E., Wickliffe, M. E., Den Hartog, E. A. & Sneden, C., 2001, ApJ, 563, 1075

Lucatello, S., Gratton, R., Cohen, J. G., Beers, T. C., Christlieb, N., Carretta, E. & Ramírez, S., 2003, AJ, 125, 875

Luck, R. E. & Bond, H. E., 1991, ApJS, 77, 515

Lucatello, S., Tsagarides, S., Beers, T. C., Carretta, E., Gratton, R. G. & Ryan, S. G., 2005, ApJ, 625, 825

Lucatello, S. *et al.*, 2006, in preparation

Matsuura, M. *et al.*, 2005, A&A, 434, 691

Marigo, P., Bernard-Salas, J., Pottasch, S. R., Tielens, A. G. G. M. & Wesselius, P. R., 2003, A&A, 409, 619

Marsteller, B., Beers, T. C., Rossi, S., Christlieb, N., Bessell, M. & Rhee, J., 2004, in *Eighth Nuclei in the Cosmos*, Nuclear Physics A (Astro-ph/0408380)

McClure, R. D., 1984, ApJ, 280, L31

McClure, R. D., 1985, JRASC, 79, 277

McClure, R. D. & Woodsworth, A. W., 1990, ApJ, 352, 709

McClure, R. D., 1997, PASP, 109, 256

McWilliam, A., Preston, G. W., Sneden, C. & Shectman, S., 1995, AJ, 109, 2736

McWilliam, A., Preston, G. W., Sneden, C. & Searle, L., 1995, AJ, 109, 2757

McWilliam, A., 1997, ARA&A, 35, 503

McWilliam, A., 1998, AJ, 115, 1640

Norris, J.E., Ryan, S. & Beers, T.C., 1997, ApJ, 489, L169

Oke, J. B. & Gunn, J. E., 1982, PASP, 94, 586

Plez, B. & Cohen, J. G., 2005, A&A, 434, 1117

Plez, B., Cohen, J. G. & Melendez, J., 2006, *From Lithium to Uranium: Elemental Tracers of Early Cosmic Evolution*, IAU Symp. 228, ed. V. Hill, P. francois & f. Primas

Preston, G. W. & Sneden, C., 2000, AJ, 120, 1014

Preston, G. W. & Sneden, C., 2001, AJ, 122, 1545

Prochascka, J. X., Naumov, S. O., Carney, B. W., McWilliam, A., & Wolfe, A. M., 2000, ApJ, 120, 2513

Querci, F., Querci, M. & Kunde, V. G., 1971, A&A, 15, 256

Querci, F., Querci, M. & Tsuji, T., 1971, A&A, 31, 265

Ramírez, S. V., Cohen, J. G., Buss, J., & Briley, M. M., 2001, AJ, 122, 1429

Rossi, S., Beers, T. C. & Sneden, C., 1999, in *The Galactic Halo*, ASP Conf. Series, 165, 264

Ryan, S. G., Aoki, W., Norris, J. E. & Beers, T. C., 2006, ApJ, in press (Astro-ph/0508475)

Scalo, J. M. & Miller, G. E., 1979, ApJ, 233, 596

Simmerer, J., Sneden, C., Cowan, J. J., Collier, J., Woolf, V. M. & Lawler, J. E., 2004, ApJ, 617, 1091

Sivarani, T. *et al.*, 2004, A&A, 413, 1073

Skrutskie, M. F., Schneider, S.E., Stiening, R., Strom, S.E., Weinberg, M.D., Beichman, C., Chester, T. *et al.*, 1997, in *The Impact of Large Scale Near-IR Sky Surveys*, ed. F.Garzon *et al.* (Dordrecht: Kluwer), p. 187

Sneden, C., 1973, Ph.D. thesis, Univ. of Texas

Spite, M. *et al.*, 2005, A&A, 430, 655

Takeda, Y., 2003, A&A, 402, 343

Takeda, Y., Zhao, G., Takad-Hidai, M., Chen, Y. Q., Saito, Y. & Zhang, H. W., 2003, Chinese Jrl. Astro., 3, 316

Travaglio, C., Gallino, R., Arnone, E., Cowan, J., Jordan, F. & Sneden, C., 2004, ApJ, 601, 864

Tsangarides, S. Ryan, S.G. & Beers, T.C., 2004, Mem. Soc. Astronom. Ital., 75, 772

Urdahl, R. S., Bao, Y. & Jackson, W. M., 1991, Chem. Phys. Lett., 178, 425

Wallace, L., Hinkle, K. & Livingston, W., 1998, 1998, N.S.O. Technical Report 98-001, http://ftp.noao.edu.fts/visatl/README

Wallerstein, G. & Greenstein, J. L., 1964, ApJ, 139, 1163

Wallerstein, G. & Knapp, G. R., 1998, ARA&A, 36, 369

Van Eck, S., Goriely, S., Jorissen, A. & Plez, B., 2003, A&A, 404, 291

Van Loon, J. T., Stanimirovic, S., Evans, A. & Muller, E., 2005, MNRAS, in press, Astro-ph/0511118

Vanture, A. D., 1992, AJ, 104, 1997

Vogt, S. E. *et al.* 1994, SPIE, 2198, 362

Yi, S., Demarque, P., Kim, Y.-C. , Lee, Y.-W., Ree, C. Lejeune, Th. & Barnes, S., 2001, ApJS, 136, 417

Table 1. The Sample of C-Stars Selected as EMP Candidates from the HES Mostly from the Palomar Sample

ID	Coords. (J2000)	V[a] (mag)	I[a] (mag)	Julian Date Obs. (– 2450000)	v_r[b] (km s^{-1})	[Fe/H](HES) (dex)
Obs. with HIRES						
HE0007−1832	00 09 52.8 −18 16 12	15.462	14.831	[f]		
HE0012−1441	00 15 27.1 −14 24 37	16.358	15.704	2547.8627	+11[g]	−2.61
HE0058−0244[c]	01 00 53.0 −02 28 20	13.727	12.933	2179.0096	−68.4	−2.81
HE0143−0441	01 45 37.8 −04 26 43	16.382	15.724	2547.0190	+121.8	−2.94
HE0212−0557	02 15 02.5 −05 43 23	14.70	···	2544.9791	−230.6	−3.45
HE0336+0113	03 38 52.8 +01 23 08	14.955	14.110	2179.0586	+66.6	−2.51
HE1031−0020	10 34 24.1 −00 36 09	14.296	13.338	3152.7297	+69.7	−3.70
HE1150−0428	11 53 06.6 −04 45 03	14.909	14.007	3152.7602	+46.6	−3.22
HE1410−0004	14 13 04.6 −00 18 33	15.494	14.712	3534.7447	+214.6	−2.65
HE1410+0213	14 13 06.5 +01 59 21	13.25	···	2396.9707	+80[e]	−3.17
HE1434−1442	14 37 26.6 −14 54 59	15.34	···	3488.9757	+146.9[e]	−3.42
HE1443+0113	14 46 16.4 +01 01 10	15.78	···	3589.7671	−1.1	−3.13
HE1509−0806	15 11 41.5 −08 17 41	14.796	13.807	2421.9292	−169.9	−3.92
HE2158−0348	22 00 40.0 −03 34 12	15.707	14.735	2178.7352	+67.6	−2.77
HE2232−0603	22 34 47.4 −05 48 17	16.513	15.738	2178.8255	−61.2	−1.99
HE2353−1758[h]	23 56 12.9 −17 42 03	15.491	14.558	3641.8915	+38.5	−2.60
HE2356−0410[d]	23 59 13.1 −03 53 49	13.622	12.710	2179.8396	−61.5	−3.22

[a]Our photometry from ANDICAM images.

[b]Heliocentric v_r.

[c]Rediscovery of CS22183−015.

[d]Rediscovery of CS22957−027.

[e]v_r only from the Mg triplet lines.

[f]See Cohen *et al.* (2004).

[g]Double lined spectroscopic binary, v_r variable

[h]HIRES spectrum obtained too late for analysis here. C-star with very strong Ba II lines.

Table 2. Stellar Parameters and Observations

ID	$T_{\rm eff}$ (K)	log(g) (dex)	v_t (km/s)	Exp. Time (sec: HIRES)	S/N[a]	Source/Follow Up
HE0012−1441	5730[d]	3.5	1.6	10,800	75	Magellan
HE0058−0244	5620	3.4	1.6	4800	100	Magellan
HE0143−0441	6240	3.7	1.6	9600	80	P200
HE0212−0557	5075	2.15	1.8	6000	100	P200
HE0336+0113	5700	3.5	1.6	12,200	100	Magellan
HE1031−0020	5080	2.2	1.6	2400	80	P200
HE1150−0428	5200	2.55	1.6	2400	70	P200
HE1410−0004	5605	3.5	1.6	2400[b]	60	P200
HE1410+0213	4985	2.0	1.8	2700	80	P200
HE1434−1442	5420	3.15	1.6	6000[c]	73	P200
HE1443+0113	4945	1.95	1.8	550[c,e]	low	P200
HE1509−0806	5185	2.5	1.6	2400	70	P200
HE2158−0348	5215	2.5	1.6	14,400	100	Magellan
HE2232−0603	5750	3.5	1.6	18,000	90	Magellan
HE2356−0410	5205	2.5	1.8	6000	100	Magellan

[a]Signal to noise ratio in the continuum near 4570 Å per 4 pixel spectral resolution element.

[b]HIRES-R spectrum with new mosaic CCD detector.

[c]HIRES-B spectrum with new mosaic CCD detector.

[d]Assumes second component does not affect the observed colors.

[e]Only one short exposure available, stopped by fog.

Table 3. Equivalent Widths for the First 5 Stars of for the Primary Sample of C-Stars from the HES

Line λ (Å)	Species	EP (eV)	Log(gf) (dex)	HE0012 −1441[a] (mÅ)	HE0058 −0244 (mÅ)	HE0143 −0441 (mÅ)	HE0212 −0557 (mÅ)	HE0336 +0113 (mÅ)
4057.52	Mg I	4.34	−1.200	34.0	19.2	21.2	···	34.4
4703.00	Mg I	4.34	−0.670	100.7	···	···	···	···
5172.70	Mg I	2.71	−0.380	258.9	144.7	163.5	183.5	210.9
5183.62	Mg I	2.72	−0.160	357.5	172.1	187.8	···	340.9
3961.52	Al I	0.00	−0.340	···	113.2	77.8	150.0	117.1
3905.53	Si I	1.91	−1.040	···	···	239.1	···	···
4226.74	Ca I	0.00	0.240	303.0	···	···	···	···
4425.44	Ca I	1.88	−0.360	···	···	25.6	···	···
4435.69	Ca I	1.89	−0.520	···	53.4	···	···	20.8
4454.79	Ca I	1.90	0.260	78.1	81.4	70.0	···	···
4578.56	Ca I	2.52	−0.558	8.0	···	···	15.0	···
4670.41	Sc II	1.36	−0.580	···	8.0	11.2	···	···
3924.53	Ti I	0.02	−0.940	···	9.6	···	···	···
3958.22	Ti I	0.05	−0.160	···	33.2	34.3	···	···
3998.64	Ti I	0.05	−0.050	···	24.7	22.4	···	19.2
4533.25	Ti I	0.85	0.480	···	20.8	10.0	55.3	17.6
4534.78	Ti I	0.84	0.280	···	16.0	···	53.0	11.2
4548.77	Ti I	0.83	−0.350	···	11.2	···	···	···
4555.49	Ti I	0.85	−0.490	···	···	···	24.1	···
4981.74	Ti I	0.85	0.500	14.0	32.6	28.8	···	···
4999.51	Ti I	0.83	0.250	14.0	17.2	19.2	···	22.4
5173.75	Ti I	0.00	−1.120	···	7.2	···	10.0	···
5210.39	Ti I	0.05	−0.880	···	8.1	···	45.7	8.0
3900.54	Ti II	1.13	−0.450	···	73.9	66.8	···	64.8
3987.61	Ti II	0.61	−2.730	···	12.8	···	···	···
4028.35	Ti II	1.89	−0.870	···	···	29.0	···	···
4443.81	Ti II	1.08	−0.700	···	72.9	63.0	···	44.8
4468.51	Ti II	1.13	−0.600	···	83.8	66.0	···	62.0
4501.28	Ti II	1.12	−0.760	52.7	64.7	55.3	112.9	55.1

Table 3—Continued

Line λ (Å)	Species	EP (eV)	Log(gf) (dex)	HE0012 −1441[a] (mÅ)	HE0058 −0244 (mÅ)	HE0143 −0441 (mÅ)	HE0212 −0557 (mÅ)	HE0336 +0113 (mÅ)
4533.97	Ti II	1.24	−0.640	58.6	82.7	55.2	136.0	44.5
4563.77	Ti II	1.22	−0.820	44.7	59.6	43.0	109.6	33.1
4571.98	Ti II	1.57	−0.340	64.0	74.7	70.3	···	51.2
4583.41	Ti II	1.16	−2.870	···	···	···	16.0	···
4589.95	Ti II	1.24	−1.650	22.0	20.8	···	44.4	···
4798.54	Ti II	1.08	−2.670	···	···	···	46.9	···
4865.62	Ti II	1.12	−2.810	···	···	···	12.0	···
4911.20	Ti II	3.12	−0.340	···	11.2	···	···	···
5185.91	Ti II	1.89	−1.460	···	···	···	35.2	···
5206.04	Cr I	0.94	0.030	44.1	29.4	24.0	96.0	33.8
5298.28	Cr I	0.98	−1.170	···	···	···	32.0	···
4030.75	Mn I	0.00	−0.470	···	69.4	45.0	140.0	81.8
4033.06	Mn I	0.00	−0.620	···	57.8	24.0	124.0	68.3
4754.04	Mn I	2.28	−0.090	···	···	···	13.0	···
4823.51	Mn I	2.32	0.140	···	7.0	···	31.0	···
3865.52	Fe I	1.01	−0.980	···	103.1	65.3	···	77.9
3899.72	Fe I	0.09	−1.530	···	87.1	79.8	···	96.0
3902.96	Fe I	1.56	−0.470	···	···	82.5	···	···
3906.49	Fe I	0.11	−2.240	···	76.3	79.7	···	72.0
3916.74	Fe I	3.24	−0.560	···	8.0	···	···	11.7
3920.27	Fe I	0.12	−1.750	···	···	72.1	···	···
3922.92	Fe I	0.05	−1.650	···	···	86.5	···	···
3949.96	Fe I	2.18	−1.160	···	14.4	···	···	27.2
4005.24	Fe I	1.56	−0.610	···	72.5	68.2	···	67.2
4045.81	Fe I	1.49	0.280	···	109.7	116.2	···	···
4063.59	Fe I	1.56	0.060	···	93.2	105.1	···	96.1
4071.74	Fe I	1.61	−0.020	···	89.4	87.6	···	86.7
4118.55	Fe I	3.57	0.140	···	29.4	34.0	···	29.6
4132.06	Fe I	1.61	−0.820	···	73.6	63.9	···	77.0

Table 3—Continued

Line λ (Å)	Species	EP (eV)	Log(gf) (dex)	HE0012 −1441[a] (mÅ)	HE0058 −0244 (mÅ)	HE0143 −0441 (mÅ)	HE0212 −0557 (mÅ)	HE0336 +0113 (mÅ)
4143.87	Fe I	1.56	−0.620	···	72.5	63.9	···	73.3
4147.67	Fe I	1.49	−2.100	···	21.3	···	···	13.3
4427.32	Fe I	0.05	−3.040	···	···	37.8	···	···
4447.73	Fe I	2.22	−1.340	···	···	29.5	···	···
4459.14	Fe I	2.18	−1.280	···	27.1	16.0	···	22.5
4461.66	Fe I	0.09	−3.210	···	47.7	24.0	···	34.2
4494.57	Fe I	2.20	−1.140	···	37.5	21.6	···	48.7
4531.16	Fe I	1.49	−2.150	···	25.6	16.0	···	30.3
4592.66	Fe I	1.56	−2.450	···	12.0	···	42.0	···
4602.95	Fe I	1.49	−2.220	···	19.7	···	···	···
4871.33	Fe I	2.86	−0.360	38.0	41.1	37.2	100.4	53.1
4872.14	Fe I	2.88	−0.570	39.9	···	27.9	90.0	29.2
4890.75	Fe I	2.87	−0.424	···	37.0	36.6	···	39.0
4891.50	Fe I	2.85	−0.110	57.9	53.2	47.9	120.3	49.9
4919.00	Fe I	2.86	−0.340	43.0	32.0	20.8	79.0	45.0
4920.51	Fe I	2.83	0.150	91.0	52.6	61.5	···	78.4
4957.61	Fe I	2.81	0.230	94.8	65.3	69.3	104.0	82.0
5083.34	Fe I	0.96	−2.960	26.0	···	···	···	···
5166.28	Fe I	0.00	−4.200	···	9.9	···	58.4	···
5171.61	Fe I	1.48	−1.790	39.1	34.8	···	82.2	37.7
5192.35	Fe I	3.00	−0.420	30.0	28.5	30.4	58.0	25.2
5194.95	Fe I	1.56	−2.090	34.2	20.9	17.7	80.5	15.0
5198.72	Fe I	2.22	−2.140	···	···	···	31.0	···
5216.28	Fe I	1.61	−2.150	···	15.7	···	65.8	18.2
5217.40	Fe I	3.21	−1.070	···	9.0	···	35.5	···
5227.19	Fe I	1.56	−1.350	74.8	61.4	43.5	117.6	51.7
5232.95	Fe I	2.94	−0.100	61.9	43.5	46.7	89.9	49.6
5269.55	Fe I	0.86	−1.320	87.5	81.3	87.4	127.5	72.0
5324.19	Fe I	3.21	−0.100	43.9	24.4	···	72.8	21.8

Table 3—Continued

Line λ (Å)	Species	EP (eV)	Log(gf) (dex)	HE0012 −1441[a] (mÅ)	HE0058 −0244 (mÅ)	HE0143 −0441 (mÅ)	HE0212 −0557 (mÅ)	HE0336 +0113 (mÅ)
4508.30	Fe II	2.84	−2.280	16.5	16.8	16.0	63.1	···
4555.89	Fe II	2.82	−2.170	25.6	18.8	16.8	46.4	8.5
4576.34	Fe II	2.83	−2.900	···	5.6	···	55.0	···
4583.84	Fe II	2.81	−2.020	31.1	30.9	28.2	65.7	14.4
4923.93	Fe II	2.88	−1.320	39.9	48.3	49.1	108.2	58.4
5018.45	Fe II	2.89	−1.220	49.0	61.1	55.3	···	44.3
5197.58	Fe II	3.23	−2.230	···	7.2	···	45.6	···
5234.63	Fe II	3.22	−2.220	···	···	···	43.0	···
3845.46	Co I	0.92	0.009	···	···	43.8	···	···
4121.31	Co I	0.92	−0.315	···	25.3	···	···	22.5
3858.30	Ni I	0.42	−0.967	···	61.8	52.7	···	···
4810.54	Zn I	4.08	−0.170	···	···	10.4	···	···
4077.71	Sr II	0.00	0.170	···	112.6	136.2	170.0	309.0
3950.36	Y II	0.10	−0.490	···	23.3	18.3	···	51.5
4883.69	Y II	1.08	0.070	···	12.8	18.9	74.6	54.8
5200.42	Y II	0.99	−0.570	···	···	···	36.0	···
5205.73	Y II	1.03	−0.340	···	···	···	43.0	···
4496.97	Zr II	0.71	−0.590	···	···	14.4	···	···
4130.65	Ba II	2.72	0.560	···	55.2	60.5	···	78.0
4554.04	Ba II	0.00	0.170	130.7	177.5	195.8	560.3	306.0
4934.16	Ba II	0.00	−0.150	96.8	171.7	180.7	416.6	230.0
3988.52	La II	0.40	0.210	···	38.5	44.5	156.0	54.3
3995.75	La II	0.17	−0.060	···	35.8	34.2	150.0	47.5
4086.71	La II	0.00	−0.070	···	41.2	44.0	140.0	47.3
4123.23	La II	0.32	0.130	···	37.2	30.9	···	44.8
4073.47	Ce II	0.48	0.320	···	31.9	25.6	···	41.4
4083.23	Ce II	0.70	0.240	···	22.4	20.1	···	23.8
4120.84	Ce II	0.32	−0.240	···	···	···	···	24.4
4127.38	Ce II	0.68	0.240	···	···	···	···	32.0

Table 3—Continued

Line λ (Å)	Species	EP (eV)	Log(gf) (dex)	HE0012 −1441[a] (mÅ)	HE0058 −0244 (mÅ)	HE0143 −0441 (mÅ)	HE0212 −0557 (mÅ)	HE0336 +0113 (mÅ)
4486.91	Ce II	0.30	−0.360	···	7.2	···	···	30.1
4562.37	Ce II	0.48	0.330	···	28.2	18.0	95.0	29.1
4628.16	Ce II	0.52	0.260	···	15.0	···	···	···
5220.12	Pr II	0.80	0.170	···	···	···	58.0	···
4021.34	Nd II	0.32	−0.170	···	13.6	···	···	17.0
4061.09	Nd II	0.47	0.300	···	27.9	29.7	···	40.0
4069.27	Nd II	0.06	−0.400	···	17.6	···	···	12.8
4109.46	Nd II	0.32	0.180	···	···	38.4	···	40.0
4446.39	Nd II	0.20	−0.630	···	···	···	···	19.2
4462.99	Nd II	0.56	−0.070	···	29.0	29.6	···	35.2
5212.35	Nd II	0.20	−0.700	···	···	···	68.2	···
3819.67	Eu II	0.00	0.510	···	51.0	30.4	···	30.0
3907.11	Eu II	0.21	0.170	···	25.0	22.4	···	···
4129.70	Eu II	0.00	0.220	···	29.0	22.8	···	12.0
4057.81	Pb I[b]	1.32	−0.220	<38.0	80.4	48.0	···	33.9

[a]W_λ given as a guide. Synthesis used throughout for this binary star. See text.

[b]Synthesis used to derive Pb abundance. W_λ given as a guidance to line strength.

Table 4. Equivalent Widths for the Next 5 Stars of for the Primary Sample of C-Stars from the HES

Line λ (Å)	Species	EP (eV)	Log(gf) (dex)	HE1031 −0020 (mÅ)	HE1150 −0428 (mÅ)	HE1410 +0213 (mÅ)	HE1410 −0004 (mÅ)	HE1434 −1442 (mÅ)
4057.52	Mg I	4.34	−1.200	18.0	···	···	13.9	···
4703.00	Mg I	4.34	−0.670	···	···	···	31.4	···
5172.70	Mg I	2.71	−0.380	160.3	115.2	218.6	128.6	191.7
5183.62	Mg I	2.72	−0.160	189.2	130.4	246.3	142.9	241.6
3961.52	Al I	0.00	−0.340	174.5	···	···	···	···
4435.69	Ca I	1.89	−0.520	55.0	32.4	···	···	···
4454.79	Ca I	1.90	0.260	110.0	74.0	···	···	···
4578.56	Ca I	2.52	−0.558	36.0	9.0	···	···	···
3924.53	Ti I	0.02	−0.940	32.4	···	···	···	···
3958.22	Ti I	0.05	−0.160	47.4	23.4	···	···	···
3998.64	Ti I	0.05	−0.050	33.4	25.2	···	···	···
4533.25	Ti I	0.85	0.480	23.0	11.0	···	8.4	27.3
4534.78	Ti I	0.84	0.280	31.0	11.0	···	···	27.6
4555.49	Ti I	0.85	−0.490	11.7	···	···	···	···
4981.74	Ti I	0.85	0.500	58.0	23.4	···	···	49.7
4999.51	Ti I	0.83	0.250	37.1	···	···	11.7	42.9
5022.87	Ti I	0.83	−0.430	20.0	···	···	···	···
5173.75	Ti I	0.00	−1.120	7.0	···	47.4	···	···
5210.39	Ti I	0.05	−0.880	24.5	···	54.0	···	22.5
3900.54	Ti II	1.13	−0.450	109.4	···	···	···	···
3987.61	Ti II	0.61	−2.730	32.4	···	···	···	···
4012.39	Ti II	0.57	−1.610	98.2	24.3	···	···	···
4028.35	Ti II	1.89	−0.870	84.4	···	···	···	···
4443.81	Ti II	1.08	−0.700	84.8	56.5	···	···	···
4468.51	Ti II	1.13	−0.600	120.0	94.0	···	···	···
4501.28	Ti II	1.12	−0.760	79.9	48.4	···	34.3	85.0
4533.97	Ti II	1.24	−0.640	115.0	88.0	···	45.6	110.8
4563.77	Ti II	1.22	−0.820	96.1	55.1	···	32.3	86.5
4571.98	Ti II	1.57	−0.340	112.0	78.0	···	40.8	110.0

Table 4—Continued

Line λ (Å)	Species	EP (eV)	Log(gf) (dex)	HE1031 −0020 (mÅ)	HE1150 −0428 (mÅ)	HE1410 +0213 (mÅ)	HE1410 −0004 (mÅ)	HE1434 −1442 (mÅ)
4589.95	Ti II	1.24	−1.650	···	···	···	···	32.5
4657.20	Ti II	1.24	−2.320	9.8	···	···	···	···
4798.54	Ti II	1.08	−2.670	23.0	···	···	···	23.8
4865.62	Ti II	1.12	−2.810	11.0	···	···	···	24.7
4911.20	Ti II	3.12	−0.340	36.0	···	···	···	···
5185.91	Ti II	1.89	−1.460	23.8	···	54.6	···	···
5336.79	Ti II	1.58	−1.630	···	···	···	···	36.1
5206.04	Cr I	0.94	0.030	50.0	11.0	83.0	23.7	55.3
5409.80	Cr I	1.03	−0.710	···	···	···	6.0	26.1
4030.75	Mn I	0.00	−0.470	120.0	···	···	37.0	···
4033.06	Mn I	0.00	−0.620	100.0	···	···	44.1	···
4451.59	Mn I	2.89	0.280	24.0	···	···	···	···
4754.04	Mn I	2.28	−0.090	7.0	···	···	···	6.9
4783.42	Mn I	2.30	0.042	14.0	···	···	···	8.4
4823.51	Mn I	2.32	0.140	···	18.0	···	···	19.2
3899.72	Fe I	0.09	−1.530	96.5	100.2	···	···	···
3902.96	Fe I	1.56	−0.470	94.0	66.4	···	···	···
3906.49	Fe I	0.11	−2.240	94.9	72.7	···	···	···
3916.74	Fe I	3.24	−0.560	17.2	···	···	···	···
3922.92	Fe I	0.05	−1.650	97.5	89.5	···	···	···
3930.31	Fe I	0.09	−1.590	···	93.5	···	···	···
3949.96	Fe I	2.18	−1.160	24.0	···	···	···	···
4005.24	Fe I	1.56	−0.610	75.3	66.6	···	···	···
4045.81	Fe I	1.49	0.280	130.2	110.9	···	···	···
4063.59	Fe I	1.56	0.060	130.2	85.3	···	···	···
4071.74	Fe I	1.61	−0.020	126.7	75.0	···	···	···
4118.55	Fe I	3.57	0.140	17.7	···	···	···	···
4459.14	Fe I	2.18	−1.280	48.9	20.7	···	···	···
4461.66	Fe I	0.09	−3.210	80.0	58.6	···	···	···

Table 4—Continued

Line λ (Å)	Species	EP (eV)	Log(gf) (dex)	HE1031 −0020 (mÅ)	HE1150 −0428 (mÅ)	HE1410 +0213 (mÅ)	HE1410 −0004 (mÅ)	HE1434 −1442 (mÅ)
4494.57	Fe I	2.20	−1.140	54.0	···	···	21.2	63.5
4531.16	Fe I	1.49	−2.150	54.0	30.0	···	9.7	54.3
4602.95	Fe I	1.49	−2.220	41.7	18.5	···	11.6	···
4654.50	Fe I	1.56	−2.780	30.0	···	···	···	···
4871.33	Fe I	2.86	−0.360	67.8	32.5	···	18.2	68.1
4872.14	Fe I	2.88	−0.570	···	···	···	22.3	···
4890.75	Fe I	2.87	−0.424	···	···	···	···	61.0
4891.50	Fe I	2.85	−0.110	83.0	52.0	77.6	41.5	78.0
4919.00	Fe I	2.86	−0.340	66.0	17.3	80.7	16.9	55.0
4920.51	Fe I	2.83	0.150	74.3	27.4	95.8	35.2	83.5
4957.61	Fe I	2.81	0.230	94.0	57.2	···	69.3	94.7
5166.28	Fe I	0.00	−4.200	29.5	···	···	···	···
5171.61	Fe I	1.48	−1.790	58.1	26.0	115.0	26.6	···
5192.35	Fe I	3.00	−0.420	36.7	13.0	83.8	···	···
5194.95	Fe I	1.56	−2.090	33.8	···	92.0	11.7	···
5198.72	Fe I	2.22	−2.140	13.0	···	39.6	···	···
5216.28	Fe I	1.61	−2.150	34.7	···	85.4	···	42.5
5217.40	Fe I	3.21	−1.070	20.9	···	44.7	···	19.0
5227.19	Fe I	1.56	−1.350	77.2	45.2	132.9	41.9	87.9
5232.95	Fe I	2.94	−0.100	57.2	30.0	98.4	28.6	65.8
5269.55	Fe I	0.86	−1.320	99.7	80.2	163.3	64.8	106.6
5324.19	Fe I	3.21	−0.100	39.8	···	···	···	52.5
5393.18	Fe I	3.24	−0.720	···	···	···	···	26.7
5405.78	Fe I	0.99	−1.840	···	···	···	49.5	86.2
4491.40	Fe II	2.84	−2.600	7.0	···	···	···	···
4508.30	Fe II	2.84	−2.280	13.8	···	···	5.9	···
4555.89	Fe II	2.82	−2.170	18.1	12.0	···	11.7	27.0
4583.84	Fe II	2.81	−2.020	37.2	20.0	···	16.9	42.6
4923.93	Fe II	2.88	−1.320	82.4	41.7	85.0	37.9	75.2

Table 4—Continued

Line λ (Å)	Species	EP (eV)	Log(gf) (dex)	HE1031 −0020 (mÅ)	HE1150 −0428 (mÅ)	HE1410 +0213 (mÅ)	HE1410 −0004 (mÅ)	HE1434 −1442 (mÅ)
5018.45	Fe II	2.89	−1.220	95.0	55.8	···	44.1	85.4
5197.58	Fe II	3.23	−2.230	13.0	···	40.9	···	14.0
5234.63	Fe II	3.22	−2.220	19.7	···	29.5	···	26.9
4077.71	Sr II	0.00	0.170	140.6	79.8	···	93.0	···
3950.36	Y II	0.10	−0.490	38.5	<14.0	···	···	···
4883.69	Y II	1.08	0.070	···	···	···	···	25.0
5205.73	Y II	1.03	−0.340	11.0	···	<5.0	···	12.8
4554.04	Ba II	0.00	0.170	176.3	38.0	···	108.9	175.0
4934.16	Ba II	0.00	−0.150	194.1	18.0	141.3	104.9	185.0
3988.52	La II	0.40	0.210	38.4	<7.0	···	···	···
3995.75	La II	0.17	−0.060	30.9	<18.0	···	···	···
4086.71	La II	0.00	−0.070	55.3	<18.0	···	···	···
4123.23	La II	0.32	0.130	40.5	···	···	···	···
4073.47	Ce II	0.48	0.320	···	<17.8	···	···	···
4120.84	Ce II	0.32	−0.240	···	<48.0	···	···	···
4562.37	Ce II	0.48	0.330	34.0	<18.0	···	···	···
4021.34	Nd II	0.32	−0.170	39.5	···	···	···	···
4061.09	Nd II	0.47	0.300	44.8	<11.0	···	···	···
4069.27	Nd II	0.06	−0.400	41.8	···	···	···	···
4446.39	Nd II	0.20	−0.630	30.0	<11.0	···	···	···
5212.35	Nd II	0.20	−0.700	···	···	23.5	···	···
3907.11	Eu II	0.21	0.170	<15.0	<14.0	···	···	···
4057.81	Pb I[a]	1.32	−0.220	118.0	79.3	···	<29.5	66.0

[a]Synthesis used to derive Pb abundance. W_λ given as a guidance to line strength.

Table 5. Equivalent Widths for the Last 5 Stars of for the Primary Sample of C-Stars from the HES

Line λ (Å)	Species	EP (eV)	Log(gf) (dex)	HE1443 +0113 (mÅ)	HE1509 −0806 (mÅ)	HE2158 −0348 (mÅ)	HE2232 −0603 (mÅ)	HE2356 −0410 (mÅ)
4057.52	Mg I	4.34	−1.200	···	···	29.0	72.0	18.0
4167.28	Mg I	4.34	−1.000	···	···	···	100.0	···
4703.00	Mg I	4.34	−0.670	···	···	···	105.4	···
5172.70	Mg I	2.71	−0.380	251.3	167.0	187.1	275.9	123.2
5183.62	Mg I	2.72	−0.160	333.8	211.0	237.5	356.6	141.9
3961.52	Al I	0.00	−0.340	···	119.0	129.1	140.0	111.3
4435.69	Ca I	1.89	−0.520	···	29.0	56.0	60.3	26.7
4454.79	Ca I	1.90	0.260	···	74.0	94.0	95.1	79.6
4670.41	Sc II	1.36	−0.580	···	···	···	12.5	9.0
3958.22	Ti I	0.05	−0.160	···	···	50.0	62.3	21.0
3998.64	Ti I	0.05	−0.050	···	···	36.3	65.8	29.0
4518.03	Ti I	0.83	−0.230	···	···	···	16.8	···
4533.25	Ti I	0.85	0.480	···	···	35.0	42.0	16.0
4534.78	Ti I	0.84	0.280	···	16.0	32.9	33.4	9.0
4548.77	Ti I	0.83	−0.350	···	···	···	17.6	···
4681.92	Ti I	0.05	−1.070	···	···	···	21.2	···
4981.74	Ti I	0.85	0.500	···	32.0	···	40.4	25.0
4999.51	Ti I	0.83	0.250	···	18.0	49.3	48.8	18.0
5022.87	Ti I	0.83	−0.430	···	···	···	9.4	···
5173.75	Ti I	0.00	−1.120	···	9.0	···	22.4	···
5210.39	Ti I	0.05	−0.880	···	10.0	28.1	22.5	···
3900.54	Ti II	1.13	−0.450	···	124.0	···	80.9	···
3987.61	Ti II	0.61	−2.730	···	22.4	···	···	···
4012.39	Ti II	0.57	−1.610	···	···	···	···	39.5
4028.35	Ti II	1.89	−0.870	···	75.0	···	53.4	···
4417.72	Ti II	1.16	−1.160	···	···	···	73.7	···
4443.81	Ti II	1.08	−0.700	···	107.2	94.0	87.1	71.9
4468.51	Ti II	1.13	−0.600	···	110.0	108.0	90.4	89.7
4501.28	Ti II	1.12	−0.760	···	106.2	80.0	82.3	68.5

Table 5—Continued

Line λ (Å)	Species	EP (eV)	Log(gf) (dex)	HE1443 +0113 (mÅ)	HE1509 −0806 (mÅ)	HE2158 −0348 (mÅ)	HE2232 −0603 (mÅ)	HE2356 −0410 (mÅ)
4533.97	Ti II	1.24	−0.640	···	108.0	110.0	91.5	89.4
4563.77	Ti II	1.22	−0.820	···	94.7	96.6	73.0	58.0
4571.98	Ti II	1.57	−0.340	···	100.0	110.0	77.5	79.2
4589.95	Ti II	1.24	−1.650	···	38.4	···	36.2	18.0
4865.62	Ti II	1.12	−2.810	···	···	10.0	···	···
4911.20	Ti II	3.12	−0.340	···	···	···	14.4	···
5185.91	Ti II	1.89	−1.460	···	18.0	18.0	···	···
4652.17	Cr I	1.00	−1.030	···	···	···	29.1	···
5206.04	Cr I	0.94	0.030	···	···	37.0	64.0	34.7
5298.28	Cr I	0.98	−1.170	···	8.0	···	23.3	···
4030.75	Mn I	0.00	−0.470	···	105.1	107.4	104.9	105.0
4033.06	Mn I	0.00	−0.620	···	100.0	101.7	79.0	89.0
4823.51	Mn I	2.32	0.140	···	8.0	···	28.0	12.0
3865.52	Fe I	1.01	−0.980	···	···	···	90.0	···
3899.72	Fe I	0.09	−1.530	···	···	···	116.0	···
3902.96	Fe I	1.56	−0.470	···	···	···	121.0	···
3906.49	Fe I	0.11	−2.240	···	···	···	80.6	···
3916.74	Fe I	3.24	−0.560	···	···	···	45.0	···
3920.27	Fe I	0.12	−1.750	···	···	···	109.5	···
3922.92	Fe I	0.05	−1.650	···	···	···	112.7	···
3949.96	Fe I	2.18	−1.160	···	···	33.5	40.4	···
4005.24	Fe I	1.56	−0.610	···	86.9	83.0	109.7	88.0
4045.81	Fe I	1.49	0.280	···	···	145.6	···	136.0
4063.59	Fe I	1.56	0.060	···	···	111.2	162.7	97.8
4071.74	Fe I	1.61	−0.020	···	···	105.0	132.4	130.0
4118.55	Fe I	3.57	0.140	···	···	32.4	61.2	···
4132.06	Fe I	1.61	−0.820	···	···	80.9	101.9	74.7
4143.87	Fe I	1.56	−0.620	···	···	89.2	112.0	79.0
4147.67	Fe I	1.49	−2.100	···	···	44.4	45.4	35.3

Table 5—Continued

Line λ (Å)	Species	EP (eV)	Log(gf) (dex)	HE1443 +0113 (mÅ)	HE1509 −0806 (mÅ)	HE2158 −0348 (mÅ)	HE2232 −0603 (mÅ)	HE2356 −0410 (mÅ)
4415.13	Fe I	1.61	−0.610	···	···	···	121.2	···
4447.73	Fe I	2.22	−1.340	···	···	···	···	43.0
4459.14	Fe I	2.18	−1.280	···	···	55.0	···	33.0
4461.66	Fe I	0.09	−3.210	···	61.2	···	57.3	59.8
4489.75	Fe I	0.12	−3.970	···	···	···	29.7	10.0
4494.57	Fe I	2.20	−1.140	···	55.4	···	64.2	35.7
4531.16	Fe I	1.49	−2.150	···	36.0	55.6	42.1	32.0
4592.66	Fe I	1.56	−2.450	···	···	···	30.9	···
4602.95	Fe I	1.49	−2.220	···	25.0	44.0	42.5	22.4
4871.33	Fe I	2.86	−0.360	···	42.0	77.0	81.6	47.9
4872.14	Fe I	2.88	−0.570	···	31.0	···	74.0	43.0
4890.75	Fe I	2.87	−0.424	···	41.0	53.9	···	···
4891.50	Fe I	2.85	−0.110	···	72.1	94.0	90.6	51.1
4919.00	Fe I	2.86	−0.340	···	37.7	65.8	77.8	25.7
4920.51	Fe I	2.83	0.150	···	63.0	86.7	95.5	48.0
4957.61	Fe I	2.81	0.230	···	76.0	88.0	113.8	66.7
5166.28	Fe I	0.00	−4.200	···	···	30.0	38.0	···
5171.61	Fe I	1.48	−1.790	···	52.2	59.2	75.9	40.6
5192.35	Fe I	3.00	−0.420	···	···	41.0	70.7	23.4
5194.95	Fe I	1.56	−2.090	···	33.9	36.8	52.4	23.4
5216.28	Fe I	1.61	−2.150	94.0	···	31.8	35.1	19.6
5217.40	Fe I	3.21	−1.070	39.4	···	20.8	13.0	···
5227.19	Fe I	1.56	−1.350	109.4	61.2	78.5	95.8	68.1
5232.95	Fe I	2.94	−0.100	108.7	62.3	60.2	82.6	43.7
5269.55	Fe I	0.86	−1.320	156.8	109.4	93.3	116.3	93.1
5324.19	Fe I	3.21	−0.100	88.0	29.1	36.3	60.4	28.4
5393.18	Fe I	3.24	−0.720	78.8	···	···	···	···
5405.78	Fe I	0.99	−1.840	115.9	···	···	···	···
4491.40	Fe II	2.84	−2.600	···	···	20.8	···	8.0

Table 5—Continued

Line λ (Å)	Species	EP (eV)	Log(gf) (dex)	HE1443 +0113 (mÅ)	HE1509 −0806 (mÅ)	HE2158 −0348 (mÅ)	HE2232 −0603 (mÅ)	HE2356 −0410 (mÅ)
4508.30	Fe II	2.84	−2.280	···	18.0	28.7	28.6	19.1
4555.89	Fe II	2.82	−2.170	···	25.0	28.0	41.3	15.6
4583.84	Fe II	2.81	−2.020	···	···	39.6	50.4	33.7
4923.93	Fe II	2.88	−1.320	···	87.7	66.0	68.8	52.2
5018.45	Fe II	2.89	−1.220	···	···	81.0	86.9	64.2
5197.58	Fe II	3.23	−2.230	···	16.0	13.0	25.4	5.0
5234.63	Fe II	3.22	−2.220	···	16.0	19.1	26.4	5.0
3842.05	Co I	0.92	−0.763	···	···	···	25.0	···
3845.46	Co I	0.92	0.009	···	···	···	62.8	···
4121.31	Co I	0.92	−0.315	···	42.0	40.8	46.9	36.0
3858.30	Ni I	0.42	−0.967	···	···	···	73.8	···
4810.54	Zn I	4.08	−0.170	···	···	···	···	9.0
4077.71	Sr II	0.00	0.170	···	226.9	158.6	190.0	72.2
3950.36	Y II	0.10	−0.490	···	···	59.5	45.5	−9.0
4883.69	Y II	1.08	0.070	···	48.0	57.7	46.0	−9.0
5087.43	Y II	1.08	−0.170	···	···	···	41.0	···
5200.42	Y II	0.99	−0.570	···	16.0	···	···	···
5205.73	Y II	1.03	−0.340	···	···	28.1	···	···
4161.21	Zr II	0.71	−0.720	···	···	68.8	···	···
4496.97	Zr II	0.71	−0.590	···	···	59.1	···	···
4130.65	Ba II	2.72	0.560	···	···	···	63.2	···
4554.04	Ba II	0.00	0.170	···	225.1	208.1	211.6	26.8
4934.16	Ba II	0.00	−0.150	284.9	239.3	199.0	180.2	29.6
3988.52	La II	0.40	0.210	···	67.0	65.3	···	···
3995.75	La II	0.17	−0.060	···	57.0	50.3	57.2	···
4086.71	La II	0.00	−0.070	···	65.2	55.0	42.6	<9.0
4123.23	La II	0.32	0.130	···	55.3	57.0	47.2	···
4073.47	Ce II	0.48	0.320	···	···	43.0	···	···
4083.23	Ce II	0.70	0.240	···	···	27.3	···	···

Table 5—Continued

Line λ (Å)	Species	EP (eV)	Log(gf) (dex)	HE1443 +0113 (mÅ)	HE1509 −0806 (mÅ)	HE2158 −0348 (mÅ)	HE2232 −0603 (mÅ)	HE2356 −0410 (mÅ)
4120.84	Ce II	0.32	−0.240	···	45.0	47.2	···	···
4486.91	Ce II	0.30	−0.360	···	···	35.2	···	···
4562.37	Ce II	0.48	0.330	···	32.0	57.5	38.0	<9.0
4628.16	Ce II	0.52	0.260	···	36.0	···	···	···
4021.34	Nd II	0.32	−0.170	···	···	···	···	<16.0
4061.09	Nd II	0.47	0.300	···	···	···	···	<9.0
4069.27	Nd II	0.06	−0.400	···	···	23.4	···	<9.0
4109.46	Nd II	0.32	0.180	···	92.0	50.0	···	<13.0
4446.39	Nd II	0.20	−0.630	···	29.0	···	···	···
4462.99	Nd II	0.56	−0.070	···	50.0	···	···	···
5212.35	Nd II	0.20	−0.700	···	9.0	···	···	···
3819.67	Eu II	0.00	0.510	···	···	43.0	···	<36.0
3907.11	Eu II	0.21	0.170	···	<15.0	···	···	···
4129.70	Eu II	0.00	0.220	···	<15.0	24.0	···	<10.0
4057.81	Pb I[a]	1.32	−0.220	···	52.0	110.0	34.0	56.0

[a]Synthesis used to derive Pb abundance. W_λ given as a guidance to line strength.

Table 6. Equivalent Widths for Redder Lines in the Spectra of Three C-Stars

Line λ (Å)	Species	EP (eV)	Log(gf) (dex)	HE1410−0004 (W_λ – mÅ)	HE1434−1442 (W_λ – mÅ)	HE1443+0113 (W_λ – mÅ)
6707.76	Li I	0.00	0.178	<10.0	···	···
6300.30	O I	0.00	−9.78	<6.0	···	···
7771.94	O I	9.15	0.369	7.0	···	···
5688.19	Na I	2.10	−0.420	7.0	···	···
5889.95	Na I	0.00	0.110	148.5	178.8	363.0
5895.92	Na I	0.00	−0.190	127.0	176.5	210.0
5528.41	Mg I	4.34	−0.480	29.5	71.8	···
5711.09	Mg I	4.34	−0.167	6.0	···	···
6696.02	Al I	3.14	−1.34	4.2	···	···
5690.43	Si I	4.93	−1.870	···	6.0	···
5948.54	Si I	5.08	−1.230	···	8.0	···
7698.97	K I	0.00	−0.168	12.6	···	···
5588.75	Ca I	2.52	0.437	11.1	36.3	···
5590.11	Ca I	2.52	−0.710	···	9.9	···
5594.46	Ca I	2.52	−0.050	6.9	33.1	···
5601.28	Ca I	2.52	−0.438	···	22.0	···
5857.45	Ca I	2.93	0.230	···	16.8	···
6162.17	Ca I	1.90	−0.090	17.3	···	···
6493.78	Ca I	2.52	0.140	5.6	···	···
7148.15	Ca I	2.71	0.218	9.8	···	···
5526.79	Sc II	1.77	0.130	···	17.5	···
5657.90	Sc II	1.51	−0.500	···	11.7	···
5424.08	Fe I	4.32	0.510	35.2	52.6	88.0
5434.53	Fe I	1.01	−2.130	···	75.4	107.0
5497.52	Fe I	1.01	−2.830	10.4	27.2	···
5506.79	Fe I	0.99	−2.790	···	35.7	···
5569.61	Fe I	3.42	−0.486	9.1	···	···
5586.76	Fe I	3.37	−0.140	10.4	···	···
6137.69	Fe I	2.59	−1.350	11.2	···	···
6430.84	Fe I	2.18	−1.950	6.9	···	···

Table 6—Continued

Line λ (Å)	Species	EP (eV)	Log(gf) (dex)	HE1410−0004 (W_λ – mÅ)	HE1434−1442 (W_λ – mÅ)	HE1443+0113 (W_λ – mÅ)
6494.98	Fe I	2.40	−1.240	13.0	···	···
5425.26	Fe II	3.00	−3.240	···	11.0	···
5534.85	Fe II	3.25	−2.640	···	6.3	···
5530.79	Co I	1.71	−2.060	···	<9.0	···
5846.99	Ni I	1.68	−3.210	···	<4.0	···
4722.16	Zn I	4.03	−0.390	<8.0	···	···
5853.70	Ba II	0.60	−1.010	19.0	73.5	121.0
6141.70	Ba II	0.70	−0.070	61.1	···	···
6496.90	Ba II	0.60	−0.380	57.4	···	···
4959.12	Nd II	0.06	−0.800	···	32.0	···
5249.58	Nd II	0.98	0.200	···	16.5	···
6645.11	Eu II	1.38	0.120	<6.0	···	···

Table 7. Fit Fe I Slopes With EP, Equivalent Width and Wavelength

Star ID	Δ[X/Fe]/Δ(EP)[a] (dex/eV)	Δ[X/Fe]/$\Delta[W_\lambda/\lambda]$ (dex)	Δ[X/Fe]/$\Delta\lambda$ (10^{-4}dex/$\mathring{A}$)
HE0012−1441	[b]	[b]	[b]
HE0058−0244	−0.013	−0.198	1.02
HE0143−0441	−0.026	0.024	0.65
HE0212−0557	0.088	0.207	−5.33
HE0336+0113	0.075	−0.121	0.98
HE1031−0020	0.039	−0.117	2.02
HE1150−0428	−0.066	−0.027	0.14
HE1410−0004	−0.014	0.001	−0.08
HE1410+0213	[c]	[c]	[c]
HE1434−1442	0.056	0.006	−1.38
HE1443+0113	[d]	[d]	[d]
HE1509−0806	[e]	[e]	[e]
HE2158−0348	0.068	−0.248	1.63
HE2232−0603	0.057	−0.013	1.87
HE2356−0410	−0.036	0.006	−0.83

[a]Typical range of EP is 3 eV.

[b]There were only 14 measured Fe I lines in this star.

[c]There were only 12 detected Fe I lines in this star.

[d]There were only 10 measured Fe I lines in this star.

[e]There were only 17 detected Fe I lines in this star.

Table 8. Abundances for the First Four EMP C-Stars From the HES

Species	HE0012−1441				HE0058−0244				HE0143−0441				HE0212−0557			
	[X/Fe] (dex)	log$\epsilon(X)$ (dex)	No. Lines	σ (dex)	[X/Fe] (dex)	log$\epsilon(X)$ (dex)	No. Lines	σ (dex)	[X/Fe] (dex)	log$\epsilon(X)$ (dex)	No. Lines	σ (dex)	[X/Fe] (dex)	log$\epsilon(X)$ (dex)	No. Lines	σ (dex)
C−CH	1.59	7.66	1	···	1.92	7.76	1	···	1.98	8.26	1	···	1.74	8.06	1	···
N−CN	0.64	6.05	1	···	1.77	6.95	1	···	1.73[d]	7.35[d]	1	···	1.09	6.75	1	···
MgI	0.91	5.93	4	0.16	0.54	5.33	3	0.19	0.63	5.86	3	0.08	0.04	5.32	1	···
AlI	···	···	···	···	0.34	4.06	1	···	−0.22	3.94	1	···	0.01	4.21	1	···
CaI	0.42	4.26	3	0.11	0.96	4.57	2	0.20	0.43	4.48	2	0.17	0.14	4.23	1	···
ScII	···	···	···	···	0.56	0.91	1	···	0.67	1.46	1	···	···	···	···	···
TiI	0.03	2.50	2	0.10	0.57	2.81	10	0.17	0.54	3.22	5	0.26	0.14	2.87	5	0.32
TiII	0.13	2.60	5	0.08	0.55	2.79	10	0.16	0.26	2.94	8	0.16	0.32	3.04	8	0.32
CrI	−0.18	2.97	1	···	−0.35	2.57	1	···	−0.38	2.98	1	···	−0.09	3.31	2	0.03
MnI	···	···	···	···	−0.39	2.24	3	0.11	−0.72	2.36	2	0.23	−0.55	2.57	4	0.46
FeI	−2.52[a]	4.93	14	0.16	−2.75[a]	4.70	35	0.21	−2.31[a]	5.14	31	0.18	−2.27[a]	5.18	17	0.26
FeII	−0.15	4.78	5	0.19	0.02	4.72	7	0.12	−0.22	4.92	5	0.11	0.04	5.23	7	0.28
CoI	···	···	···	···	0.17	2.34	1	···	0.47	3.08	1	···	···	···	···	···
NiI	···	···	···	···	−0.33	3.17	1	···	−0.31	3.63	1	···	···	···	···	···
ZnI	···	···	···	···	···	···	···	···	0.46	2.76	1	···	···	···	···	···
SrII	···	···	···	···	0.34	0.49	1	···	0.86	1.45	1	···	−0.05	0.59	1	···
YII	···	···	···	···	0.52	0.01	2	0.03	0.59	0.52	2	0.21	0.55	0.53	3	0.16
ZrII	···	···	···	···	···	···	···	···	1.05	1.34	1	···	···	···	···	···
BaII	1.15	0.76	2	0.27	2.04	1.42	3	0.16	2.32	2.14	3	0.12	2.18	2.04	2	0.06
LaII	···	···	···	···	1.70	0.09	4	0.04	1.78	0.61	4	0.15	2.28	1.15	3	0.22
CeII	···	···	···	···	1.88	0.68	5	0.22	1.93	1.17	3	0.21	2.14	1.42	1	···
PrII	···	···	···	···	···	···	···	···	···	···	···	···	2.37	0.81	1	···
NdII	···	···	···	···	1.91	0.66	4	0.24	2.17	1.37	3	0.21	1.90	1.13	1	···
EuII	···	···	···	···	1.70	−0.54	3	0.14	1.46	−0.34	3	0.17	···	···	···	···
PbI	<1.92	<1.35	1	···	2.79	1.99	1	···	3.11	2.75	1	···	[c]	···	···	···

[a] This is [Fe/H].

[b] Pb I 4057 line is swamped by molecular features.

[c] No Pb abundance as the large negative v_r moves the 4057 Å Pb I line onto a CCD defect.

[d] This value supercedes that given in Cohen *et al.* (2004).

Table 9. Abundances for the Second Four EMP C-Stars From the HES

Species	HE0336+0113				HE1031−0020				HE1150−0428				HE1410+0213			
	[X/Fe] (dex)	log$\epsilon(X)$ (dex)	No. Lines	σ (dex)	[X/Fe] (dex)	log$\epsilon(X)$ (dex)	No. Lines	σ (dex)	[X/Fe] (dex)	log$\epsilon(X)$ (dex)	No. Lines	σ (dex)	[X/Fe] (dex)	log$\epsilon(X)$ (dex)	No. Lines	σ (dex)
C−CH	2.25	8.16	1	···	1.63	7.36	1	···	2.37	7.66	1	···	1.73	8.16	1	···
N−CN	1.60	6.85	1	···	2.48	7.55	1	···	2.52	7.15	1	···	1.78	7.55	1	···
NaI	···	···	···	···	···	···	···	···	···	···	···	···	···	···	···	···
MgI	1.04	5.90	3	0.18	0.50	5.19	3	0.18	0.34	4.58	2	0.06	0.18	5.56	2	0.03
AlI	0.34	4.13	1	···	0.88	4.49	1	···	···	···	···	···	···	···	···	···
SiI	···	···	···	···	···	···	···	···	···	···	···	···	···	···	···	···
CaI	0.42	4.10	1	···	1.12	4.62	3	0.22	1.03	4.09	3	0.04	···	···	···	···
TiI	0.39	2.70	5	0.19	0.46	2.60	11	0.31	0.49	2.17	5	0.12	0.29	3.12	2	0.04
TiII	0.11	2.42	7	0.13	0.80	2.93	15	0.37	0.50	2.19	7	0.45	0.36	3.19	1	···
CrI	−0.26	2.73	1	···	−0.38	2.43	1	···	−0.70	1.67	1	···	−0.55	2.96	1	···
MnI	−0.21	2.50	2	0.14	0.03	2.56	5	0.45	···	···	···	···	···	···	···	···
FeI	−2.68[a]	4.77	31	0.22	−2.86[a]	4.59	33	0.30	−3.30[a]	4.15	23	0.26	−2.16[a]	0.00	5.29	12	0.31
FeII	−0.23	4.55	4	0.19	−0.05	4.54	8	0.32	0.00	4.15	4	0.09	−0.41	4.88	3	0.21
CoI	0.15	2.40	1	···	···	···	···	···	···	···	···	···	···	···	···	···
ZnI	···	···	···	···	···	···	···	···	···	···	···	···	···	···	···	···
SrII	1.68	1.91	1	···	0.31	0.35	1	···	−0.39	−0.80	1	···	···	···	···	···
YII	1.40	0.96	2	0.29	0.25	−0.37	2	0.02	<0.23	< −0.83	1	···	···	···	···	···
BaII	2.63	2.08	3	0.32	1.21	0.48	2	0.24	−0.61	−1.78	2	0.14	0.07	0.04	1	···
LaII	1.93	0.39	4	0.14	1.16	−0.56	4	0.15	<1.16	< −1.00	3	0.25	···	···	···	···
CeII	2.30	1.17	6	0.18	1.40	0.09	1	···	<2.04	<0.29	3	0.65	···	···	···	···
NdII	2.12	0.94	6	0.27	1.72	0.36	4	0.11	<1.59	< −0.21	2	0.41	···	···	···	···
EuII	1.18	−0.99	2	0.13	<0.87	< −1.48	1	···	<1.45	< −1.34	1	···	···	···	···	···
PbI	<2.28	<1.55	1	···	2.66	1.75	1	···	···	···	···	···	[b]	···	···	···

[a] This is [Fe/H].

[b] Pb I 4057 line is swamped by molecular features.

[c] No Pb abundance as the large negative v_r moves the 4057 Å Pb I line onto a CCD defect.

Table 10. Abundances for the Third Four EMP C-Stars From the HES

Species	HE1410−0004				HE1434−1442				HE1443+0113				HE1509−0806			
	[X/Fe] (dex)	log$\epsilon(X)$ (dex)	No. Lines	σ (dex)	[X/Fe] (dex)	log$\epsilon(X)$ (dex)	No. Lines	σ (dex)	[X/Fe] (dex)	log$\epsilon(X)$ (dex)	No. Lines	σ (dex)	[X/Fe] (dex)	log$\epsilon(X)$ (dex)	No. Lines	σ (dex)
Li I	<1.03[d]	<1.32	1	···	···	···	···	···	···	···	···	···	···	···	···	···
C−CH	1.99	7.56	1	···	1.95	8.16	1	···	1.84	8.36	1	···	1.98	7.66	1	···
N−CN	···	···	···	···	1.40	6.95	1	···	···	···	···	···	2.23	7.25	1	···
O I	1.18	6.90	1	···	···	···	···	···	···	···	···	···	···	···	···	···
NaI	0.48	3.78	3	0.20	0.03	3.97	4	0.23	0.37	4.62	2	0.27	···	···	···	···
MgI	0.58	5.10	6	0.29	0.30	5.45	3	0.05	0.37	5.84	2	0.09	0.64	5.27	2	0.11
AlI	···	···	···	···	···	···	···	···	···	···	···	···	0.28	3.84	1	···
SiI	···	···	···	···	0.74	5.91	2	0.26	···	···	···	···	···	···	···	···
KI	0.71	2.81	1	···	···	···	···	···	···	···	···	···	···	···	···	···
CaI	0.11	3.45	5	0.16	0.24	4.21	5	0.23	···	···	···	···	0.55	4.00	2	0.06
ScII	···	···	···	···	0.18	0.90	2	0.10	···	···	···	···	···	···	···	···
TiI	0.38	2.35	2	0.24	0.31	2.91	5	0.19	···	···	···	···	0.28	2.36	5	0.08
TiII	0.22	2.20	4	0.09	0.68	3.29	8	0.32	···	···	···	···	0.96	3.04	11	0.28
CrI	−0.19	2.47	2	0.09	−0.30	2.99	2	0.19	···	···	···	···	−0.08	2.68	1	···
MnI	−0.61	1.76	2	0.21	−0.40	2.60	3	0.19	···	···	···	···	−0.05	2.43	3	0.42
FeI	−3.02[a]	4.43	22	0.17	−2.39[a]	5.07	20	0.18	−2.07[a]	5.38	10	0.21	−2.91[a]	4.54	18	0.16
FeII	0.02	4.45	5	0.09	0.03	5.09	8	0.23	···	···	···	···	0.17	4.71	5	0.24
CoI	···	···	···	···	<1.53	<4.07	1	···	···	···	···	···	0.10	2.11	1	···
NiI	···	···	···	···	0.76	4.63	1	···	···	···	···	···	···	···	···	···
ZnI	<0.90	<2.48	1	···	···	···	···	···	···	···	···	···	···	···	···	···
SrII	0.18	0.06	1	···	···	···	···	···	···	···	···	···	1.12	1.11	1	···
YII	···	···	···	···	0.37	0.23	2	0.03	···	···	···	···	0.95	0.28	2	0.16
BaII	1.06	0.17	5	0.24	1.23	0.98	3	0.17	1.40	1.46	2	0.04	1.93	1.15	2	0.18
LaII	···	···	···	···	···	···	···	···	···	···	···	···	1.67	−0.10	4	0.16
CeII	···	···	···	···	···	···	···	···	···	···	···	···	1.89	0.53	3	0.38
NdII	···	···	···	···	1.70	0.81	2	0.31	···	···	···	···	2.18	0.77	4	0.70
EuII	<2.40	< −0.11	1	···	···	···	···	···	···	···	···	···	<0.93	< −1.47	2	0.23
PbI	<3.17	<2.11	1	···	2.18	1.75	1	···	···	···	···	···	2.61	1.65	1	···

[a]This is [Fe/H].

[b]Pb I 4057 line is swamped by molecular features.

[c]No Pb abundance as the large negative v_r moves the 4057 Å Pb I line onto a CCD defect.

[d]The meteoritic abundance is used for Li, rather than the solar one.

Table 11. Abundances for the Last Three EMP C-Stars From the HES

Species	HE2158−0348				HE2232−0603				HE2356−0410			
	[X/Fe] (dex)	log$\epsilon(X)$ (dex)	No. Lines	σ (dex)	[X/Fe] (dex)	log$\epsilon(X)$ (dex)	No. Lines	σ (dex)	[X/Fe] (dex)	log$\epsilon(X)$ (dex)	No. Lines	σ (dex)
C−CH	1.87	7.76	1	···	1.22	7.96	1	···	2.14	7.66	1	···
N−CN	1.52	6.75	1	···	0.47	6.55	1	···	1.89	6.75	1	···
MgI	0.68	5.52	3	0.18	0.85	6.54	5	0.32	0.36	4.83	3	0.50
AlI	0.47	4.24	1	···	0.26	4.88	1	···	0.25	3.65	1	···
CaI	0.82	4.48	2	0.05	0.35	4.86	2	0.15	0.71	4.01	2	0.13
ScII	···	···	···	···	0.05	1.31	1	···	0.48	0.51	1	···
TiI	0.43	2.72	6	0.24	0.35	3.50	13	0.21	0.25	2.17	6	0.13
TiII	0.65	2.94	8	0.28	0.11	3.25	11	0.17	0.33	2.25	8	0.23
CrI	−0.66	2.31	1	···	−0.06	3.76	3	0.25	−0.36	2.24	1	···
MnI	−0.19	2.50	2	0.01	−0.41	3.14	3	0.34	−0.10	2.22	4	0.28
FeI	−2.70[a]	4.75	28	0.26	−1.85[a]	5.60	38	0.23	−3.07[a]	4.38	28	0.21
FeII	−0.03	4.72	8	0.12	−0.28	5.32	7	0.13	−0.06	4.32	8	0.15
CoI	−0.06	2.16	1	···	0.02	3.09	3	0.06	0.18	2.03	1	···
NiI	···	···	···	···	−0.65	3.76	1	···	···	···	···	···
ZnI	···	···	···	···	···	···	···	···	0.51	2.04	1	···
SrII	0.52	0.72	1	···	0.55	1.61	1	···	−0.98	−1.15	1	···
YII	0.87	0.41	3	0.19	0.60	0.99	3	0.24	< -0.01	< -0.84	2	0.25
ZrII	1.74	1.64	2	0.32	···	···	···	···	···	···	···	···
BaII	1.59	1.02	2	0.15	1.41	1.69	3	0.19	−0.78	−1.72	2	0.25
LaII	1.55	0.00	4	0.21	1.23	0.53	3	0.27	<0.60	< -1.33	1	···
CeII	1.89	0.75	5	0.21	1.45	1.15	1	···	<1.04	< -0.48	1	···
NdII	1.51	0.31	2	0.23	···	···	···	···	<1.20	< -0.36	4	0.26
SmII	<2.40	<0.71	1	···	···	···	···	···	···	···	···	···
EuII	0.80	−1.38	2	0.15	···	···	···	···	<0.97	< -1.59	2	0.35
PbI	2.60	1.85	1	···	1.55	1.65	1	···	···	···	···	···

[a]This is [Fe/H].

Table 12. $^{12}C/^{13}C$ Ratios for EMP C-Stars From the HES

ID	$^{12}C/^{13}C(C_2)$[a]	$^{12}C/^{13}C(CH)$
HE0007−1832	>2.0	···
HE0012−1441	>3.0	···
HE0058−0244	3.5	8 – 10
HE0143−0411	>4.0	···
HE0212−0557	4.0	3 – 4
HE0336+0113	2.5	7.5
HE1031−0020	5.0	···
HE1150−0428	4.0	···
HE1410+0213	2.0	2.5
HE1410−0004	>3.0	···
HE1434−1442	5.0	···
HE1443+0113	5.0	···
HE1509−0806	4.0	···
HE2158−0348	6.0	3 – 5
HE2232−0603	>6.0	≥30
HE2356−0410	4.0	3 – 5

[a]The uncertainty in the deduced $^{12}C/^{13}C$ ratios is 30% of the isotopic ratio.

Table 13. Abundance Changes for Small Changes in Stellar Parameters[a]

Species	Δ[X/Fe] ($T_{\rm eff}$−150K) (dex)	Δ[X/Fe] (log(g)−0.4 dex) (dex)	Δ[X/Fe] Model[Fe/H]-0.5 (dex)	Δ[X/Fe] (v_t-0.2 km s^{-1}) (dex)	Δ[X/Fe] W_λ Unc. (dex)	Δ[X/Fe][b] 1 Star (1σ)(dex)
C(CH)	−0.18	0.14	−0.04	−0.02	···	0.23
N(CN)[f]	0.04	0.09	0.00	0.00	···	0.26[g]
MgI	0.00	0.11	0.01	0.03	0.05	0.13
AlI	−0.02	0.10	0.02	0.10	0.08	0.16
CaI	0.04	0.03	0.01	0.06	0.06	0.10
TiI	−0.01	−0.01	−0.01	0.02	0.03	0.04
TiII	0.08	−0.14	−0.01	0.11	0.03	0.20
TiII[h]	−0.06	0.03	0.01	0.11	0.03	0.13
CrI	0.00	−0.01	−0.01	0.02	0.08	0.08
MnI[c]	−0.06	0.05	0.02	0.16	0.06	0.19
FeI[d]	−0.16[d]	0.03[d]	0.13[d]	0.08[d]	0.02[d]	0.22[d]
FeII	0.14	−0.17	−0.02	0.03	0.03	0.23
CoI[c]	−0.02	−0.01	−0.01	0.03	0.08	0.09
SrII	0.00	−0.02	0.00	0.08	0.08	0.11
SrII[h]	−0.14	0.15	0.02	0.08	0.08	0.24
YII	0.07	−0.15	−0.02	0.06	0.05	0.19
YII[h]	−0.07	0.02	0.00	0.06	0.05	0.11
ZrII	0.08	−0.15	−0.02	0.11	0.06	0.21
ZrII[h]	−0.07	0.02	0.00	0.11	0.06	0.14
BaII[c]	−0.04	0.03	0.00	0.04	0.06	0.09
BaII[c*h*]	−0.19	0.20	0.02	0.04	0.06	0.28
LaII[c]	0.06	−0.14	−0.02	0.09	0.04	0.19
LaII [c*h*]	−0.08	0.02	0.00	0.09	0.04	0.13
CeII	0.06	−0.15	−0.02	0.05	0.04	0.18
CeII[h]	−0.08	0.02	0.00	0.05	0.04	0.11
NdII	0.04	−0.14	−0.03	0.04	0.06	0.17
NdII[h]	−0.10	0.02	−0.01	0.04	0.06	0.13
SmII	0.06	−0.15	−0.02	0.06	0.08	0.19
SmII[h]	−0.08	0.02	0.00	0.06	0.08	0.13
EuII[c]	0.05	−0.15	−0.02	0.03	0.06	0.18
EuII[c*h*]	−0.09	0.02	0.00	0.03	0.06	0.11

Table 13—Continued

Species	Δ[X/Fe] ($T_{\rm eff}$−150K) (dex)	Δ[X/Fe] (log(g)−0.4 dex) (dex)	Δ[X/Fe] Model[Fe/H]-0.5 (dex)	Δ[X/Fe] (v_t-0.2 km s^{-1}) (dex)	Δ[X/Fe] W_λ Unc. (dex)	Δ[X/Fe][b] 1 Star (1σ)(dex)
PbI[e]	−0.05	0.12	0.02	0.14	0.08	0.21

[a]Computed from the line list and the stellar parameters of HE2158−0348 with respect to Fe I for all species.

[b]1σ uncertainty in [X/Fe] for a single (typical) star including the 5 sources of uncertainties.

[c]Treated as individual absorption lines without HFS corrections.

[d]Change in log[ϵ(Fe)].

[e]4057 Å feature treated as a single Pb I line.

[f]Assumes logϵ(C) varies as for CH.

[g]This includes the uncertainty in ϵ(C), as ϵ(N) is derived from lines of CN.

[h]Changes computed with respect to Fe II.

Table 14. Additional C-Stars From the Literature

Star ID	Ref.[a]	Binary	Period, v_r Amp (days, km s^{-1})	[Ba/Fe] (dex)	^{12}C/^{13}C
G77–61	1,2	Yes	245, 20	···	···
CS22880–074	8	···	···	+1.34	>40
CS22881–036	8	···	···	+1.93	40:
CS22898–027	8	···	···	+2.27	>20
CS22942-019	4, 8	Yes	2800, 5	+1.92	30:
CS22948–027	8,9	Yes	505, 5	+1.67	14
CS29497–030	6,7	Yes	342, 4	+2.17	>10
CS29497–034	9	···	···	+2.03	12
CS29498–043	3	···	···	−0.45	6
CS30301–015	4	···	···	+1.45	···
CS31062–050	4,5	···	···	+2.61	···

[a]1. Plez & Cohen (2005), Plez, Cohen & Melendez (2006) 2. Dearborn *et al.* (1986), 3. Aoki *et al.* (2002b), 4. Aoki *et al.* (2003), 5. Johnson & Bolte (2004), 6. Sivarani *et al.* (2004), 7. Preston & Sneden (2000), 8. Preston & Sneden (2001), 9. Hill *et al.* (2000).

Table 15. Statistics for Selected Abundance Ratios For the Primary Sample of 16 C-Stars From the HES[a]

Species[h]	Nstars[b]	Min. [X/Y] (dex)	Max. [X/Y] (dex)	Median [X/Y] (dex)	σ[X/Y] (dex)	EMP Dwarfs[c] (dex)
[C/Fe]	16	1.22	2.52	1.93	0.31	0.2[f]
[N/Fe]	14	0.47	2.52	1.75	0.59	0.0[f]
[Na/Fe]	3	0.03	0.48	0.37	0.23	0.41[g]
[Mg/Fe]	12	0.04	1.04	0.55	0.27	0.56
[Al/Fe][d]	10	−0.55	0.88	0.27	0.39	−0.09
[Ca/Fe]	14	0.11	1.12	0.42	0.34	0.31
[ScII/Fe][d]	5	0.05	0.67	0.48	0.26	0.24
[TiI/Fe]	14	0.03	0.57	0.36	0.15	0.36
[TiII/Fe]	15	0.11	0.96	0.36	0.26	0.36
[Cr/Fe]	14	−0.70	−0.06	−0.32	0.21	−0.23
[Mn/Fe]	12	−0.72	0.03	−0.31	0.23	−0.59
[FeII/FeI]	15	−0.41	0.17	−0.04	0.16	0.00
[Co/Fe][d]	8	−0.06	0.67	0.16	0.24	0.42
[NiI]	4	−0.65	0.02	−0.32	0.27	−0.02
[Sr/Fe]	12	−0.98	1.68	0.32	0.69	−0.19
[Y/Fe]	11	−0.01	1.40	0.55	0.39	···
[Ba/Fe]	16	−0.78	2.63	1.30	1.01	−0.20
[C/Ba]	16	−0.44	2.98	0.43	1.15	···
[C/Ba][e]	12	−0.44	0.93	0.15	0.49	···
[Sr/Ba]	12	−2.23	0.21	−0.94	0.69	···
[Sr/Ba][e]	8	−2.23	−0.85	−1.11	0.51	···
[Y/Ba]	9	−1.73	−0.72	−1.21	0.35	···
[Y/Sr]	8	−0.28	0.60	−0.03	0.32	···
[La/Ba]	8	−0.71	0.10	−0.32	0.26	···
[Eu/Ba]	4	−1.47	−0.34	−0.82	0.46	···
[Pb/Ba]	7	0.14	1.21	0.79	0.34	···

[a]We include the dwarf C-star HE0007−1832 from Cohen *et al.* (2004).

[b]Upper limits are ignored.

[c]Data from Cohen *et al.* (2004).

[d]Only 1 line used, with possible blending by molecular features.

[e]Here we exclude the four C-stars with [Ba/Fe]< 0.2 dex.

[f]Data for unmixed giants from Spite *et al.* (2005).

[g]Data for giants from Cayrel *et al.* (2004).

[h]Detection in a minimum of three stars is required.

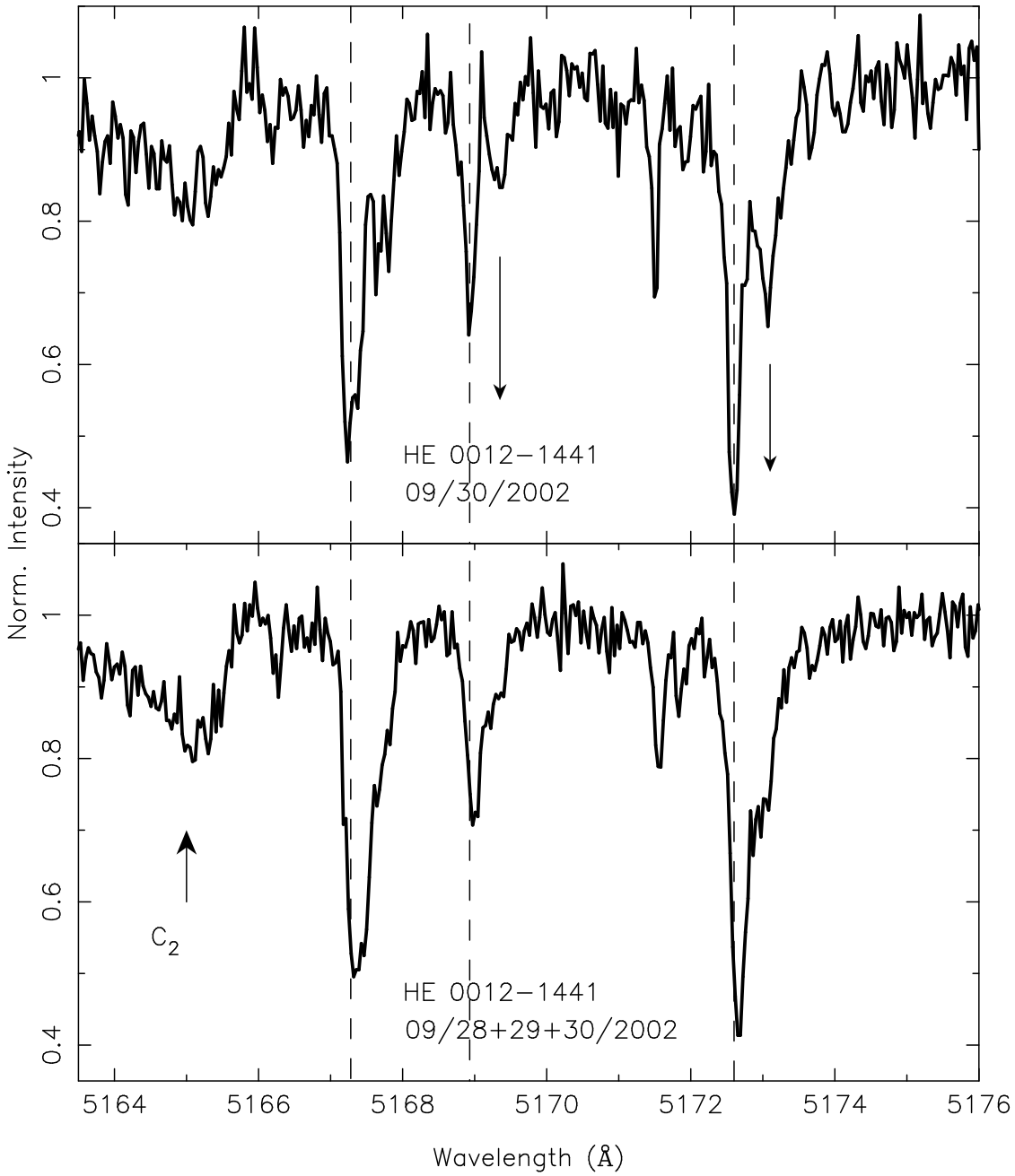

Fig. 1.— Upper panel: the spectrum of the spectroscopic binary HE0012−1441 from the night of 09/30/2002 in the region of the Mg triplet. The arrows indicate two lines from the secondary star. lower panel: the same, but using the data summed over 3 nights from the Sep. 2002 HIRES run. Note the difference in the line profiles of the Mg triplet lines (and some of the weaker lines as well). Note also that the lines from the secondary star are noticably broader than those from the primary. The dashed vertical lines guide the eye to indicate the changing relative v_r of the two components over a timespan of 48 hours.

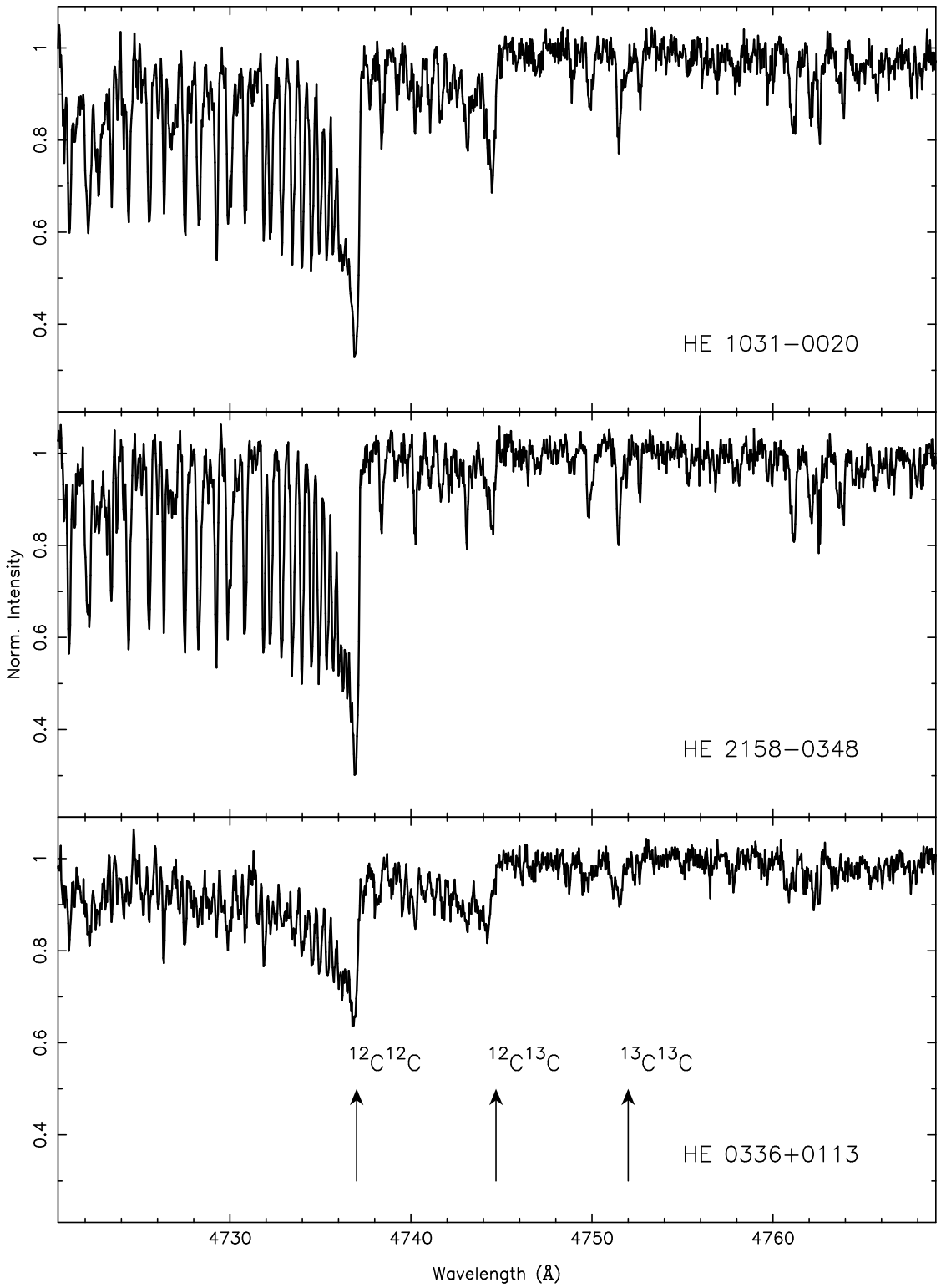

Fig. 2.— The HIRES spectra of three C-stars from our sample in the region of 4740 Å. The bandheads of $^{12}C^{12}C$, $^{12}C^{13}C$ and $^{13}C^{13}C$ are indicated. The vertical range is the same for each panel. The derived $^{12}C/^{13}C$ ratio for these three stars ranges from 3.5 to 6, identical to within the observational errors of ±30%.

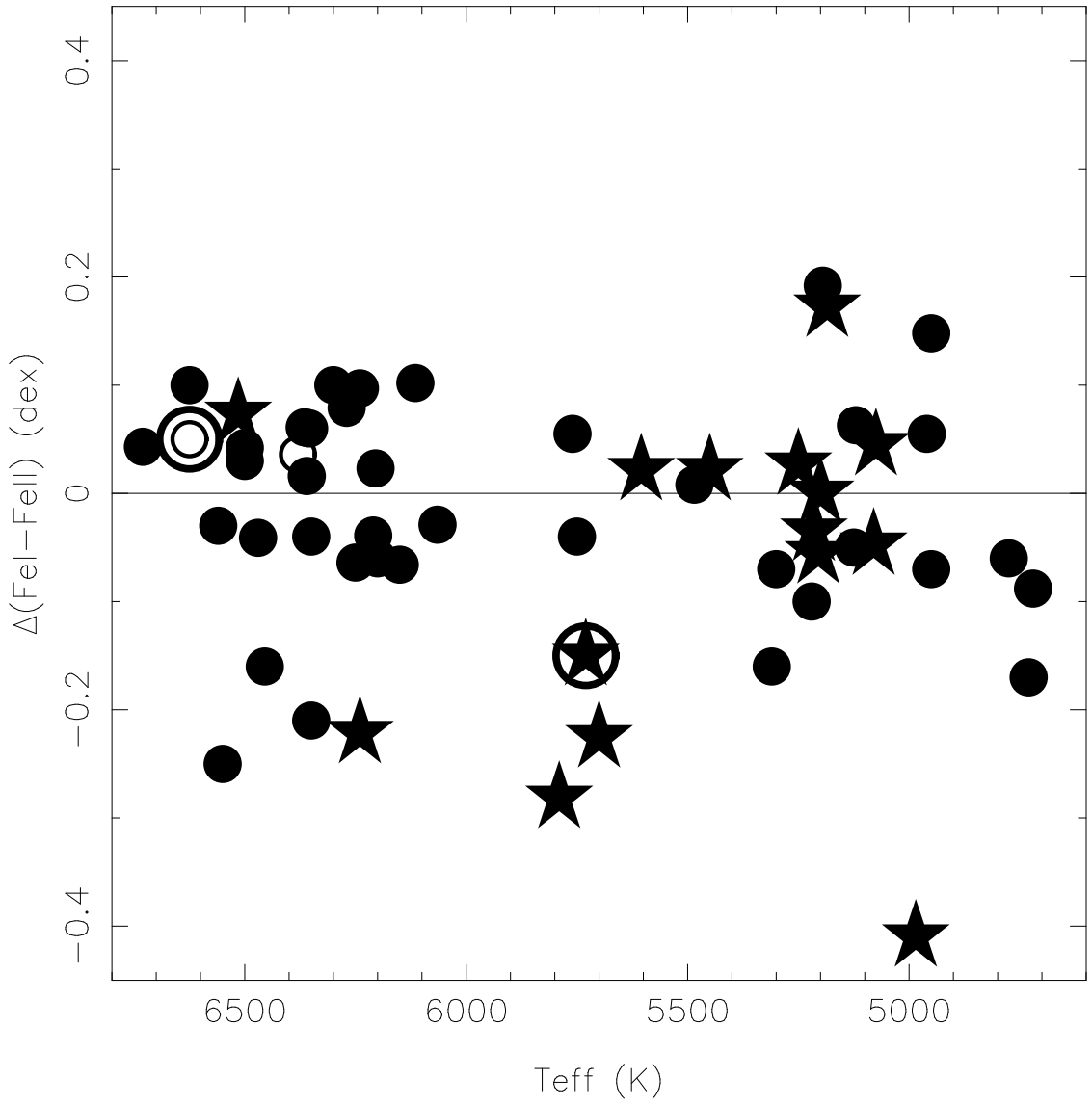

Fig. 3.— The Fe ionization equilibrium for the 16 VMP and EMP C-stars in the present sample. The C-stars are indicated as large stars, the C-enhanced stars as open circles, and the C-normal stars from our published and unpublished analyses as filled circles. The three known spectroscopic binaries in this sample are circled. (One of these is an apparently C-normal star (HE0218−2736) which is too hot and too metal-poor to show any Fe II lines, hence does not appear in this figure.)

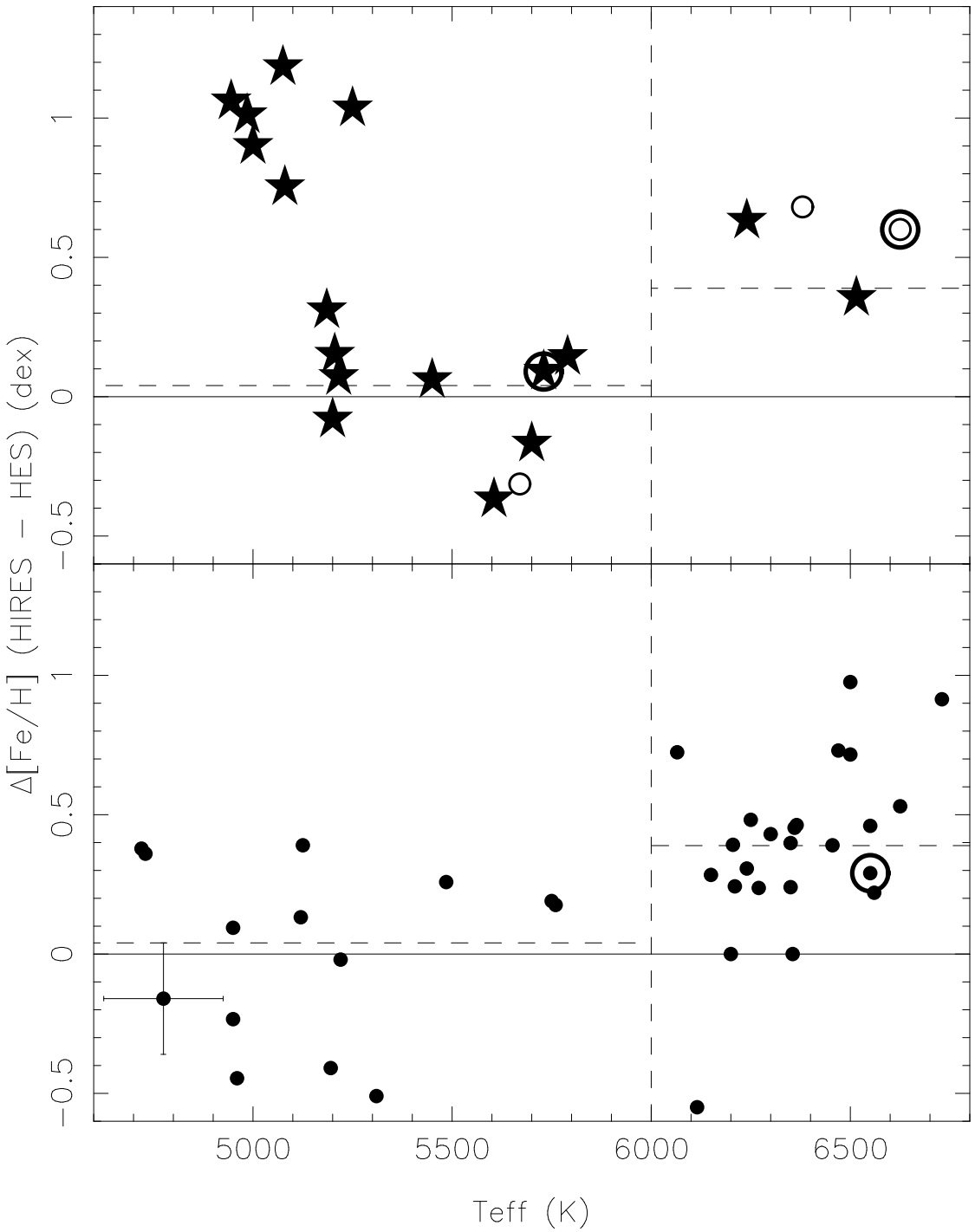

Fig. 4.— The difference between [Fe/H](HES) and [Fe/H](HIRES) is shown as a function of $T_{\rm eff}$ for the C-stars (upper panel) and for the C-normal stars (lower panel) for those EMP candidates from the HES with analyses based on Keck/HIRES spectra. The symbols are those of Fig. 3. The vertical dashed line separates the giants from the dwarfs, while the horizontal dashed lines are represent the mean Δ for the C-normal giants and for the C-normal dwarfs. A typical error is indicated for a single star.

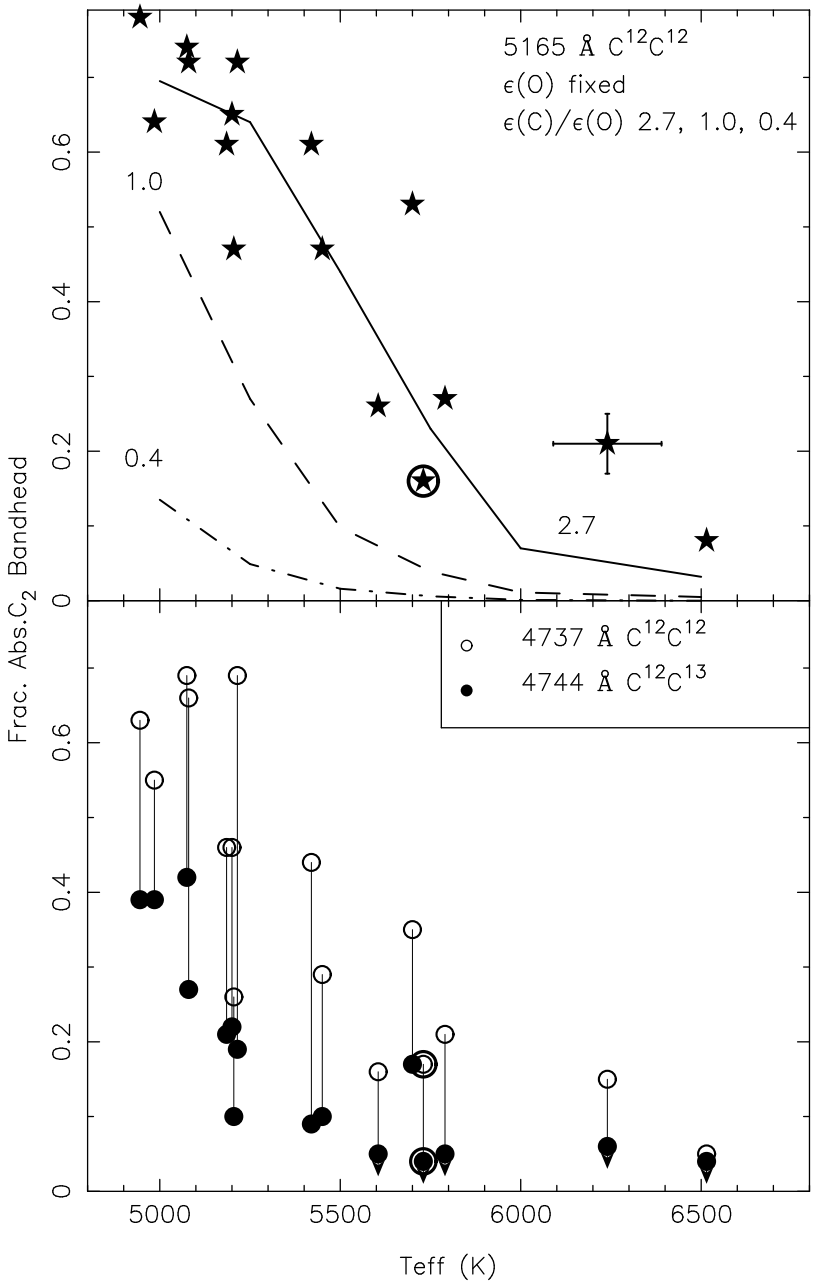

Fig. 5.— The fractional absorption at several C_2 bandheads measured from our Keck/HIRES spectra is shown for our sample of C-stars from the HES as a function of $T_{\rm eff}$. The symbols are those of Fig. 3. Upper panel: the fractional absorption at 5165.0 Å (the 0,0 bandhead of the Swan system) is shown. The solid curve indicates the predicted behavior for $\log[\epsilon({\rm C,N,O})] =$ 7.56, 6.55, and 7.13 dex (C/O 2.7), the dashed curve is that for C/O=1 and the dot-dashed curve for C/O 1/2.7, keeping ϵ(O) fixed. Lower panel: the 4737 Å bandhead of $^{12}C^{12}C$ is shown as open circles while the 4744 Å bandhead of $^{12}C^{13}C$ is shown as filled circles. Vertical lines connect the two values for each C-star. All C-stars in our sample hotter than 5500 K only have upper limits for the latter.

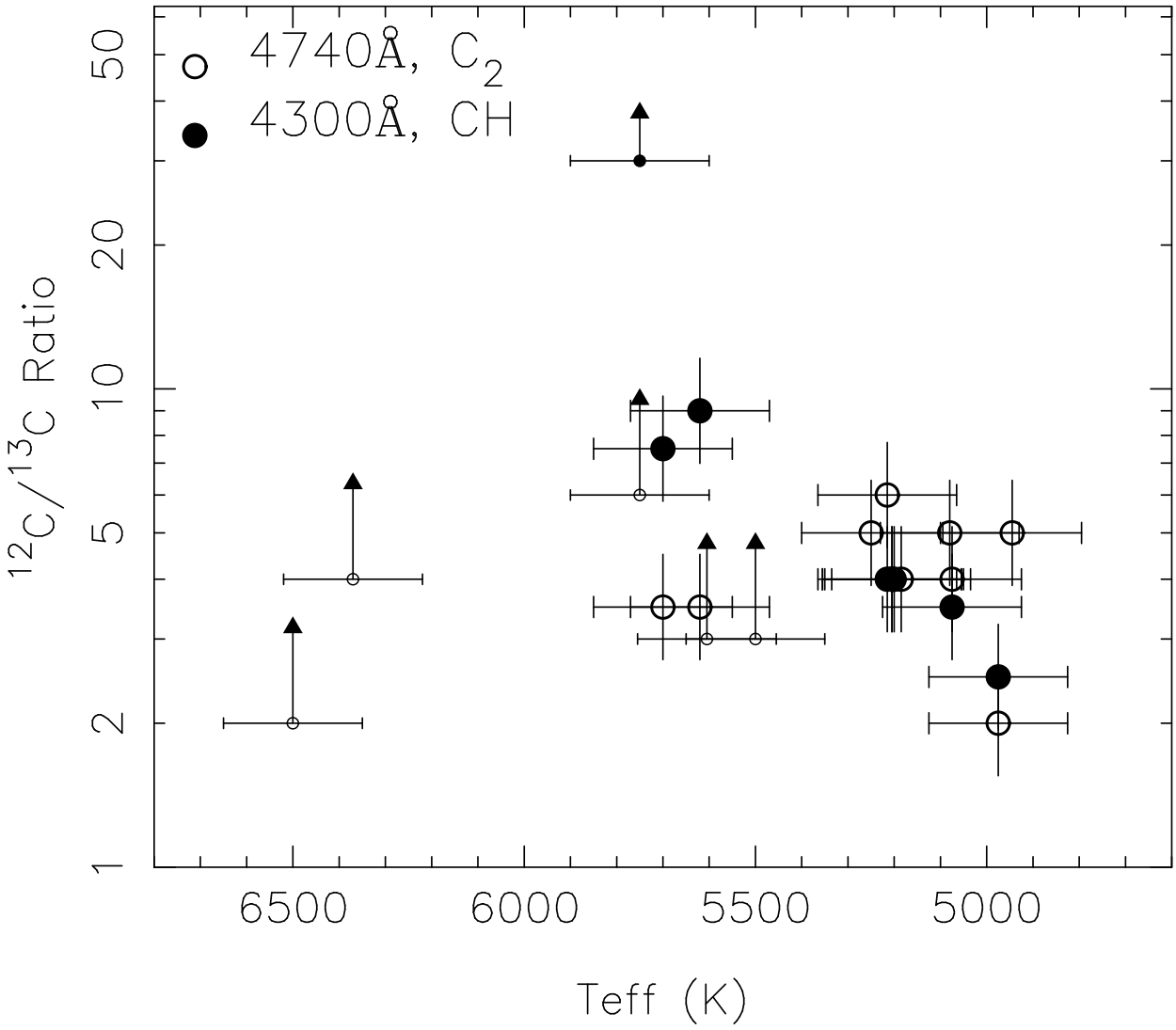

Fig. 6.— $^{12}C/^{13}C$ ratios measured from the C_2 (1,0) Swan band and from the G band of CH are shown as a function of $T_{\rm eff}$ for the C-stars in our sample. All C-stars with $T_{\rm eff} > 5700$ K have only lower limits to the $^{12}C/^{13}C$ ratio from the present spectra.

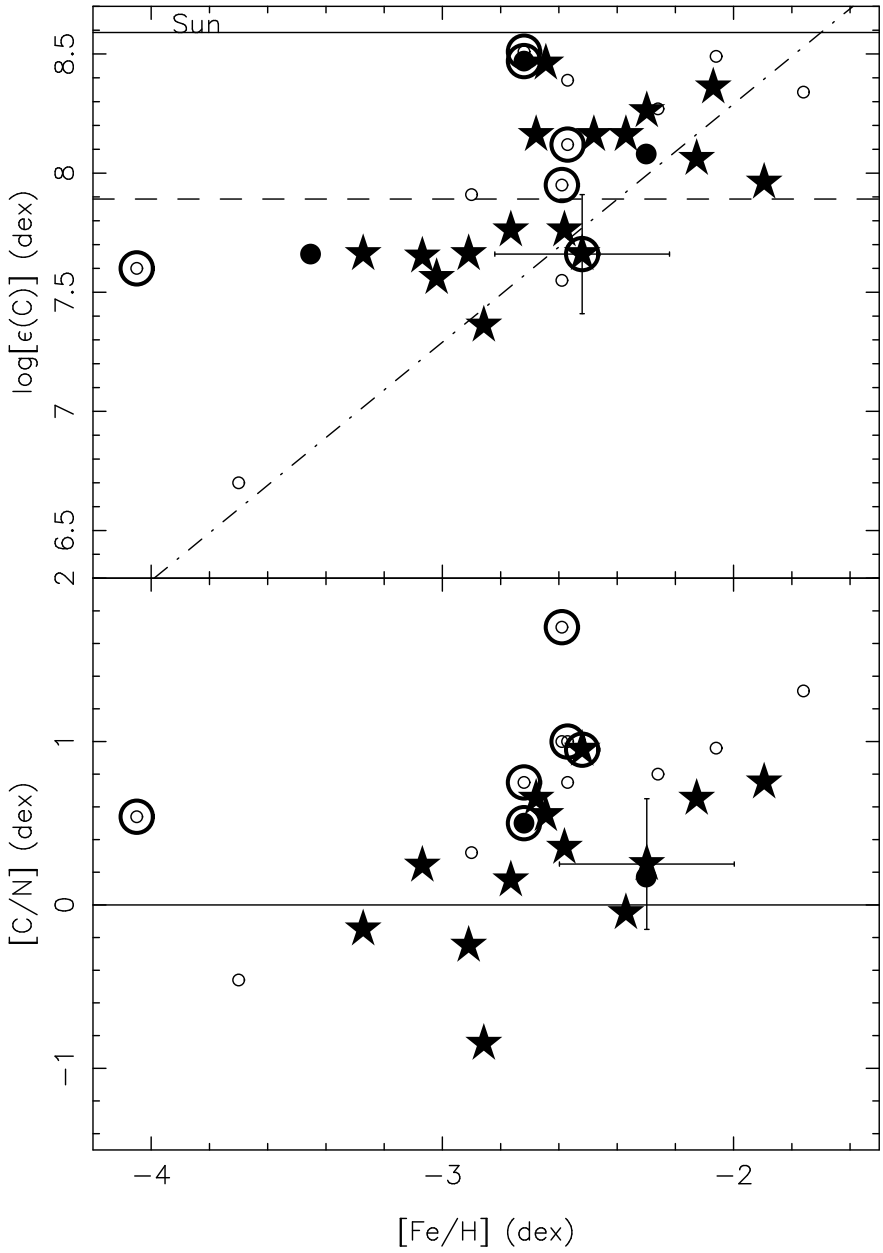

Fig. 7.— Upper panel: logϵ(C) is shown as a function of [Fe/H] for C-stars (marked by large stars) and the C-enhanced stars (indicated by filled circles) with detailed abundance analyses from the HES by our group. The augmented sample of very metal-poor C-stars from the literature (see Table 14 for details) is shown as small open circles. Known spectroscopic binaries are circled. The dashed horizontal line indicates a fixed ϵ(C) of 20% that of the Sun. The sloping line indicates the locus of [C/Fe] = +1.7 dex. Lower panel: the same for [C/N]. The horizontal line indicates the Solar ratio. A typical error bar is indicated for a single star in each panel.

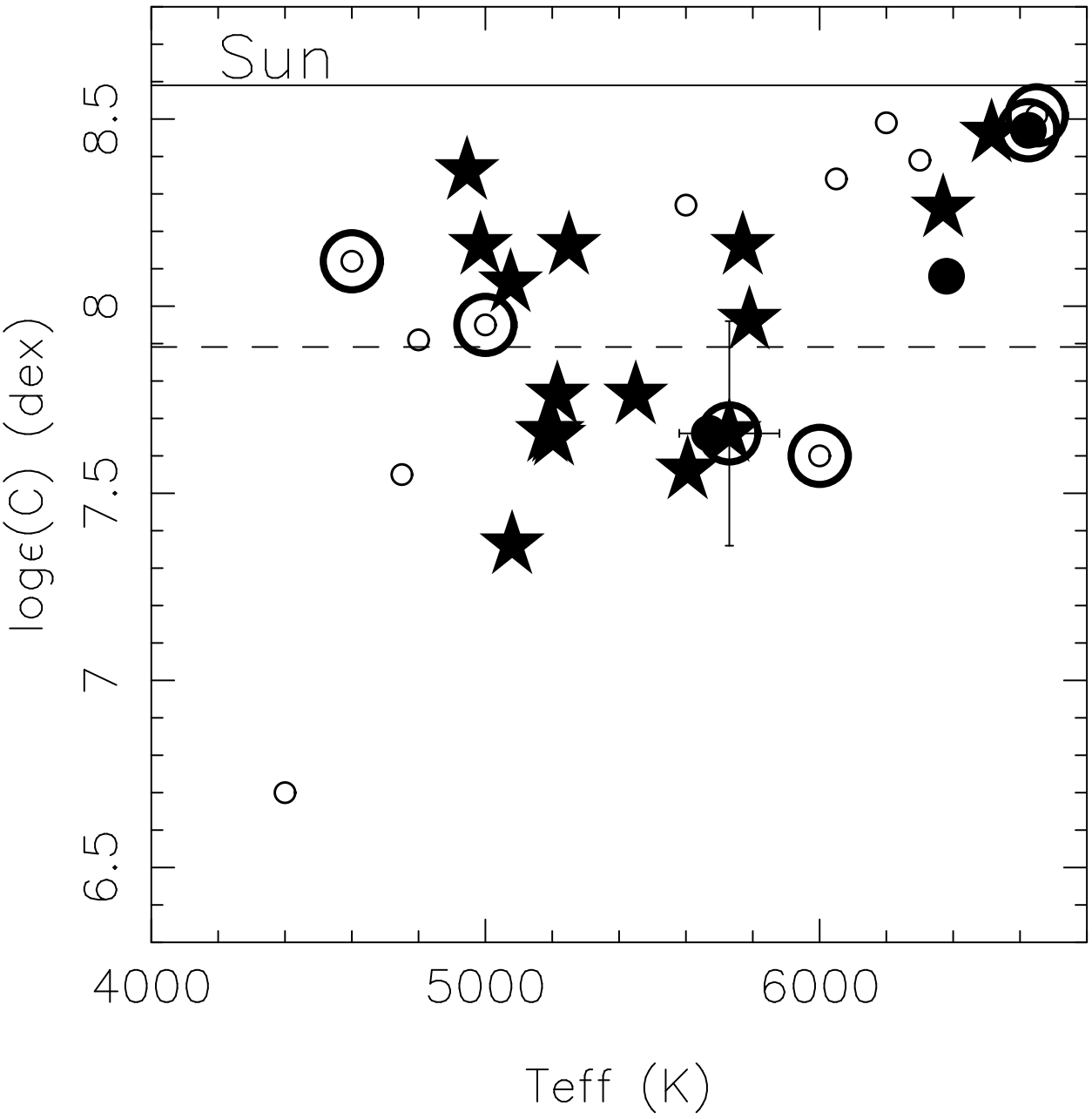

Fig. 8.— log[ϵ(C)] is shown as a function of $T_{\rm eff}$ for C-stars (large stars) and C-enhanced stars (large filled circles) from our sample. The augmented sample of very metal-poor C-stars with recent detailed abundance analyses from the literature (see Table 14 for details) is shown as small open circles. Known spectroscopic binaries are circled. The solid horizontal line represents the Solar ratio, while the horizontal dashed line represents 20% of Solar. G77–61 is plotted as a dwarf with $T_{\rm eff}$ = 6000 K.

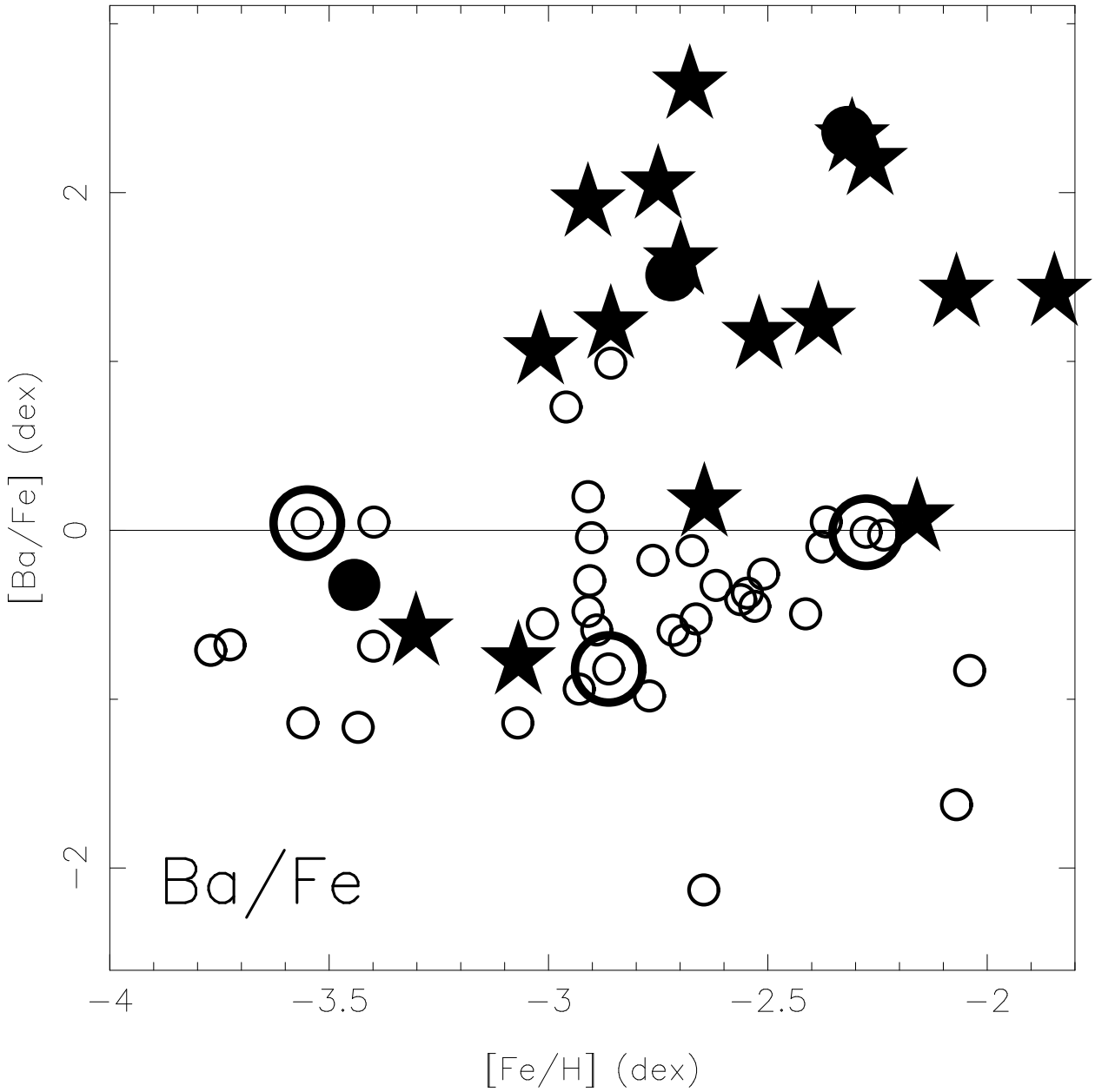

Fig. 9.— The abundance ratio [Ba/Fe] as a function of [Fe/H] for HES EMP C-stars (large stars) and C-enhanced stars (large filled circles) with detailed abundance analyses. All C-normal stars from the HES analyzed to date by us are shown as small open circles. The additional C-stars from the literature are not shown. Known spectroscopic binaries are circled.

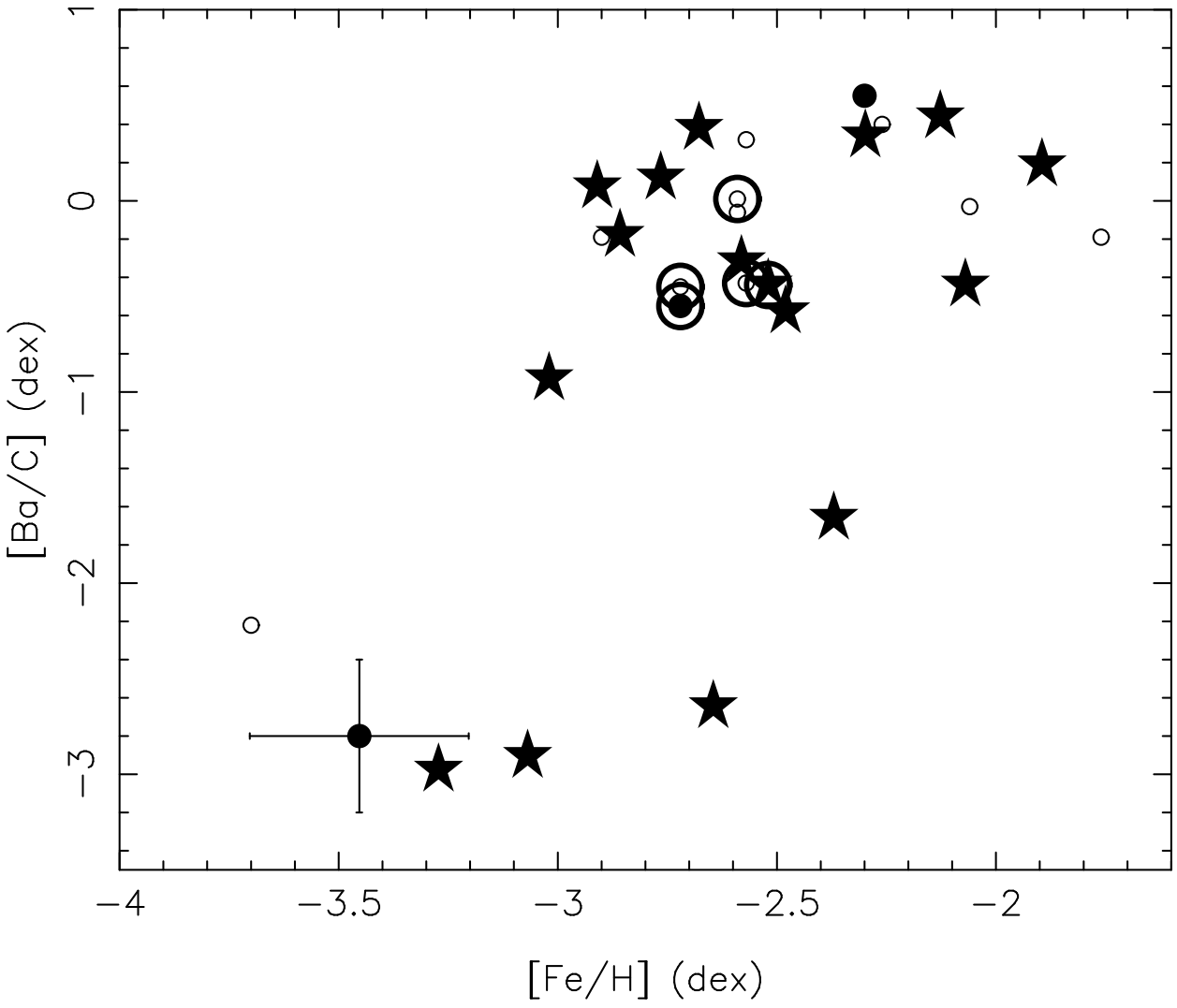

Fig. 10.— The abundance ratio [Ba/C] as a function of [Fe/H] for HES EMP C and C-enhanced stars with detailed abundance analyses and for the augmented sample of very metal-poor C-stars from the literature. The symbols are those used in Fig. 8; known spectroscopic binaries are circled. A typical error bar is indicated for a single star.

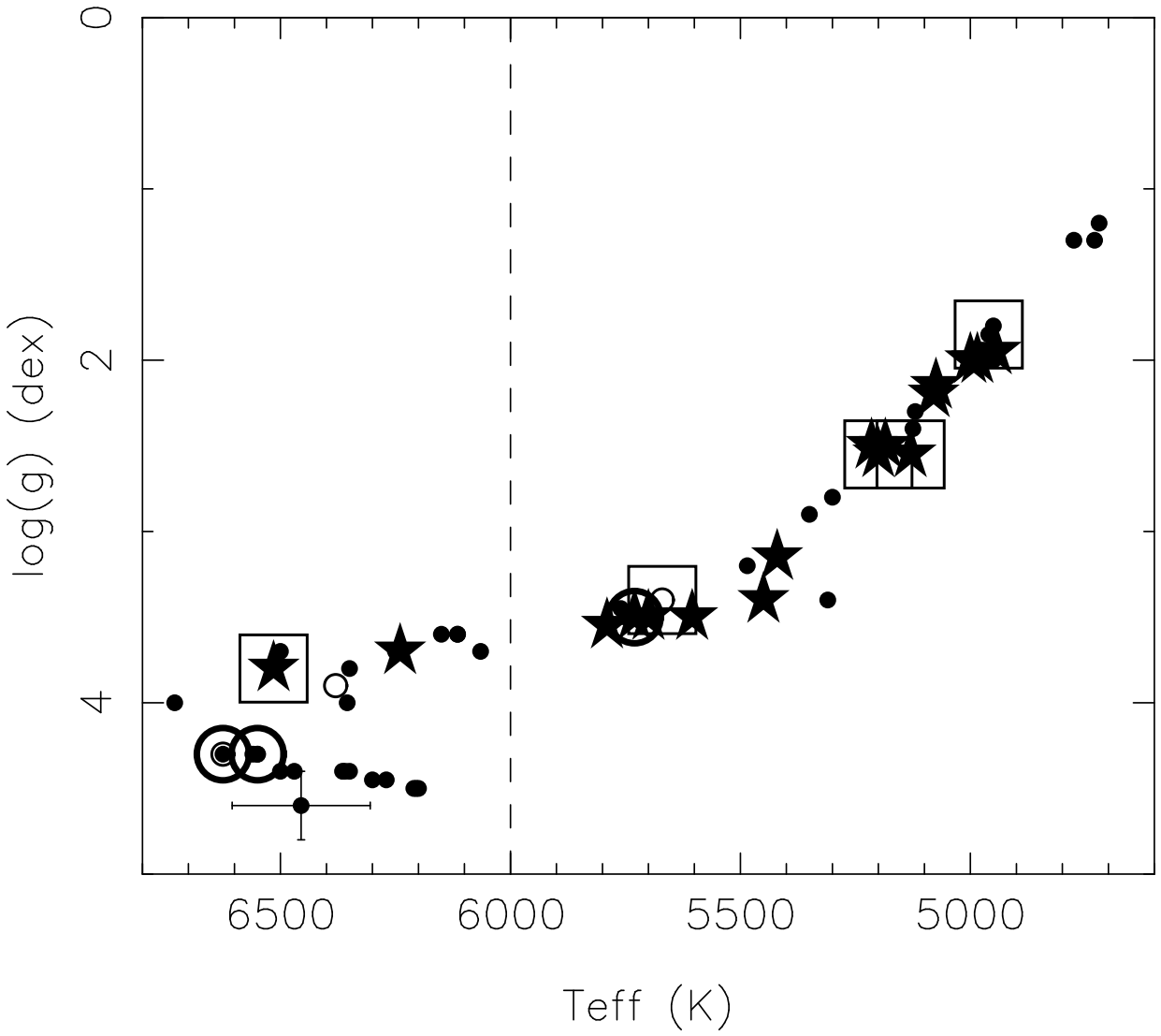

Fig. 11.— The HR-diagram ($T_{\rm eff}$ versus $\log(g)$) is shown for our sample of 16 C-stars and 3 C-enhanced stars denoted by filled stars for the former and by open circles for the latter. The small filled circles indicate all the other EMP candidates from the HES that we have analyzed to date. The five Ba-poor, C-rich stars from our sample are enclosed in squares. The three known binaries are circled. The additional C-stars from the literature are not shown. A typical error bar is indicated for a single star.